



LTH
FACULTY OF
ENGINEERING

Faculty of Engineering LTH
Department of Biomedical Engineering

Master's Thesis in Biomedical Engineering

November 2020 - June 2021

**Cardiovascular effects of exposure
to biodiesel exhaust**

Student: Youna Marc-Derrien

Supervisor:
Frida Sandberg
Associate Professor

Examiner:
Leif Sörnmo
Professor

Abstract

Context: Urban air pollution is considered a significant factor contributing to increased respiratory and cardiovascular mortality in cities. Many studies focused on the relationship between exposure to diesel exhaust and human health effects, demonstrating the toxicity of such gases. Biodiesel is described as a more carbon-neutral alternative to petroleum derivatives, but few studies have been conducted yet to assess its effects on human health. *Objective:* The present work investigates the influence of exposure to biodiesel exhaust gases on cardiovascular function in human. *Methods:* PPG and ECG recordings of 19 study participants are recorded during exposure to various gases, including biodiesel exhaust. PPG pulses are decomposed into five waves by implementing a pulse decomposition analysis (PDA). Morphological features, including the percentage of amplitude loss between waves, are calculated among others. Measures of changes in PPG waveforms, complemented by computation of pulse transit time (PTT) are performed for assessment of vascular compliance properties. In addition, calculation of heart rate variability (HRV) indicators is used for evaluation of the state of the autonomic nervous system (ANS). *Results:* Statistically significant individual differences between exposure to pure air and biodiesel exhaust were found regarding percentage of amplitude loss in the second and third reflected waves. Increase in those parameters after three hours was reasonably consistent among study participants. There was no effect of exposure to biodiesel exhaust on PTT intervals and HRV indicators. *Conclusion:* An increase in amplitude loss in reflected waves is associated with reduced vascular compliance. Exposure to biodiesel may thus induce a slight increase in arterial stiffness. Further studies are necessary to assess the effects of biofuel exhaust on cardiovascular function and should be based on larger groups of study participants to compensate for the large range of responses obtained by PDA and HRV analysis.

Key words: photoplethysmography, electrocardiography, signal processing, pulse decomposition analysis, heart rate variability, pulse transit time, biodiesel, arterial stiffness.

Acknowledgements

First and foremost, I would like to thank my supervisor at LTH, Frida Sandberg, for her guidance in the biomedical engineering aspects for my research. But also for her support and her feedback regarding the content of the thesis.

Further thanks to my home university, Ecole Centrale de Marseille, for allowing me to complete this 2-year double degree at Lund University. I am very grateful for this opportunity.

Selected abbreviations

ANS	Autonomic Nervous System
EC	Elemental Carbon
ECG	Electrocardiogram
HC	Hydro-Carbon
HRV	Heart Rate Variability
ICG	Impedance Cardiogram
NO	Nitric Oxide
NO ₂	Nitrogen Dioxide
PAT	Pulse Arrival Time
PDA	Pulse Decomposition Analysis
PEP	Pre-Ejection Period
PM	Particulate Matter
PPG	Photoplethysmogram
PRV	Pulse Rate Variability
PTT	Pulse Transit Time

A _{1j}	Percentage of amplitude loss between the first and j^{th} inner waves
HF	Power in high-frequency band (0.15-0.40 Hz)
LF	Power in low-frequency band (0.04-0.15 Hz)
LF/HF	Ratio of LF over HF
NN	Mean of NN intervals
pNN50	Percentage of adjacent NN interval pairs differing by more than 50ms
rMSSD	Root mean square of successive differences of adjacent NN intervals
rMSSD ^{PTT}	Root mean square of differences of successive PTT intervals
SDNN	Standard deviation of NN intervals
SDPTT	Standard deviation of PTT intervals
SDSD	Standard deviation of adjacent NN interval differences
SDSD ^{PTT}	Standard deviation of successive PTT interval differences
T _{1j}	Time delay between the first and j^{th} inner waves
W _j	Width at half-maximum of the j^{th} inner wave

Contents

1	Introduction	1
2	Background	5
2.1	Photoplethysmography	5
2.1.1	Principle	5
2.1.2	Artefacts	6
2.2	Pulse waveform analysis	8
2.2.1	PPG pulse waveform	8
2.2.2	Features and applications	8
2.2.3	Pulse decomposition analysis	10
2.3	Heart rate variability	12
2.3.1	Acquisition of NN-intervals	12
2.3.2	Time domain measures	13
2.3.3	Frequency domain measures	14
2.4	Pulse rate variability	15
2.4.1	Pulse rate variability analysis	15
2.4.2	Pulse transit time	15
3	Methodology	18
3.1	Experimental protocol and data acquisition	18
3.2	Data pre-processing	20
3.2.1	Baseline wander removal	20
3.2.2	Motion artefact detection	20
3.2.3	Low-pass filtering	21
3.3	Pulse detection	22
3.4	Pulse waveform analysis	24
3.4.1	Pulse decomposition analysis	24
3.4.2	Features extraction	26
3.4.3	Statistical analysis	27
3.5	PTT and HRV analysis	29
3.5.1	Acquisition of beat detection times	29
3.5.2	Heart rate variability analysis	29
3.5.3	Pulse transit time analysis	30
3.5.4	Statistical analysis	31

4	Results	34
4.1	Pulse waveform analysis	34
4.1.1	Changes in pulse waveform features over time	35
4.1.2	Variability of pulse waveform features at basal condition	35
4.1.3	Changes in pulse waveform features with exposure type	38
4.2	HRV analysis	43
4.2.1	Changes in HRV parameters over exposure time	43
4.2.2	Variability of HRV parameters at basal condition	43
4.2.3	Changes in HRV parameters with exposure type	46
4.3	PTT Analysis	49
4.3.1	Changes in PTT characteristics over exposure time	49
4.3.2	Variability of PTT characteristics at basal condition	52
4.3.3	Changes in PTT characteristics with exposure type	52
4.4	Correlation analysis	54
4.4.1	Correlation between features at basal condition	54
4.4.2	Correlation between relative changes in features after three hours into exposure	54
5	Discussion	61
5.1	Critical review of the results	61
5.2	Limits of the study	62
5.3	Ethical considerations	63
5.4	Future work	64
6	Conclusion	66
A	Pulse waveform analysis	72
A.1	Changes in PDA-derived features over time	72
A.2	Variability of PDA-derived features at basal condition	75
A.3	Changes in PDA-derived features with exposure type	78
B	Heart rate variability analysis	81
B.1	Changes in HRV parameters over time	82
B.2	Variability of HRV parameters at basal condition	85
B.3	Changes in HRV parameters with exposure type	88
C	Pulse transit time analysis	92
C.1	Changes in PTT characteristics over time	92
C.2	Variability of PTT characteristics at basal condition	94
C.3	Changes in PTT characteristics with exposure type	95

Chapter 1

Introduction

Diesel exhaust emission is considered one of the main sources of air pollution in cities, and contributes to the enhancement of greenhouse effect, leading to global warming. Moreover, energy security concerns, such as the predicted shortage of fossil fuel, encourage the search for alternatives to petroleum derivatives. This results in the production of a substitute fuel, named "biodiesel". Contrary to diesel, it is obtained from alkyl esters of vegetable oils or animal fats. It can be pure or merged with fossil fuel in various proportions [1]. Biodiesel constitutes a renewable form of energy, often assumed to be carbon-neutral. As its use is supposed to release marginal levels of pollutants into the air, biodiesel is a potentially attractive surrogate to fossil fuel. But far from being perfect, its fabrication process is way more expensive than conventional fuels. In addition, its production generates a lot of greenhouse gases, making the global carbon-balance of biodiesel not neutral, but negative. In terms of energy performance, biodiesel fuel has also a lower energy density compared to fossil fuel.

In the past, a large number of toxicological studies clearly demonstrated that diesel engine exhaust affects human health through emission of toxicant particles, such as organic compounds, sulfur and metals [2]. Toxic gases, such as carbon monoxide (CO) and dioxide (CO₂), nitric oxide (NO) and nitrogen dioxide (NO₂) are emitted. Also, hydrocarbons (HC), polyaromatic hydrocarbons (PAHs), nitrated PAHs (nPAHs) and fine particulate matter (PM) compose diesel exhaust. Based on these studies, it has been judged as mutagenic and carcinogenic to human by the World Health Organization (WHO) in 2010, and classified as a group 1 carcinogen to human by the International Agency for Research on Cancer (IARC) in 2012. After that, laboratory studies showed that the composition of biodiesel fuel influences not only exhaust gas composition but human health effects from exhaust exposure. A reduction in hydrocarbon (HC) and carbon (CO and CO₂) emissions with increasing concentration of bio-components in fuel was demonstrated. Biodiesel is also expected to decrease PAH and nPAH

emissions, but information regarding those compounds is limited and inconsistent [3].

By now, many studies demonstrated that air pollution, including diesel exhaust, seriously influences human health. Urban air pollution is considered a significant factor contributing to increased respiratory and cardiovascular morbidity and mortality [4]. Exposure studies showed that inhalation of fine particulate matter induces inflammation and injuries to the pulmonary system, but also cardiovascular alterations in healthy rats [5]. Epidemiological analyses demonstrated that this exposure type may also promote changes in mean heart rate and heart rate variability (HRV) in elderly subjects [6]. Moreover, acute exposure to diesel exhaust is associated with an immediate and transient increase in arterial stiffness [7]. Finally, cardiovascular and inflammatory toxicity of diesel and biodiesel particles were assessed. The study concluded that biodiesel is to be considered more toxic than fossil fuel [8].

Since the relationship between biodiesel exhaust and human health requires further investigations, a research project is developed at the Division of Ergonomics and Aerosol Technology of Lund University. Its general purpose is to characterize emissions from vehicles powered by renewable fuels and to determine how humans are affected by being exposed to the exhaust gases. Within the project, chamber studies are carried out where test persons are exposed to biodiesel exhaust gases in a controlled and ethically approved manner and potential negative health effects are measured. Photoplethysmograms (PPG), as well as electrocardiograms (ECG) data from the test subjects are recorded during the chamber exposures.

If ECG is a common and extensively exploited diagnostic tool, PPG might be lesser-known. Photoplethysmography is an optical technique for measuring changes in blood circulation. It offers many advantages, such as simplicity, low cost and non-invasiveness. Recent studies emphasized the potential information embedded in the waveform signal about cardiovascular activity. For instance, PPG's waveform analysis was proven useful as an investigator to changes in elastic properties of the vascular system. Derivations of quantitative measures characterizing pulse shape and specific indexes were used in the assessment of health and diseases [9]. It was also demonstrated that Pulse Rate Variability (PRV) can be used as a surrogate of Heart Rate Variability (HRV) to provide valuable information related to autonomic nervous system (ANS). Both methods provide very similar results, although different due to variations of the so-called pulse transit time (PTT) closely related to arterial compliance [10].

This thesis aims at studying the acute effects of exposure to biodiesel exhaust gases on cardiovascular function in human. For this purpose, PPG and ECG signal recordings from the chamber studies are analyzed. First, an algorithm for modeling PPG pulse waveforms is implemented. PPG pulses are split into five inner waves, by pulse decomposition analysis. Pulse shape features related to arterial stiffness are extracted and compared. In a second phase, HRV analysis is performed, based on ECG signals, to provide information connected to autonomic nervous system. Lastly, PTT computation from both ECG and PPG is carried out to provide additional results linked to vascular compliance properties.

Chapter 2

Background

The theoretical chapter will give a setting for the project. The first part introduces basic information regarding the principle of photoplethysmography. Methods for analyzing PPG pulse waveform are brought up in the next part. The last one relates to analysis of HRV and computation of PTT series.

2.1 Photoplethysmography

2.1.1 Principle

Photoplethysmography (PPG) is a simple optical technique for determining volumetric changes in blood in peripheral circulation which occur with every heartbeat. This method has many advantages: it is easy to set-up, convenient, inexpensive and noninvasive. PPG has been applied in many different clinical settings, such as monitoring of blood oxygen saturation, heart rate, blood pressure, cardiac output and respiration [9].

Fingertip PPG is one of the most commonly used measurement method in medicine. The PPG finger sensor consists of a light emitting diode (LED) and a photo-detector (PD). In transmission mode, PD and LED are on the opposite sides of the finger. The light is emitted from the LED to the skin, and partially absorbed by bones, skin and both venous and arterial blood when travelling through biological tissues. The PD detects transmitted light, while reflectance mode detects light that is back-scattered or reflected. Since light is more strongly absorbed by blood than the surrounding tissues, variations in blood flow can be detected as changes in light intensity received by the PD. The voltage signal obtained by PPG is directly proportional to the quantity of blood flowing through the vessels.

The interaction of light with biological tissues can be quite complex. Several factors determine its penetration depth, namely the wavelength and the distance between the LED and PD. By now, IR or near-IR wavelengths have been used, since the corresponding radiations pass easily without being absorbed and thus provide accurate measurements of deep-tissue blood flow. However, green light is becoming increasingly popular due to large intensity variations observed during the cardiac cycle using these wavelengths. It is also highly suitable for measurements of superficial blood flow in skin. [11]

Finally, the recorded PPG signal contains both a DC and an AC component. The first one is due to the non-pulsatile blood volume part. Tissues surrounding the arteries attenuate light, and produce a signal that varies slowly. Subtle energy changes in the body may also affect this component. The AC component is synchronous with the heart rate and depends on changes in pulsatile pressure and blood volume [10].

2.1.2 Artefacts

The quality of the PPG signal depends on the location and the properties of the subject's skin at measurement, such as the skin structure, its temperature or whether the patient is at rest. These factors generate different types of artefacts which may be contained within the PPG signal segments. The main challenges in processing PPG signals are described hereafter.

First, electromagnetic fields caused by a powerline represents a common noise source in the PPG, as well as in any other electrical signal recorded from the body surface. This type of artefact, also named powerline interference, introduces a sinusoidal component into the recorded signal at a frequency around 50-60 Hz, but also at its higher harmonics. Although precautions can be taken to reduce the effect of powerline interference, for example by selecting a recording location with few surrounding electrical devices, it may still be necessary to perform signal processing to remove such interference [9].

Then, removal of baseline wander is required in order to minimize variations in pulse morphology which do not come from cardiac origin. The frequency content of baseline wander is usually below 0.5 Hz. It is often removed by linear phase high-pass filtering to prevent signal distortion [12].

Motion artefact may be caused by poor contact to the fingertip PPG sensor, as well as vibrations or subject's movement. One way to limit its impact is to ensure a fixed position of the arm during signal recording and to limit the duration of measurements to a few seconds [9].

Finally, the PPG waveform can be subject to sudden amplitude changes due to the automatic gain controller (AGC), which is automatically adjusted to the input signal amplitude. It may induce amplitude saturation at a maximum value, or at a minimum value. This problem is device dependent and is often already accounted for. In this study, the used device had no AGC.

2.2 Pulse waveform analysis

2.2.1 PPG pulse waveform

The PPG pulse waveform is divided into two phases. The anacrotic phase corresponds to the rising edge of the pulse and is primarily concerned with systole. The catacrotic phase, which is the falling edge, is concerned with diastole and wave reflections. During this second phase, a diastolic notch is usually seen in subjects with healthy compliant arteries. As can be seen in Figure 2.1, the PPG pulse waveform is very simple but it is sometimes difficult to detect changes in the phase of inflections. Therefore, most methods for pulse wave analysis require first, second or higher derivatives to be calculated. The use of derivatives facilitates the interpretation of original PPG waves and enables a more accurate recognition of inflection points.

2.2.2 Features and applications

Many features based on the PPG pulse waveform and its derivatives have been described in literature. First of all, the systolic amplitude, denoted as x , is an indicator of the pulsatile changes in blood volume caused by arterial blood flow around the measurement site. This point is easily recognizable since it corresponds to the maximum amplitude of the pulse, as shown on Figure 2.1.

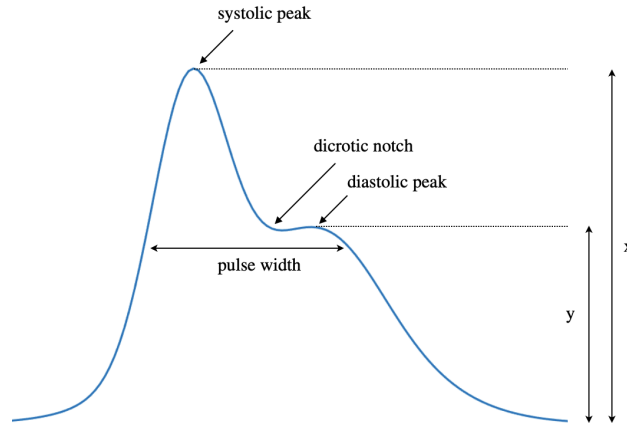


Figure 2.1: PPG pulse waveform, adapted from [9].

More difficult to detect is the diastolic point, requiring the first derivative of PPG waveform (FDPPG) to be calculated. It is defined as the point at which the first derivative is closest to zero, as shown on Figure 2.2b. The diastolic amplitude is denoted as y . Based on these two features,

an Augmentation Index (AI) is defined and corresponds to the relative loss in amplitude between the systolic and diastolic points as expressed by equation 2.1 [13].

$$AI = \frac{x - y}{x} \quad (2.1)$$

It is a measure of the contribution of wave reflection to systolic arterial pressure. In fact, reduced compliance of the elastic arteries causes an earlier return of the reflected wave and a disproportionate rise in systolic pressure, with a consequent decrease in diastolic blood pressure.

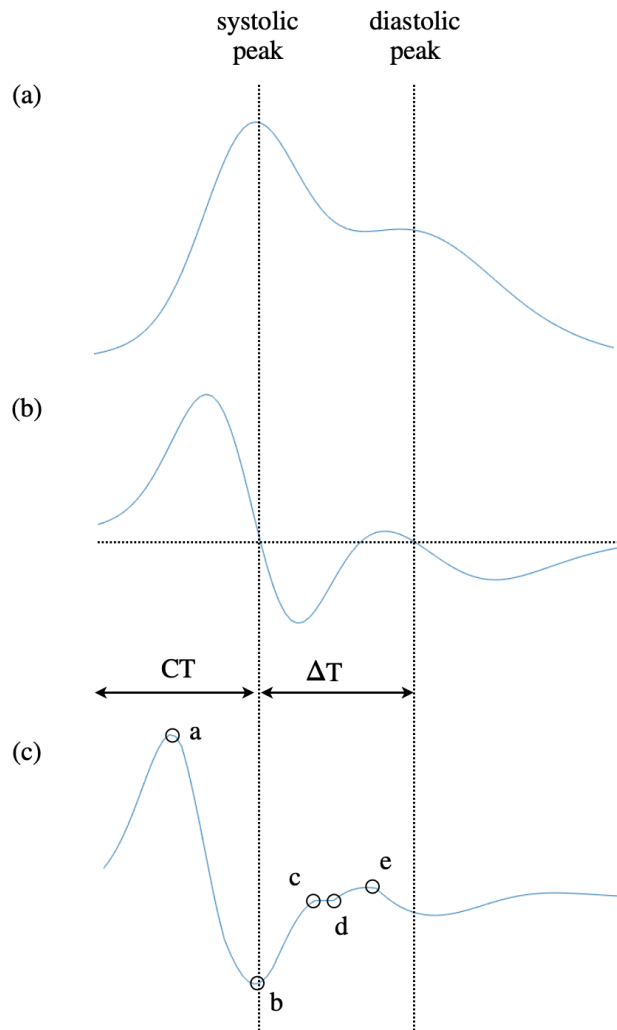


Figure 2.2: Signal measurements, adapted from [9].
 (a) PPG pulse waveform, (b) first derivative, (c) second derivative.

The ΔT interval is the time between the systolic and diastolic points. When the second peak is not easy to distinguish, the time interval is defined

as the time between the peak of the waveform and the inflection point of the falling edge which is a local maximum of the first derivative [9]. From this feature, the Large Artery Stiffness Index (SI) was defined as expressed by equation 2.2, with h is the subject height [14].

$$\text{SI} = \frac{h}{\Delta T} \quad (2.2)$$

The time delay between the systolic and diastolic peaks decreases with increasing artery stiffness and pulse wave velocity in large arteries, which makes the SI an useful indicator for artery compliance evaluation.

The pulse width is defined as the width at half height of the systolic peak. Some studies suggested that this feature correlates with the systemic vascular resistance [9]. Also, the crest time (CT) defined as the time interval from the the foot of the PPG waveform to the systolic peak, was proven useful for cardiovascular disease classification [9].

Finally, the second derivative of PPG waveform (SDPPF) is more commonly used than the first derivative. Its waveform includes four systolic waves, named a , b , c and d , and one diastolic wave, named e , as shown on Figure 2.2c. This latter one corresponds to the dicrotic notch. The height of each wave is measured from the baseline, with the values above the baseline being positive and those under it negative. The ratios of each wave height to that of a provide valuable information for arterial stiffness evaluation. For instance, it was proven that the b/a ratio reflects increased arterial stiffness, whereas c/a , d/a and e/a ratios correspond to decreased arterial stiffness. Based on these results, an Ageing Index (AGI) was defined as expressed by equation 2.3 [15].

$$\text{AGI} = \frac{b - c - d - e}{a} \quad (2.3)$$

2.2.3 Pulse decomposition analysis

Traditional methods based on PPG derivatives have proven efficient for arterial stiffness evaluation. However, they are limited to cases when the signal is not too weak, noisy, or when the diastolic part of the pulse is not damped out [13]. As an alternative, PPG pulse waveforms were recently modelled by curve fitting with Gaussian functions. Making no physiological assumptions, it constitutes a simple and accurate manner for reproducing and analyzing original waveforms.

Several methods were proposed. One approach would be to first separate the diastolic and systolic parts of the pulse waveform and then fit each

of them with the sum of two Gaussian functions [13], as shown on Figure 2.3.a. In a similar way, the entire pulse waveform can also be decomposed using the sum of up to three Gaussians [16], as illustrated on Figure 2.3.b. In both cases, the best combination of Gaussian functions is obtained by minimizing the mean absolute error with the original waveform. In [17], another method is developed, where this time three Gaussian-inspired inner waves are sequentially defined and subtracted to the original waveform. Each function is obtained by fitting the residual signal. This method is presented on Figure 2.3.c.

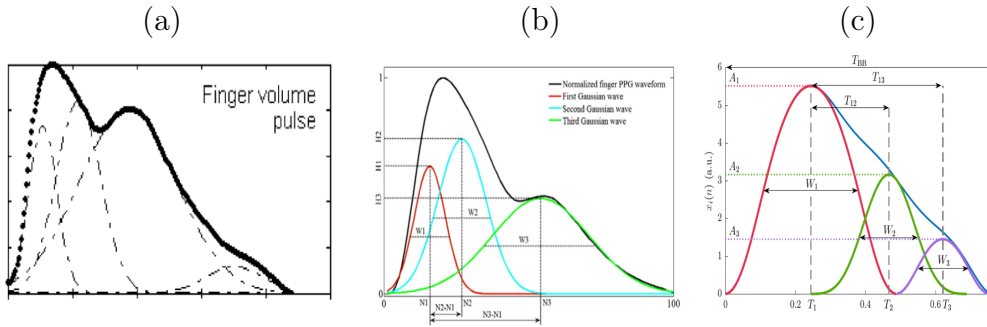


Figure 2.3: Pulse waveform decomposition using Gaussian curve fitting. (a) taken from [13], (b) taken from [16], (c) taken from [17].

Using such methods, features are directly extracted from the Gaussian curves, instead of the original signal. In most cases, the position in time, width and amplitude of each Gaussian function are considered relevant morphological characteristics. Studies demonstrated that they were highly related to cardiac hemodynamic parameters, including arterial elasticity and vascular aging, and correlated with those obtained with the derivative method [13]. Also they were proven useful for many applications, such as identifying waveform changes during exercise and recovery [18] or for assessing autonomic reactivity in depression [17].

2.3 Heart rate variability

By now, heart rate variability (HRV) is one of the most widely used technique for evaluation of autonomic nervous system and cardiovascular function. Indeed, it allows for non-invasive investigations using basic signal processing techniques.

2.3.1 Acquisition of NN-intervals

An electrocardiogram (ECG) describes the different electrical phases of a cardiac cycle, recorded by electrodes placed on the body surface. Each cycle is composed of two phases, which are referred to as depolarization and repolarization. Initialization of the cycle occurs in the sinoatrial node, the natural pacemaker determining the heart rate. On the ECG signal, several waves can be defined, as illustrated on Figure 2.4. The first one, named P wave, reflects atrial fibrillation. The QRS complex then relates to ventricular depolarization. Finally, the T wave corresponds to ventricular repolarization [12]. ECG recording constitutes the starting point for HRV analysis.

The analysis of HRV is based on the series of occurrence times, originally produced by the QRS detector. Traditionally, the onset of the P wave is considered the most appropriate fiducial point of the heartbeat, since it directly relates to sinoatrial activity. Its position is nevertheless difficult to define accurately, because the P wave has a very low amplitude, as shown on Figure 2.4. Given that the R wave has the largest amplitude, it is easier to define with precision. In addition, the PR interval is relatively fixed. For these two reasons, the use of the R wave as fiducial point has now been generally accepted.

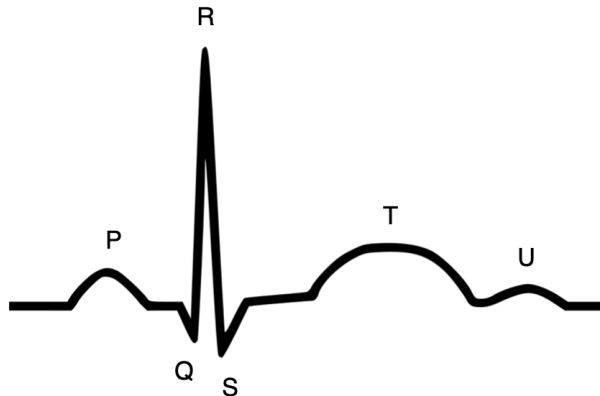


Figure 2.4: QRS complex.

Once the interval series is defined, an important step consists in the

exclusion of irregular intervals, for instance due to the presence of ectopic beats. This is necessary in order to make HRV analysis more reliable. A simple approach would be to apply an exclusion criterion, for example to consider an interval abnormal if it deviates more than a certain percentage from the mean length of the preceding intervals. The resulting series is commonly referred to as the normal-to-normal (NN) interval series [12].

2.3.2 Time domain measures

Several techniques have been developed for characterizing HRV. Among them, simple time domain methods are the most-widely used, since they are less sensitive to the presence of artefacts than measures derived from the power spectrum. Such methods take the NN interval series as starting point.

Statistical measures are first described. A common approach to quantify HRV involves calculating the standard deviation of the available NN intervals, denoted as SDNN and expressed by equation 2.4:

$$\text{SDNN} = \sqrt{\frac{1}{M-1} \sum_{k=1}^M (r_k - \bar{T})^2} \quad (2.4)$$

where r_k notes the k^{th} NN interval and \bar{T} the mean length of all intervals [12]. In a similar way, the standard deviation of the averages of NN intervals in all 5-min segments of the entire recording, abbreviated to SDANN, is used [12]. Also, the mean of the standard deviations of all NN intervals for all 5-min segments of the entire recording constitutes a statistical measure, named SDNN index [19].

Complementary measures have also been developed through analysis of the difference between successive NN intervals. As an example, the standard deviation of adjacent NN interval differences is a frequently used dispersion measure, named SDSD [19]. The square root of the mean of the sum of the squares of differences between adjacent NN intervals is another well-known HRV measure, commonly denoted as rMSSD [12]. Also, the percentage of intervals differing more than a certain limit value from the preceding interval constitutes another relevant measure. The threshold value being often set to 50 ms, the measure is usually referred to as pNN50 [12].

Other time domain measures based on geometrical properties of the series histogram have proven useful. For instance, the histogram can be well-characterized by fitting a simple triangle shape to its dominant peak.

In this manner, the width of the triangle base provides a relevant measure of heart rate variability. This measure is referred to as the triangular interpolation index (TINN) [12]. Moreover, the HRV triangular index, that is defined as the total number of all NN intervals divided by the height of the histogram measured on a discrete scale, has been widely used for HRV analysis [19].

2.3.3 Frequency domain measures

Frequency domain measures have been defined to provide further information. Spontaneous variability in heart rate exhibits indeed an oscillatory behavior, influenced by breathing, temperature regulation or blood pressure. It can be characterized by quantifying the power of spectral components. However, specific oscillations can sometimes be poorly pronounced and difficult to detect on a spectrum.

An alternative consists in instead quantifying the power of low and high frequencies in two specific intervals, 0.04-0.15 Hz and 0.15-0.4 Hz [19]. The spectral power measured in these two intervals is of primary interest because it relates closely to autonomic balance. Indeed, low frequency power (LF) directly relates to sympathetic activity, while high frequency power (HF) is connected to parasympathetic activity. Finally, the ratio of these two spectral power measures (LF/HF) is used as an indicator of the state of the autonomic balance [12].

2.4 Pulse rate variability

Recent studies have shown that pulse rate variability (PRV) is a relevant surrogate of HRV. This is for instance useful in applications where electrocardiogram is not available or of poor quality, due to electrical artefacts [10].

2.4.1 Pulse rate variability analysis

The analysis of PRV is based on the series of occurrence times, produced by the PPG pulse detector. The systolic peak is considered an appropriate fiducial point since it has the highest amplitude in the PPG pulse waveform. The corresponding series is named peak-to-peak interval series, as shown on Figure 2.5. As an alternative, the pulse onset point, also named basal point, could be chosen as fiducial point. In this case, the output corresponds to the series of pulse-to-pulse intervals.

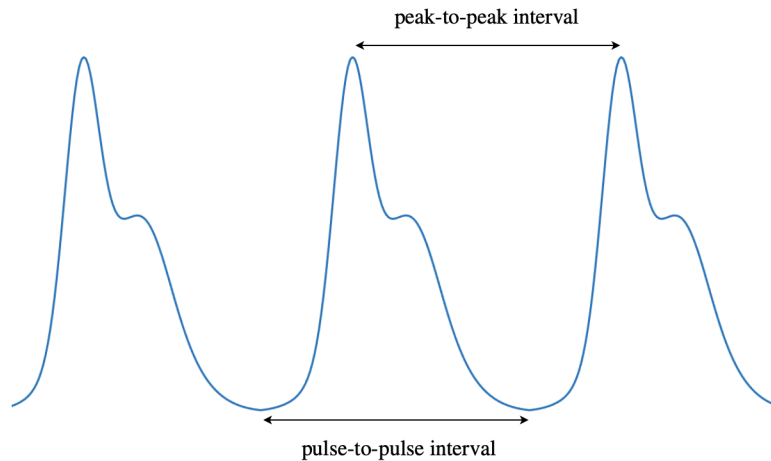


Figure 2.5: PPG pulse intervals, adapted from [9].

Once the series of intervals is defined, non-normal intervals are excluded in the same way as for HRV analysis. Finally, PRV measures are the same as those that have been applied for HRV.

2.4.2 Pulse transit time

The main difference between HRV and PRV is the variability of the time that the pulse wave takes to travel from the heart to the finger. This time delay is usually called pulse arrival time (PAT). In practice, it is measured as the difference between the position of the peak of the R-wave on the ECG and the onset of the corresponding pulse on the PPG signal [20].

PAT can be decomposed into two sub-intervals: the pulse transit time (PTT) and the pre-ejection period (PEP), as shown on Figure 2.6. Accurate measurement of PTT requires proper recording of proximal PPG waveforms in the first instance, for example using impedance cardiography (ICG). Therefore, PEP is often neglected and PAT and PTT are considered almost equivalent.

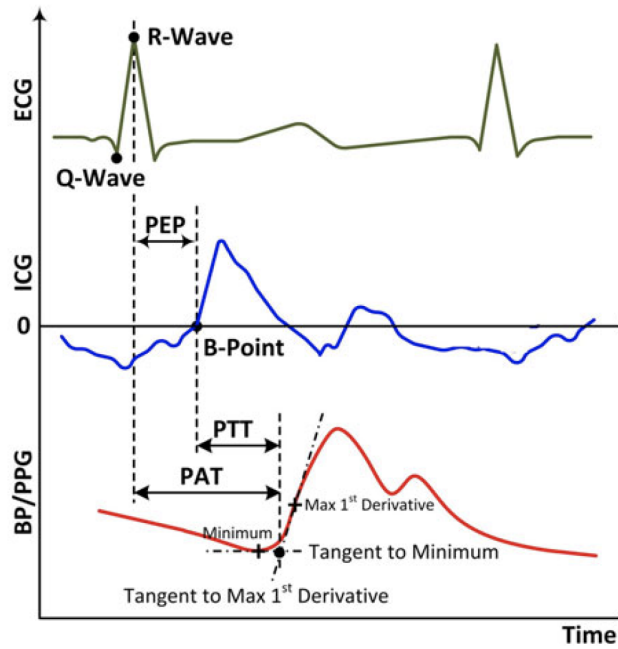


Figure 2.6: Pulse Transit Time, taken from [20].

PTT is highly related to arterial compliance and varies beat to beat. To study short and long-term PTT variability, the time domain measures defined below can also be applied to PTT series.

Chapter 3

Methodology

This chapter explains the overall methods and terminology used throughout the project. All steps from experimental protocol to pulse detection are first described. Analysis of PPG pulse morphology is performed by pulse decomposition analysis. Methods for HRV analysis and PTT computation are presented in the last section.

3.1 Experimental protocol and data acquisition

A database of 19 healthy volunteers was recorded at the Division of Ergonomics and Aerosol Technology of Lund University. The test group is composed of nine female subjects and ten male subjects from 20 to 55 years old.

The experimental protocol consists of four chamber studies of three hours each, with a starting time between 09:00 am and 10:00 am. During session \mathcal{A} , the subjects are exposed to filtered air ($\text{PM} \simeq 1 \mu\text{g}/\text{m}^3$) and during \mathcal{B} to air enriched with NaCl salt particles. This second stage is supposed to mimic exposure to sea breeze. During sessions \mathcal{C} and \mathcal{D} , the participants are exposed to, respectively, exhaust from a wheel loader operated with HVO without exhaust after-treatment ($\text{PM} \simeq 90 \mu\text{g}/\text{m}^3$, $\text{EC} = 54 \mu\text{g}/\text{m}^3$, $\text{NO} = 3.4 \text{ ppm}$, $\text{NO}_2 = 0.6 \text{ ppm}$) and exhaust from a wheel loader operated with HVO with after-treatment ($\text{PM} \simeq 1 \mu\text{g}/\text{m}^3$, $\text{NO} = 2.0 \text{ ppm}$, $\text{NO}_2 = 0.7 \text{ ppm}$). The chosen concentrations of exhaust gases correspond to absolute maximum levels people could be exposed to in everyday life in Sweden. All patients complete one chamber study per day maximum, in a randomized order. The concentrations are monitored with battery of real time measuring instruments and off-line collection techniques. Cham-

ber studies are carried out in a controlled and ethically approved manner. Among the 19 test persons, one participant only attended two sessions, corresponding to exposures \mathcal{B} and \mathcal{D} .

PPG and ECG measurements are performed with the Cardio Holter system [21]. During the whole experimental protocol, three-lead ECG signal is continuously recorded at a sampling frequency of 1 kHz. Fingertip PPG signal is recorded at a sampling frequency of 250 Hz at wavelengths of 635 nm (RED) and 960 nm (IR). Recordings is performed only during four 15-minute sessions, at basal condition and after one, two and three hours into exposure. It was not recorded continuously for practical reasons: PPG measurement requires to stay as still as possible, which is difficult to set up during three-hour sessions.

3.2 Data pre-processing

3.2.1 Baseline wander removal

PPG signals are first filtered using a 2nd order high-pass Butterworth filter, with cut-off frequency of 0.5 Hz, for the purpose of baseline removal. Forward-backward filtering is applied for preserving signal morphology. Filtered PPG signal segments constitute the basis of this thesis.

3.2.2 Motion artefact detection

Due to high sensitivity of PPG data acquisition to motion artefacts, an artefact detector is implemented. Intervals of the PPG signal containing artefacts are removed using the energy-related approach proposed in [22]. This method is based on the assumption that motion artefacts are characterized by higher energy than clean PPG signal segments, as shown on Figure 3.1.

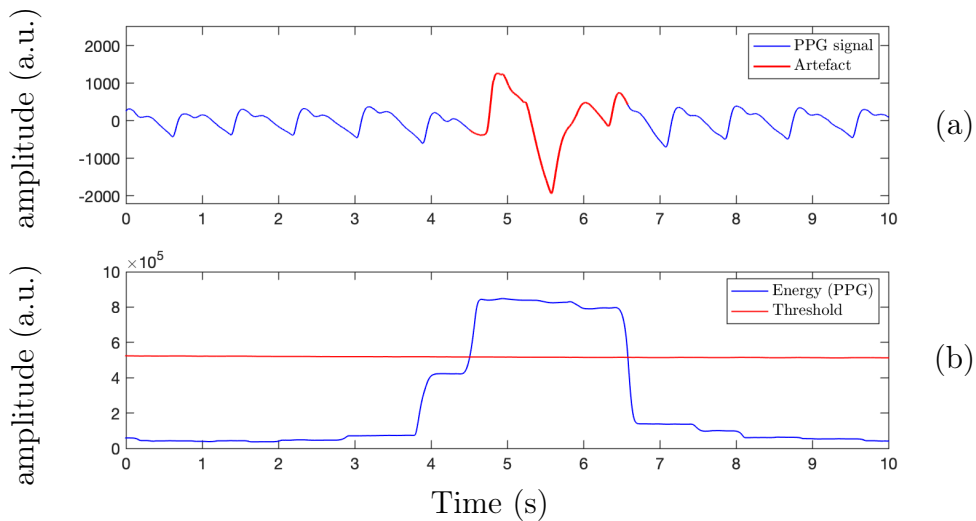


Figure 3.1: Artefact Detection based on the energy of the signal. (a) PPG signal where artefacts were defined, (b) decision criterion.

Procedure requires multiple steps. Firstly, the signal is squared to emphasize the segments with high energy. Secondly, the moving variance, $s(n)$, of the squared signal is computed over a 2-second window, while the moving median, $m(n)$, is calculated over a 100-second window. Lastly, if the decision criterion, $s(n) > 4 \times m(n)$, is fulfilled, the sample n is considered as artefact, since a large deviation of the moving median value is detected. In addition, PPG pulses immediately preceding and following detected artefacts are excluded from further analysis.

3.2.3 Low-pass filtering

To conclude the pre-processing part, PPG signal segments are subjected to low-pass filtering for attenuating high frequency noise. Forward-backward filtering is performed using a 4th order IIR low-pass filter, with cut-off frequency of 10 Hz. It should be noted that the zero-phase transfer function of the whole filtering step prevents phase distortion of the signal.

3.3 Pulse detection

Pulse detection is carried out using the Mountaineer’s Method for Peak Detection (MMPD) [23]. This method is based on the similarities between a mountain range and a PPG pulse waveform. Each systolic maximum is seen as the top of a mountain. In this way, it is reached when the slope changes from positive to negative. Assuming that the rising edge preceding the systolic maximum is a strictly increasing function, denoted as f , every point on the rising edge satisfies the condition 3.1.

$$f(t_{i+1}) > f(t_i) \text{ if } t_{i+1} > t_i \quad (3.1)$$

We count the number of consecutive samples that satisfy the condition 3.1, denoted as n_{steps} . If this number reaches or exceeds a certain threshold value, denoted as T_r , a systolic peak is detected. Every time the slope changes from positive to negative, n_{steps} is reset to zero, whether or not the threshold has been reached. The crest time (CT) corresponds to the time interval from the pulse onset to the systolic maximum. It was estimated around 0.2 seconds. Then, PPG signals were recorded at a sampling frequency of 250 Hz. The systolic rising edge should thus be composed of $N = 250 \times 0.2 = 50$ samples in average. The threshold T_r initializes to $0.6 \times N$ and updates its value with every detected pulse as expressed by equation 3.2:

$$T_r = 0.6 \times N_{\text{average}} \quad (3.2)$$

with N_{average} the mean of the total number of samples composing the rising edge of the ten last detected systolic peaks. Finally, setting the detection at 60% of the number of samples N enables the algorithm to detect peaks even in the event of heart rate variations.

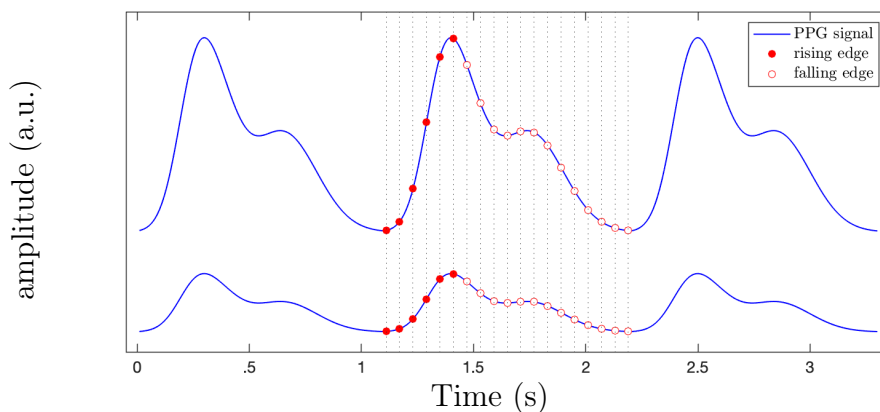


Figure 3.2: PPG pulses of different amplitudes. Regardless of the pulse amplitude, the number of points composing the rising edge remains constant.

The threshold is proportional to the number of samples composing the rising edge. Hence, it depends directly on the sampling frequency, but not on the amplitude of the PPG signal at all, as illustrated on Figure 3.2. This method can easily be applied to PPG signal segments with low or varying amplitude.

Once PPG pulses have been detected, a fiducial point corresponding to the maximum up-slope of the rising edge is defined for each pulse. It is denoted as $n_F(i)$ for the i :th PPG pulse. A percentage relative to the maximum up-slope value of the first-derivative of x_{PPG} (x'_{PPG}) is then used to define the basal point, denoted as $n_B(i)$. As implemented in [17], the point $n_B(i)$ is searched in the interval $\Omega = [n_F(i) - 0.3F_s, n_F(i)]$ and defined by equation 3.3:

$$n_B(i) = \arg \min_{n \in \Omega} \{|x'_{\text{PPG}}(n) - 0.05 \times x'_{\text{PPG}}(n_F(i))|\} \quad (3.3)$$

where $x'_{\text{PPG}}(n) = x_{\text{PPG}}(n) - x_{\text{PPG}}(n-1)$. Characteristic points defined on PPG pulses are illustrated on Figure 3.3. Finally, linear interpolation of $x_{\text{PPG}}(n_B(i))$ is subtracted from the original PPG pulse segment, so that each pulse $x_i(n)$ begins and ends with zero amplitude.

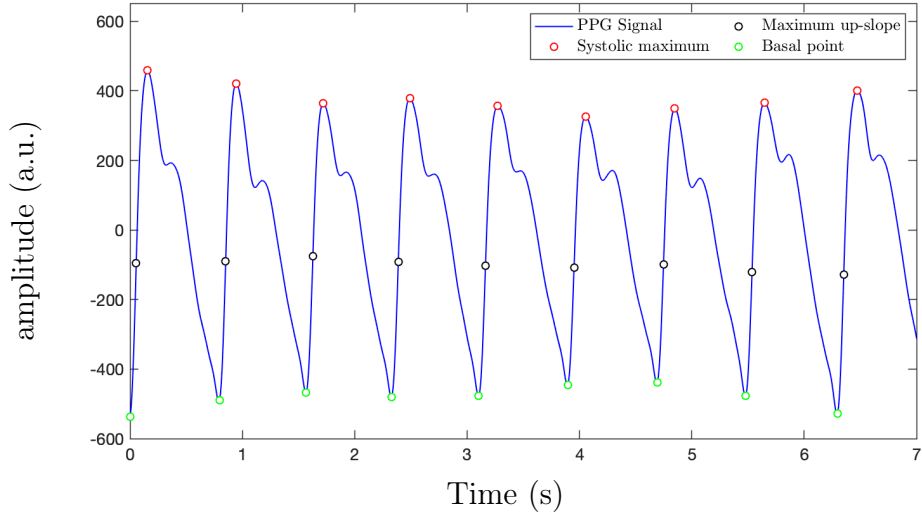


Figure 3.3: Characteristic points defined on PPG pulses.

3.4 Pulse waveform analysis

3.4.1 Pulse decomposition analysis

Pulse decomposition analysis is performed using an approach similar to that proposed by Kontaxis et al. [17]. Each detected pulse, $x_i(n)$, is decomposed into J symmetrical waves $x_{i,1}(n), \dots, x_{i,J}(n)$ and a residual signal. In this study, J is set to 5.

Inner wave computation is performed in the following steps. First, the up-slope interval of the running residual $\tilde{x}_{i,j}(n)$ is defined, with its onset denoted as n_{O_j} and its end as n_{E_j} . The inner wave is obtained by concatenating the up-slope of the residual with itself horizontally flipped as expressed by equation 3.4.

$$x_{i,j}(n) = \begin{cases} \tilde{x}_{i,j}(n), & n \in [n_{O_j}, n_{E_j}] \\ \tilde{x}_{i,j}(-n + 2n_{E_j}), & n \in [n_{E_j}, 2n_{E_j} - n_{O_j}] \\ 0, & \text{otherwise.} \end{cases} \quad (3.4)$$

The j :th inner wave is then subtracted from the running residual, i.e. $\tilde{x}_{i,j+1}(n) = \tilde{x}_{i,j}(n) - x_{i,j}(n)$ and the following inner waves are computed recursively. An example of pulse decomposition is shown on Figure 3.4. For each inner wave, the up-slope is marked with solid line and the horizontally flipped up-slope with dashed line.

To prevent erroneous definition of inner waves, a fixed amplitude threshold is used. An inner wave is considered to exist only if the absolute maximum value of the running residual $\tilde{x}_{i,j}(n)$ exceeds $A_P = 0.05 \times \max\{x_i(n)\}$. Furthermore, slope changes prior to the first relative maximum can lead to incorrect inner wave definition. To prevent this second type of error, decomposition is completed by taking into account the first derivative of the PPG pulse residual, $\tilde{x}'_{i,j}$, as illustrated on Figure 3.4. The up-slope onset is defined as the first sample after the last negative-amplitude sample of $\tilde{x}'_{i,j}$. The up-slope end is then redefined as the position of the first relative minimum of $\tilde{x}'_{i,j}$, for which $\tilde{x}_{i,j}(n_{E_j}) > A_P$ is fulfilled.

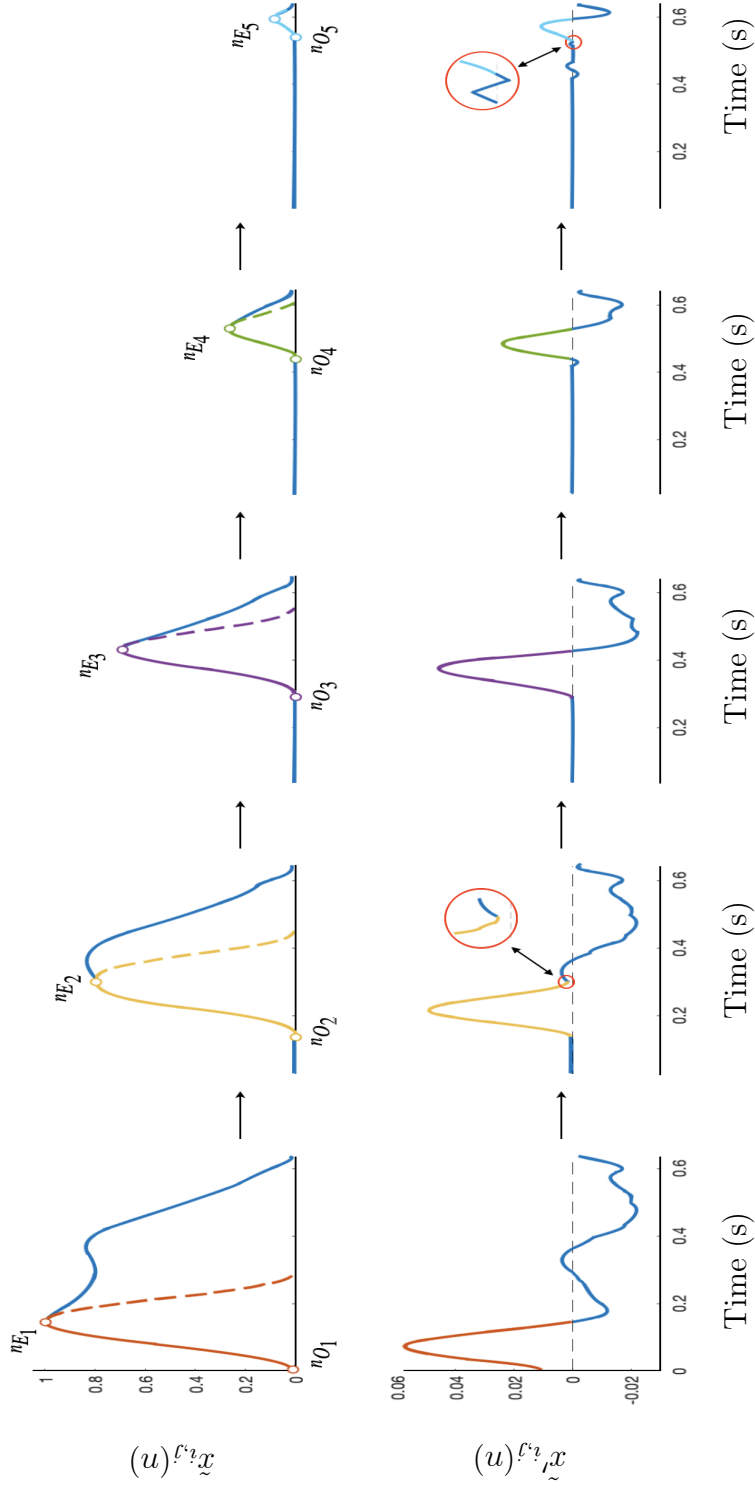


Figure 3.4: Pulse decomposition algorithm, adapted from [17].
Recursive computation of inner waves, by taking into account the first derivative of the running residual.

3.4.2 Features extraction

Morphological features are extracted from PPG pulses by pulse decomposition analysis. For every inner wave, the amplitude $A_j(i)$ is defined as the amplitude of the absolute maximum of $x_{i,j}(n)$. Similarly, the position $T_j(i)$ is defined as the position of the absolute maximum of $x_{i,j}(n)$. The width of $x_{i,j}(n)$ is finally estimated by the width at half-maximum and denoted as $W_j(i)$. Those features are illustrated on Figure 3.5.

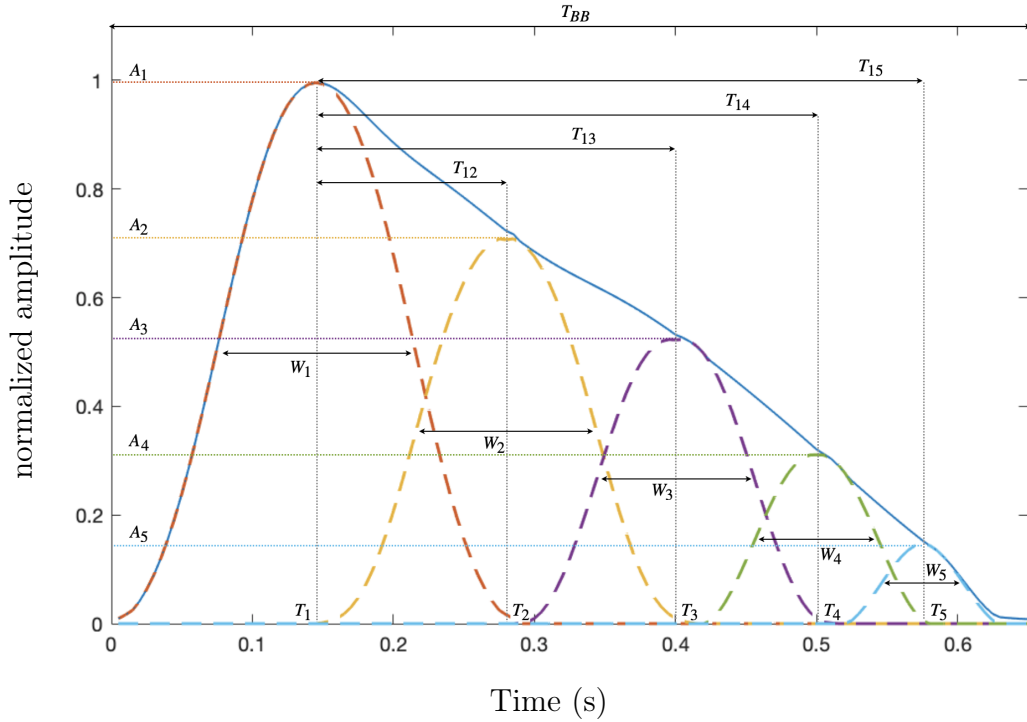


Figure 3.5: Pulse waveform characteristics, adapted from [17].

From those features, the time delay between the main wave and every reflected wave is computed as expressed by equation 3.5.

$$T_{1j} = T_j - T_1 \text{ for } j \in [2, 5] \quad (3.5)$$

The percentage of amplitude loss in each reflection is calculated as expressed by equation 3.6. The position and width of the main wave are also analyzed.

$$A_{1j} = \frac{A_1 - A_j}{A_1} \times 100 \text{ for } j \in [2, 5] \quad (3.6)$$

Finally, the pulse-to-pulse interval length $T_{BB}(i)$ is computed using the defined basal points $n_B(i)$ as expressed by equation 3.7.

$$T_{BB}(i) = \frac{n_B(i+1) - n_B(i)}{F_s} \quad (3.7)$$

In this work, pulses are considered distorted if one of the following criteria is fulfilled:

- the pulse is decomposed into less than five waves ;
- the amplitude of the main wave is not the largest of the five waves ;
- the second wave is located at the end of the pulse interval, i.e. $T_2 > 0.8T_{\text{BB}}$.
- the fifth wave is located at the beginning of the pulse interval, i.e. $T_5 < 0.4T_{\text{BB}}$.

All distorted pulses are excluded from further analysis. In addition to that, outlier rejection is completed using an exclusion criterion based on median absolute deviation (MAD). For each feature, the running median of the 50 most recent features, denoted as $m(n)$, is computed, as well as the running median absolute deviation, $\text{MAD}(n)$. If the following decision criterion is fulfilled: $|f_n - m(n)| > 5 \times \text{MAD}(n)$, with f_n the feature value of the current pulse, the pulse is excluded.

3.4.3 Statistical analysis

Median values of all pulse waveform characteristics ($T_1, T_{12}, T_{13}, T_{14}, T_{15}, W_1, A_{12}, A_{13}, A_{14}, A_{15}$) are calculated for every subject, separately for each exposure type ($\mathcal{A}, \mathcal{B}, \mathcal{C}$ and \mathcal{D}) and time into exposure (pre-exposure and after 1, 2 and 3 hours). In this study, only the last five minutes of each 15 minute session of PPG recording are taken into account.

Assessment of feature variations over exposure time: For each exposure type ($\mathcal{A}, \mathcal{B}, \mathcal{C}$ and \mathcal{D}) separately, a non-parametric Friedman test is conducted for evaluating individual differences in features over time. A multiple comparison test (post-hoc analysis) with Bonferroni correction is performed, using the Wilcoxon signed rank test, to assess the significance of feature variations over time and determine which data come from a different distribution. The significance threshold is set to $p < 0.05$.

Assessment of feature variations with exposure type: For every feature \mathcal{F} , we are interested in changes in its value at a given time point ($t = 1\text{h}, 2\text{h}$ or 3h) after exposure onset, denoted as \mathcal{F}^t , relative to the same parameter pre-exposure, \mathcal{F}^0 . Relative changes are computed as expressed by equation 3.8.

$$\Delta(\mathcal{F})^t = \frac{\mathcal{F}^t - \mathcal{F}^0}{\mathcal{F}^0} \times 100 \quad (3.8)$$

A non-parametric Friedman test is also conducted for evaluating individual differences in feature relative variations between the stages of the experimental protocol (\mathcal{A} , \mathcal{B} , \mathcal{C} and \mathcal{D}). A multiple comparison test (post-hoc analysis) with Bonferroni correction is performed, using the Wilcoxon signed rank, to determine which exposure type induces statistical changes in morphological characteristics over time. The significance threshold is set to $p < 0.05$.

3.5 PTT and HRV analysis

3.5.1 Acquisition of beat detection times

Beats from ECG signal recordings are detected to generate heart rate time series. The temporal location of each R wave in the ECG, t_{E_j} , was provided by the Division of Biomedical Engineering of Lund University. Following detection of R peaks in the ECG signals, beats are clustered and ectopic beats are identified based on heartbeat morphology [24]. RR intervals preceding and following ectopic beats are excluded from the RR series. In addition, RR intervals deviating more than 20% from the mean length of the 50 preceding intervals are considered abnormal and excluded from further analysis.

The PPG signal recordings are interpolated using cubic splines to increase the resolution in time up to 1kHz and match the temporal resolution of both signals. Then, the temporal location of each pulse wave, t_{P_j} , is detected as the pulse onset within the interval $[t_{E_j}, t_{E_{j+1}}]$, as implemented above (*see 3.3 Pulse Detection*).

3.5.2 Heart rate variability analysis

From the beat detection times of ECG signals, the inverse interval function is computed as expressed by 3.9.

$$d_{\text{IIF}}(t_{E_j}) = \frac{1}{t_{E_j} - t_{E_{j-1}}} \quad (3.9)$$

By using a cubic spline interpolation at 4 Hz, we obtain the heart rate signal, $d_{\text{HR}}(t)$. For the purpose of baseline wander removal, the mean heart rate is estimated by low-pass filtering the heart rate series with a cut-off frequency of 0.03 Hz. The HRV signal, $d_{\text{HRV}}(t)$, is finally computed by subtracting the time-varying mean heart rate from $d_{\text{HR}}(t)$. Since the filtering step may introduce artifacts at the beginning and at the end of the computed $d_{\text{HR}}(t)$ signal, the first and last five seconds are not taken into account in the final analysis. The computational steps are illustrated on Figure 3.6.

Following time domain indices are estimated from RR interval series: the mean normal to normal interval (NN), the standard deviation of NN intervals (SDNN), the root mean square of successive differences of adjacent NN intervals (rMSSD), the standard deviation of adjacent NN interval differences (SDSD) and the percentage of pairs of adjacent NN intervals differing by more than 50 ms (pNN50).

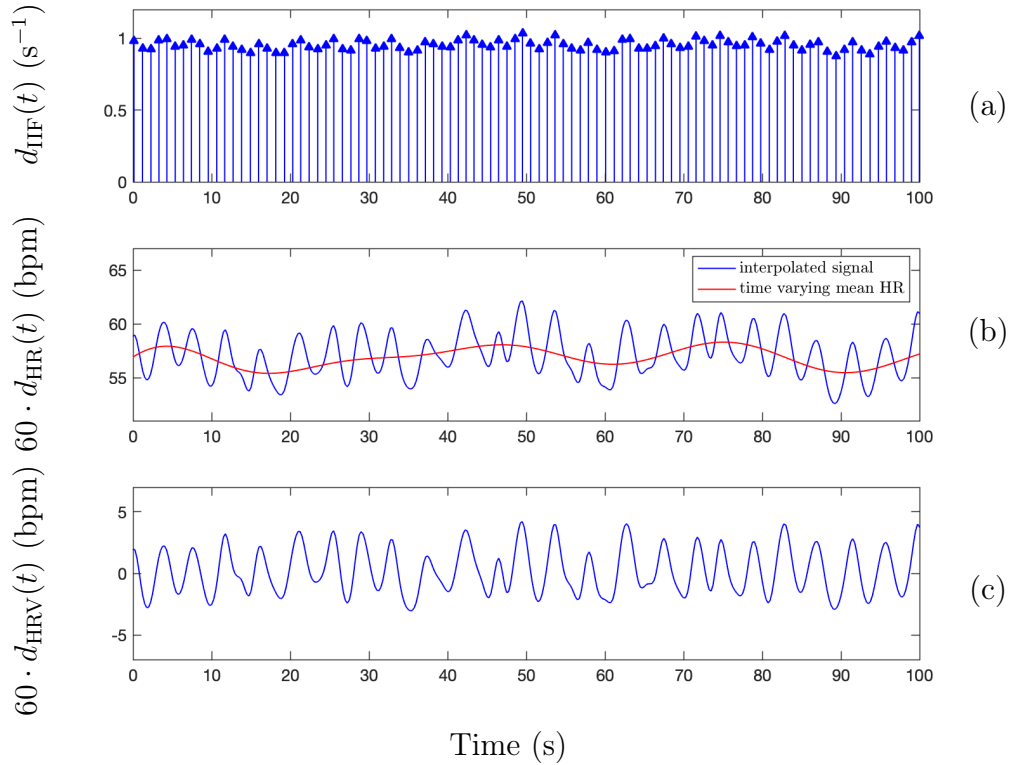


Figure 3.6: Computational steps to obtain the HRV signal. (a) inverse interval function, (b) interpolated inverse interval function and time varying mean heart rate, (c) HRV signal.

Frequency domain parameters are also measured based on HRV signals. The fast Fourier transform algorithm with a frequency resolution of 0.0020 Hz is applied to $d_{\text{HRV}}(t)$. The power in the low-frequency band 0.04-0.15 Hz (LF) and in the high frequency band 0.15-0.4 Hz (HF) are estimated, as well as the LF to HF ratio (LF/HF).

3.5.3 Pulse transit time analysis

From the beat detection times of both ECG and PPG, respectively denoted as t_{E_j} and t_{P_j} , the pulse transit time interval series is computed as expressed by 3.10 and illustrated on Figure 3.7.

$$d_{\text{PTT}}(j) = t_{P_j} - t_{E_j} \quad (3.10)$$

Outlier rejection is performed by applying an exclusion criterion, i.e. PTT intervals deviating more than 30% from the mean length of the 50 preceding intervals are considered abnormal. Classical time domain features are finally measured as in the previous section. The mean value of

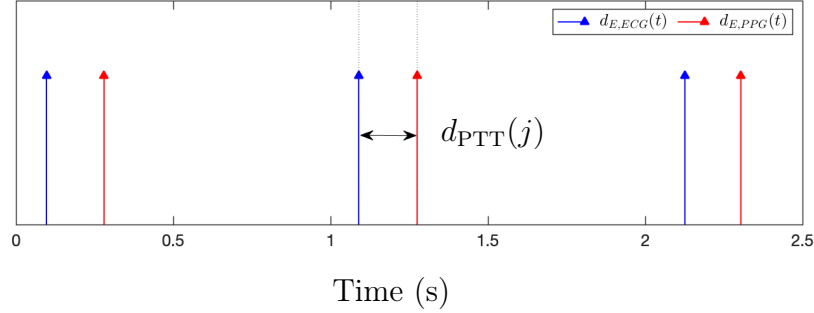


Figure 3.7: Event series representation from ECG and PPG recordings. in blue: event series from ECG which displays the beat occurrence times, in red: event series from PPG which displays the pulse occurrence times.

PTT interval (PTT), the standard deviation of PTT intervals (SDPTT), the root mean square of successive differences of adjacent PTT intervals ($\text{rMSSD}^{\text{PTT}}$) and the standard deviation of adjacent PTT interval differences (SDSD^{PTT}) are computed.

3.5.4 Statistical analysis

All HRV and PTT features described in the two previous subsections are calculated for every subject, separately for each exposure type (\mathcal{A} , \mathcal{B} , \mathcal{C} and \mathcal{D}) and time into exposure. In the same manner as above, only the last five minutes of each session of PPG recording are taken into account.

Assessment of feature variations over exposure time: For each exposure type (\mathcal{A} , \mathcal{B} , \mathcal{C} and \mathcal{D}) separately, a non-parametric Friedman test is conducted for evaluating individual differences in features over time. A multiple comparison test (post-hoc analysis) with Bonferroni correction is performed, using the Wilcoxon signed rank test, to identify data coming from a different distribution. The significance threshold is set to $p < 0.05$.

Assessment of feature variations with exposure type: For every feature \mathcal{F} , changes relative to pre-exposure level are computed as expressed by equation 3.7. A non-parametric Friedman test is conducted for evaluating individual differences in feature relative changes between the stages of the experimental protocol (\mathcal{A} , \mathcal{B} , \mathcal{C} and \mathcal{D}). A multiple comparison test (post-hoc analysis) with Bonferroni correction is then performed, using the Wilcoxon signed rank test, to determine how HRV and PTT parameters differ with exposure type. The significance threshold is set to $p < 0.05$.

Analysis of correlation between PDA, HRV and PTT parameters:

Correlation (Person) analyses are carried out for testing bivariate associations between PDA-derived features and HRV and PTT parameters. A first study is completed, based on the results obtained at basal condition ($\mathcal{F}(t = 0\text{h})$). Then, the same methodology is applied to relative changes in all extracted features after three hours into exposure ($\Delta(\mathcal{F})^{3\text{h}}$), for each exposure type separately.

Chapter 4

Results

The present chapter will display the produced results, following mainly the same structure as the method chapter. The outcomes of the PDA phase come first. Subsequently, the results regarding HRV and PTT series are detailed.

4.1 Pulse waveform analysis

A total of 19 subjects completed the experimental protocol. One patient only attended sessions \mathcal{B} and \mathcal{D} . Two patients had missing 15-minute PPG recordings at two and three hours during session \mathcal{B} and two other subjects during session \mathcal{C} . One more recording corresponding to session \mathcal{C} at two hours was excluded from further analysis due to its poor quality.

For each exposure session, the percentage of discarded pulses (mean \pm std) is $8.2 \pm 13.7\%$ (\mathcal{A}), $8.1 \pm 12.1\%$ (\mathcal{B}), $7.1 \pm 12.5\%$ (\mathcal{C}) and $9.9 \pm 14.6\%$ (\mathcal{D}). These results suggest that few distorted pulses are present in PPG signal recordings in average, but the percentages are heterogeneous. Some segments actually present a proportion of discarded pulses superior to 15%. For instance, three recordings of 15-minute sessions are concerned by a higher number of excluded pulses for exposure \mathcal{A} , three for \mathcal{B} , two for \mathcal{C} and eleven for \mathcal{D} . However, these recordings are considered suitable for further analysis. Finally, the number of analyzed pulses (mean \pm std) for each exposure type is 235 ± 98 (\mathcal{A}), 244 ± 91 (\mathcal{B}), 228 ± 108 (\mathcal{C}) and 240 ± 86 (\mathcal{D}). It is considered sufficient for proper implementation of the pulse decomposition algorithm and statistical analysis of the results.

4.1.1 Changes in pulse waveform features over time

Friedman tests were performed to analyze the variations of morphological features over time, for each exposure type separately. The results indicate that all features, except T_{14} , present significant variations over time during exposure \mathcal{D} . A similar result is observed for exposure \mathcal{C} , except regarding features A_{12} and A_{13} , and for exposure \mathcal{B} , except regarding T_{15} and A_{15} . Regarding exposure \mathcal{A} , only features T_1 , T_{12} , T_{15} and W_1 exhibit statistical changes over time. Multi-comparison tests reveal which exposure duration in particular leads to statistical changes compared to basal condition, separately for every exposure type. Tables 4.1 to 4.4 illustrate the results of the multi-comparison paired tests. Median (Q_1 - Q_3) values of features for each exposure type and time are also summarized. The results which are statistically different from those estimated at basal condition are shown in bold. Functional boxplots of all features as functions of time are presented in Figure A.1 (*see Appendix A*).

Regarding temporal parameters related to the main wave, the results show that all exposure types are concerned by a decrease in T_1 and W_1 after one hour into exposure. Both features come back to baseline values after two hours. Moreover, the pulse transit time surrogate T_{12} is found to decrease after one hour in each case, as well as T_{13} except for \mathcal{A} . After three hours into exposure, this parameter reaches its baseline value for \mathcal{C} and \mathcal{D} , but continues to decrease slightly for \mathcal{B} . For exposure \mathcal{A} , parameter T_{15} decreases at three hours. The same feature decreases after one hour for exposure \mathcal{C} , while it is found to increase at one and two hours for \mathcal{D} . In both cases, a trend toward baseline values is observed after two hours into exposure. Vascular compliance related parameters also present statistical differences over time. Features A_{14} and A_{15} exhibit a decreasing behavior after one hour for \mathcal{B} , \mathcal{C} and \mathcal{D} , as well as after two hours for \mathcal{C} . After three hours into exposure, parameters A_{12} and A_{13} increase for all exposures, but significantly for \mathcal{B} and \mathcal{D} only. Finally, parameters A_{14} and A_{15} are found to increase as well after three hours for exposure \mathcal{C} .

4.1.2 Variability of pulse waveform features at basal condition

No statistical difference is found between results of all exposure types at basal condition across the subjects. However, a high variability of the pre-exposure data is observed for every subject and indicator individually, as illustrated on Figure A.2 (*see Appendix A*). To assess the actual impact of each exposure type on extracted features, it is thus necessary to compute relative changes in parameters compared to baseline values.

\mathcal{F}	Exposure type \mathcal{A}			
	baseline	$t = 1\text{h}$	$t = 2\text{h}$	$t = 3\text{h}$
T ₁ (ms)	154 (144 - 172)	144 (128 - 162) **	156 (144 - 168)	n.s.
T ₁₂ (ms)	156 (148 - 180)	152 (140 - 168) *	158 (142 - 170)	n.s.
T ₁₃ (ms)	308 (296 - 338)	312 (292 - 328)	316 (310 - 332)	n.s.
T ₁₄ (ms)	441 (428 - 474)	448 (428 - 464)	460 (448 - 472)	n.s.
T ₁₅ (ms)	556 (532 - 584)	552 (532 - 578)	569 (556 - 584)	n.s.
W ₁ (ms)	184 (160 - 208)	168 (148 - 208) **	184 (160 - 200)	n.s.
A ₁₂ (%)	12.6 (9.0 - 18.5)	15.9 (9.2 - 22.2)	14.9 (10.3 - 18.9)	n.s.
A ₁₃ (%)	17.8 (14.2 - 31.3)	24.7 (14.9 - 31.9)	19.7 (13.9 - 28.5)	n.s.
A ₁₄ (%)	37.1 (30.9 - 49.0)	36.0 (27.5 - 45.2)	34.7 (27.3 - 46.6)	n.s.
A ₁₅ (%)	54.3 (45.6 - 69.9)	52.4 (41.3 - 65.2)	49.8 (42.7 - 62.5)	n.s.

comparison between results at t and baseline: n.s. not significant, * $p < 0.05$, ** $p < 0.01$

Table 4.1: Median (Q_1 - Q_3) values of pulse waveform features and results of statistical tests for exposure type \mathcal{A} .

\mathcal{F}	Exposure type \mathcal{B}			
	baseline	$t = 1\text{h}$	$t = 2\text{h}$	$t = 3\text{h}$
T ₁ (ms)	156 (140 - 178)	144 (128 - 156) **	160 (144 - 176)	n.s.
T ₁₂ (ms)	156 (144 - 192)	143 (136 - 152) **	158 (136 - 172)	n.s.
T ₁₃ (ms)	312 (298 - 348)	300 (288 - 308) **	312 (296 - 330)	*
T ₁₄ (ms)	454 (430 - 480)	432 (412 - 448)	448 (426 - 472)	n.s.
T ₁₅ (ms)	552 (534 - 580)	540 (516 - 562)	551 (524 - 576)	n.s.
W ₁ (ms)	184 (160 - 228)	168 (144 - 184) **	192 (168 - 212)	n.s.
A ₁₂ (%)	13.1 (9.5 - 21.7)	16.5 (11.9 - 20.6)	16.5 (10.7 - 22.9)	**
A ₁₃ (%)	23.6 (12.9 - 36.2)	16.7 (13.4 - 25.8) **	22.8 (17.3 - 32.1)	n.s.
A ₁₄ (%)	43.7 (27.9 - 54.8)	36.8 (27.0 - 41.1) *	44.0 (29.3 - 51.3)	n.s.
A ₁₅ (%)	58.8 (43.7 - 72.6)	55.1 (41.3 - 59.2)	61.9 (46.3 - 70.1)	n.s.

comparison between results at t and baseline: n.s. not significant, * $p < 0.05$, ** $p < 0.01$

Table 4.2: Median (Q_1 - Q_3) values of pulse waveform features and results of statistical tests for exposure type \mathcal{B} .

\mathcal{F}	Exposure type \mathcal{C}							
	baseline		$t = 1\text{h}$		$t = 2\text{h}$		$t = 3\text{h}$	
	T_1 (ms)	150 (144 - 172)	144 (140 - 152)	**	151 (140 - 161)	n.s.	156 (140 - 172)	n.s.
T_{12} (ms)	156 (144 - 192)	144 (140 - 156)	**	152 (144 - 164)	n.s.	152 (140 - 184)	*	
T_{13} (ms)	316 (292 - 334)	294 (278 - 316)	**	304 (283 - 324)	n.s.	308 (284 - 330)	n.s.	
T_{14} (ms)	448 (416 - 474)	424 (407 - 454)	n.s.	438 (406 - 468)	n.s.	442 (410 - 466)	n.s.	
T_{15} (ms)	554 (524 - 588)	528 (508 - 560)	*	532 (508 - 592)	n.s.	534 (496 - 564)	*	
W_1 (ms)	176 (168 - 216)	176 (160 - 188)	**	176 (168 - 204)	n.s.	184 (168 - 220)	n.s.	
A_{12} (%)	14.2 (10.1 - 19.7)	13.9 (8.5 - 17.8)	n.s.	14.8 (11.7 - 20.1)	n.s.	16.6 (13.0 - 22.4)	n.s.	
A_{13} (%)	17.7 (10.9 - 31.1)	18.4 (12.4 - 28.1)	n.s.	23.0 (10.2 - 28.8)	n.s.	22.5 (16.9 - 30.7)	n.s.	
A_{14} (%)	38.8 (30.7 - 46.5)	34.6 (29.4 - 40.6)	*	34.3 (27.7 - 45.8)	**	44.2 (34.9 - 49.7)	n.s.	
A_{15} (%)	54.3 (47.3 - 64.1)	50.0 (45.4 - 57.8)	*	52.2 (42.8 - 61.7)	**	61.0 (51.5 - 66.8)	n.s.	

comparison between results at t and baseline: n.s. not significant, * $p < 0.05$, ** $p < 0.01$

Table 4.3: Median (Q_1 - Q_3) values of of pulse waveform features and results of statistical tests for exposure type \mathcal{C} .

\mathcal{F}	Exposure type \mathcal{D}							
	baseline		$t = 1\text{h}$		$t = 2\text{h}$		$t = 3\text{h}$	
	T_1 (ms)	160 (132 - 174)	146 (136 - 156)	**	156 (146 - 174)	n.s.	156 (140 - 168)	n.s.
T_{12} (ms)	156 (148 - 190)	148 (138 - 158)	**	158 (144 - 184)	n.s.	156 (144 - 180)	n.s.	
T_{13} (ms)	314 (298 - 332)	302 (286 - 324)	*	318 (308 - 340)	n.s.	308 (284 - 328)	**	
T_{14} (ms)	444 (430 - 478)	432 (412 - 459)	n.s.	462 (444 - 480)	n.s.	436 (408 - 470)	n.s.	
T_{15} (ms)	544 (520 - 590)	554 (512 - 576)	n.s.	566 (544 - 605)	*	544 (496 - 578)	n.s.	
W_1 (ms)	184 (152 - 216)	168 (152 - 188)	**	184 (168 - 212)	n.s.	192 (168 - 214)	n.s.	
A_{12} (%)	12.1 (8.5 - 22.8)	14.0 (9.0 - 23.6)	n.s.	13.8 (7.9 - 21.3)	n.s.	14.8 (11.1 - 24.1)	**	
A_{13} (%)	20.7 (9.7 - 30.2)	20.0 (13.7 - 28.0)	n.s.	24.2 (16.4 - 27.6)	n.s.	28.3 (17.3 - 34.7)	**	
A_{14} (%)	40.0 (28.9 - 47.8)	32.3 (23.2 - 42.2)	**	37.1 (30.8 - 50.1)	n.s.	41.0 (32.6 - 48.6)	n.s.	
A_{15} (%)	56.9 (44.6 - 65.1)	49.0 (36.6 - 58.2)	**	52.3 (42.3 - 65.2)	n.s.	55.3 (48.6 - 65.0)	n.s.	

comparison between results at t and baseline: n.s. not significant, * $p < 0.05$, ** $p < 0.01$

Table 4.4: Median (Q_1 - Q_3) values of of pulse waveform features and results of statistical tests for exposure type \mathcal{D} .

4.1.3 Changes in pulse waveform features with exposure type

Friedman tests reveal statistical differences in relative variations of vascular compliance related parameters A_{13} , A_{14} and A_{15} between exposure types. However, no significant difference is found regarding temporal parameters related to the main wave, i.e. W_1 and T_1 , or pulse transit time surrogates T_{12} , T_{13} , T_{14} , and T_{15} . Multi-comparison tests indicate which exposure types in particular induce results different from those obtained during sessions \mathcal{A} or \mathcal{B} . Tables 4.5 to 4.7 illustrate the outcomes of the multi-comparison paired tests. Median (Q_1 - Q_3) values of relative changes in morphological features are also summarized. The results that are statistically different from \mathcal{A} are shown in bold. Functional boxplots of relative variations of all features are presented on Figure A.3 (see *Appendix A*).

From the tables, it can first be observed that subjects exhibit statistical differences in relative variations of parameters A_{13} and A_{15} during session \mathcal{B} , after one and two hours into exposure. The first morphological feature is indeed found to substantially decrease after one hour compared to results obtained for \mathcal{A} . A_{15} is then normalized after two hours for \mathcal{B} , while we observe a decline of this same parameter during all other sessions. Moreover, study participants present statistical differences in relative variations of parameter A_{13} during session \mathcal{D} compared to \mathcal{A} . This parameter increases after three hours into exposure for \mathcal{D} , while it remains constant for \mathcal{A} . In addition, exposure types \mathcal{B} and \mathcal{C} induce an increase in A_{14} and A_{15} , while both remain constant during session \mathcal{A} . The statistical changes in vascular compliance related parameters, that are observed between \mathcal{C} or \mathcal{D} and \mathcal{A} , are nevertheless not significant compared to results obtained during session \mathcal{B} . An example of the average pulse waveform of one arbitrary chosen subject, for all exposure types, at baseline and after three hours into exposure, is presented on Figure 4.1. This figure highlights the fact that across different stages within the same subject minimal changes in PDA-derived features, including A_{13} , A_{14} and A_{15} are observed during sessions \mathcal{C} and \mathcal{D} , while features remain constant for \mathcal{A} and \mathcal{B} .

To assess whether the increased amplitude loss A_{13} during \mathcal{D} is consistent among study participants, relative variations of the concerned feature for each patient and exposure type are presented on Figure 4.2. 13 out of 18 test persons, with available recordings, show an increased amplitude loss in the second reflection after three hours into exposure \mathcal{D} compared to \mathcal{A} . The same approach reveals that 12 out of 17 participants present an increase in A_{14} during \mathcal{C} at three hours. Finally, 11 out of 17 persons exhibit an increased amplitude loss in the fourth reflection during \mathcal{C} , and 11 out of 16 participants during \mathcal{B} compared to session \mathcal{A} .

\mathcal{F}	Relative changes $\Delta(\mathcal{F})^{\text{1h}}$ (%)					
	\mathcal{A}	\mathcal{B}	\mathcal{B} vs \mathcal{A}	\mathcal{C}	\mathcal{C} vs \mathcal{A}	\mathcal{C} vs \mathcal{B}
T ₁	-5.6 (-11.0 - 0.0)	-7.7 (-20.6 - 0.0)	n.s.	-5.4 (-15.4 - 2.7)	n.s.	n.s.
T ₁₂	-2.7 (-9.5 - 2.9)	-5.6 (-16.3 - 0.0)	n.s.	-5.6 (-13.4 - -2.5)	n.s.	n.s.
T ₁₃	0.0 (-7.7 - 4.0)	-3.9 (-9.8 - 1.4)	n.s.	-5.2 (-11.8 - -0.3)	n.s.	n.s.
T ₁₄	0.0 (-8.2 - 4.6)	-1.9 (-8.2 - 3.0)	n.s.	-3.8 (-8.5 - 0.0)	n.s.	n.s.
T ₁₅	0.0 (-6.0 - 3.1)	-2.2 (-7.3 - 4.3)	n.s.	-2.4 (-6.0 - 0.0)	n.s.	n.s.
W ₁	-7.2 (-15.8 - 4.4)	-9.3 (-23.6 - 0.0)	n.s.	-8.0 (-19.3 - 4.5)	n.s.	n.s.
A ₁₂	25.4 (-15.4 - 63.5)	13.1 (-19.2 - 56.8)	n.s.	5.0 (-33.2 - 31.1)	n.s.	n.s.
A ₁₃	23.2 (-14.5 - 51.1)	-19.7 (-46.1 - 55.4)	**	11.9 (-27.9 - 53.0)	n.s.	n.s.
A ₁₄	-7.2 (-21.9 - 6.9)	-16.3 (-22.7 - 9.6)	n.s.	-2.9 (-19.3 - 9.6)	n.s.	n.s.
A ₁₅	-6.4 (-18.9 - 3.4)	-9.0 (-18.4 - 11.8)	n.s.	-3.8 (-14.8 - 7.2)	n.s.	n.s.

n.s. not significant, * p < 0.05, ** p < 0.01.

Table 4.5: Median (Q_1 - Q_3) values of relative changes in pulse waveform features after one hour and statistical results.

\mathcal{F}	Relative changes $\Delta(\mathcal{F})^{\text{2h}}$ (%)					
	\mathcal{A}	\mathcal{B}	\mathcal{B} vs \mathcal{A}	\mathcal{C}	\mathcal{C} vs \mathcal{A}	\mathcal{C} vs \mathcal{B}
T ₁	-2.4 (-6.7 - 1.3)	0.0 (-14.1 - 6.5)	n.s.	0.0 (-13.8 - 5.4)	n.s.	n.s.
T ₁₂	-5.1 (-8.6 - 2.6)	0.0 (-10.0 - 5.1)	n.s.	0.0 (-18.9 - 2.9)	n.s.	n.s.
T ₁₃	1.3 (-4.6 - 5.4)	0.0 (-3.9 - 4.4)	n.s.	-1.4 (-10.4 - 2.1)	n.s.	n.s.
T ₁₄	2.7 (-3.5 - 5.3)	0.4 (-3.4 - 4.1)	n.s.	-0.2 (-8.0 - 1.8)	n.s.	n.s.
T ₁₅	1.8 (-3.5 - 4.2)	-0.5 (-4.0 - 4.1)	n.s.	0.0 (-9.3 - 3.8)	n.s.	n.s.
W ₁	-2.9 (-10.6 - 0.0)	-0.9 (-17.4 - 11.1)	n.s.	0.0 (-18.5 - 6.2)	n.s.	n.s.
A ₁₂	18.3 (-29.2 - 85.9)	8.2 (-15.1 - 42.8)	n.s.	-2.5 (-33.3 - 27.1)	n.s.	n.s.
A ₁₃	9.1 (-42.6 - 45.8)	0.5 (-22.6 - 31.5)	n.s.	25.6 (-36.6 - 70.3)	n.s.	n.s.
A ₁₄	0.7 (-35.5 - 21.7)	-1.1 (-21.7 - 17.3)	n.s.	-12.9 (-30.5 - 11.6)	n.s.	n.s.
A ₁₅	-7.1 (-23.5 - 12.6)	0.4 (-13.2 - 15.9)	*	-9.4 (-22.9 - 5.3)	n.s.	**

n.s. not significant, * p < 0.05, ** p < 0.01.

Table 4.6: Median (Q_1 - Q_3) values of relative changes in pulse waveform features after two hours and statistical results.

\mathcal{F}	Relative changes $\Delta(\mathcal{F})^{3h}$ (%)								
	\mathcal{A}	\mathcal{B}	\mathcal{B} vs \mathcal{A}	\mathcal{C}	\mathcal{C} vs \mathcal{A}	\mathcal{C} vs \mathcal{B}	\mathcal{D}	\mathcal{D} vs \mathcal{A}	\mathcal{D} vs \mathcal{B}
T ₁	-2.3 (-9.2 - 4.7)	0.0 (-9.6 - 5.3)	n.s.	2.4 (-8.8 - 8.7)	n.s.	n.s.	-2.5 (-9.3 - 6.1)	n.s.	n.s.
T ₁₂	-0.6 (-9.1 - 3.3)	-2.6 (-8.1 - 5.2)	n.s.	-2.7 (-12.7 - 2.4)	n.s.	n.s.	-5.2 (-12.1 - 0.8)	n.s.	n.s.
T ₁₃	-1.3 (-5.8 - 2.4)	-2.6 (-6.3 - 2.7)	n.s.	-2.8 (-7.4 - 3.0)	n.s.	n.s.	-2.8 (-9.4 - 1.3)	n.s.	n.s.
T ₁₄	-1.8 (-5.6 - 1.7)	-2.9 (-7.2 - 4.2)	n.s.	-1.5 (-7.3 - 3.2)	n.s.	n.s.	-2.3 (-7.5 - 2.8)	n.s.	n.s.
T ₁₅	-2.8 (-6.8 - 1.0)	-4.2 (-9.2 - 2.9)	n.s.	-2.1 (-8.6 - 1.6)	n.s.	n.s.	-2.4 (-7.9 - 0.7)	n.s.	n.s.
W ₁	0.0 (-10.3 - 8.1)	0.0 (-10.0 - 9.1)	n.s.	0.0 (-14.3 - 12.1)	n.s.	n.s.	1.7 (-11.2 - 10.5)	n.s.	n.s.
A ₁₂	10.9 (-15.4 - 54.9)	34.7 (-15.4 - 93.0)	n.s.	22.3 (-22.3 - 61.6)	n.s.	n.s.	20.6 (-7.4 - 79.1)	n.s.	n.s.
A ₁₃	2.2 (-24.9 - 62.3)	7.1 (-11.2 - 102.9)	n.s.	29.3 (-11.6 - 92.1)	n.s.	n.s.	30.3 (-5.2 - 87.5)	**	n.s.
A ₁₄	-4.9 (-15.3 - 16.1)	4.3 (-13.8 - 46.6)	n.s.	13.5 (-5.4 - 24.5)	**	n.s.	6.0 (-7.7 - 31.7)	n.s.	n.s.
A ₁₅	-3.3 (-13.5 - 5.7)	4.2 (-8.6 - 45.9)	**	8.8 (-4.5 - 19.3)	**	n.s.	2.7 (-6.3 - 24.1)	n.s.	n.s.

n.s. not significant, * p < 0.05, ** p < 0.01.

Table 4.7: Median (Q_1 - Q_3) values of relative changes in pulse waveform features after three hours and statistical results.

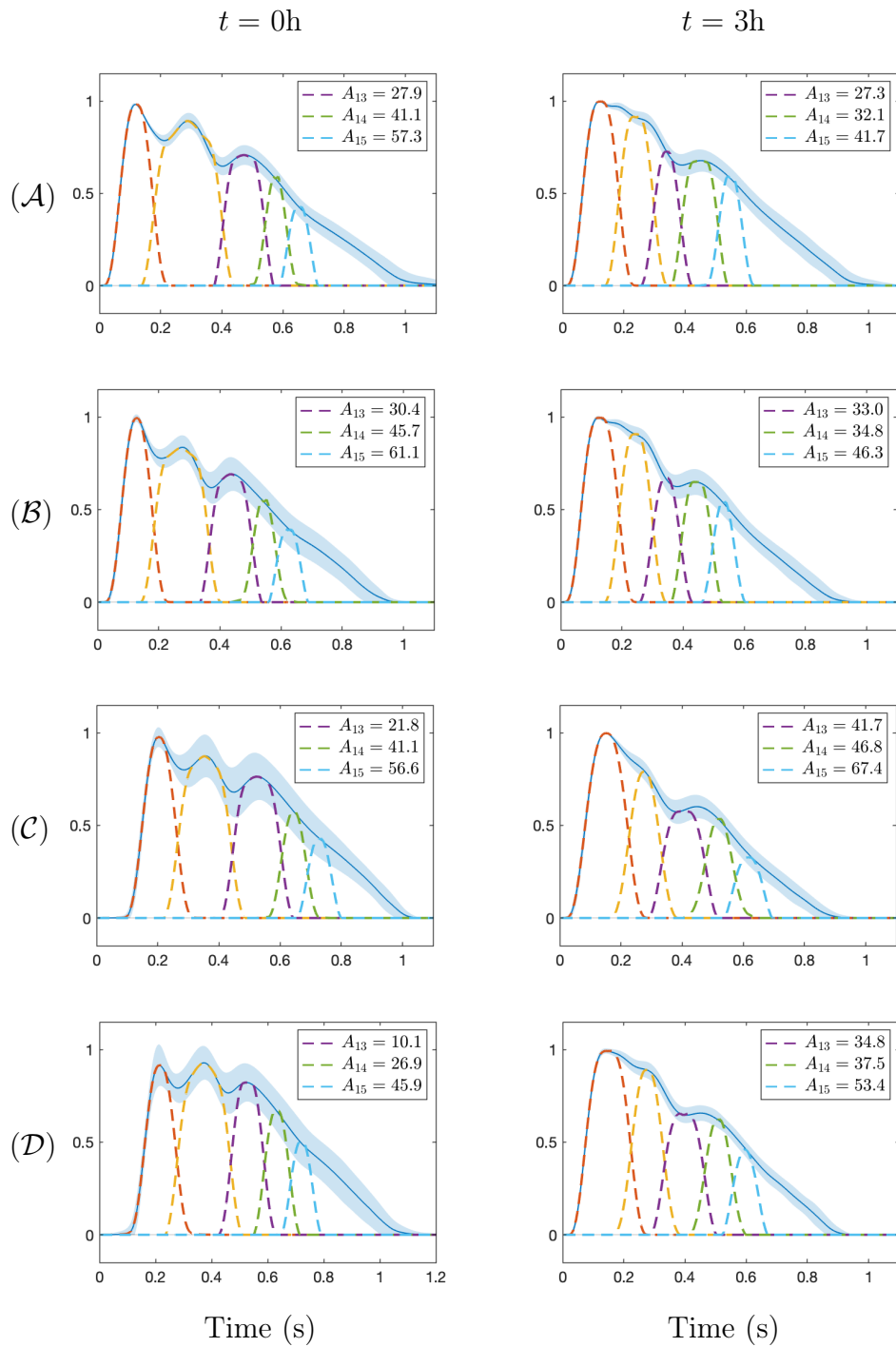


Figure 4.1: Example of average pulse waveform of one study participant for all exposure types at baseline and after three hours. The blue lines and shaded areas represent the ensemble average and standard deviation. The inner waves are marked with dashed lines. The waveform characteristics A_{13} , A_{14} and A_{15} are illustrated at the top right of each graph.

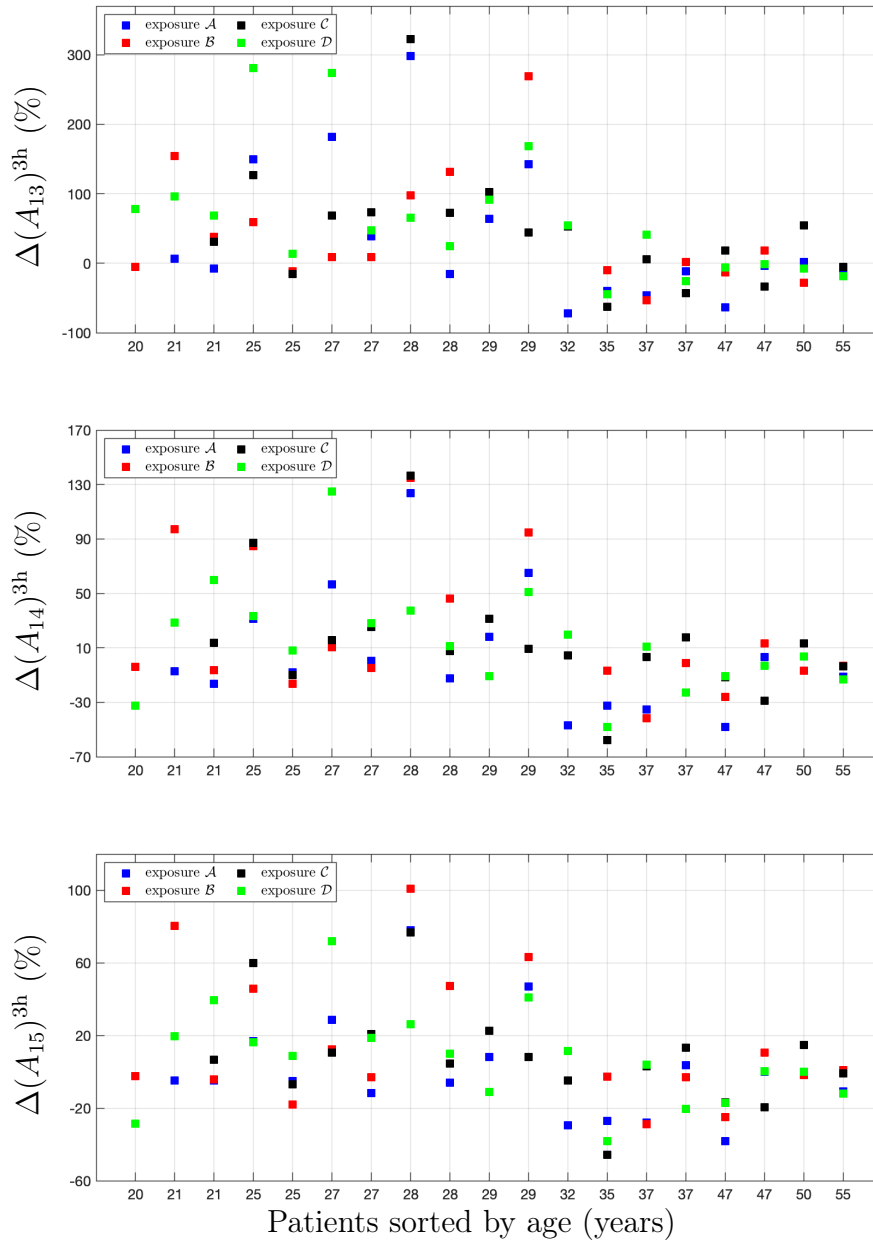


Figure 4.2: Relative changes in pulse waveform characteristics after three hours compared to basal condition, for all subjects and exposure types.

4.2 HRV analysis

Among the 19 study participants, several subjects had at least one missing 15-minute ECG recording: six for exposure \mathcal{B} , three for \mathcal{C} and two for \mathcal{D} . As a consequence, only 13 out of the 19 study participants provided data usable to assess and compare the actual influence of exposure types on HRV parameters.

The percentage of discarded RR intervals (mean \pm std) for each stage is $3.5 \pm 6.6\%$ (\mathcal{A}), $3.5 \pm 6.7\%$ (\mathcal{B}), $2.5 \pm 3.4\%$ (\mathcal{C}) and $3.9 \pm 12.1\%$ (\mathcal{D}). These results suggest that few abnormal RR intervals are present in the ECG signal recordings in average. The percentages are heterogeneous, since some records present a proportion of discarded RR intervals superior to 15%. For example, three recordings of 15-minute sessions are concerned by a larger amount of excluded intervals for exposure \mathcal{A} , two for \mathcal{B} , one for \mathcal{C} and three for \mathcal{D} . These recordings are considered suitable for further analysis. Finally, the number of analyzed RR intervals (mean \pm std) for each exposure type is 281 ± 52 (\mathcal{A}), 286 ± 47 (\mathcal{B}), 278 ± 56 (\mathcal{C}) and 278 ± 58 (\mathcal{D}). It is considered sufficient for proper computation of HRV parameters and statistical analysis of the results.

4.2.1 Changes in HRV parameters over exposure time

Friedman tests were performed to assess the variations of HRV parameters over time, for each exposure type separately. It was complemented by multi-comparison tests to determine which specific exposure duration induces results statistically different from those obtained at basal condition. The tests show that no exposure type is concerned by significant variations of HRV parameters over time. Tables 4.8 to 4.11 illustrate the outputs of the multi-comparison paired tests. Median (Q_1 - Q_3) values of HRV parameters for each exposure type and time are also summarized. Functional boxplots of features as functions of time are presented in Figure B.1 (*see Appendix B*).

4.2.2 Variability of HRV parameters at basal condition

No statistically significant difference is found between HRV characteristics of all exposure types at basal condition across the subjects. However, a high variability of the pre-exposure data is observed for every subject and indicator individually, as illustrated on Figure B.2 (*see Appendix B*). To assess the actual impact of each exposure type on extracted features, it is thus necessary to compute relative changes in HRV parameters compared to baseline values.

\mathcal{F}	Exposure type \mathcal{A}						
	baseline	$t = 1\text{h}$		$t = 2\text{h}$		$t = 3\text{h}$	
RR (s)	1.044 (0.926 - 1.111)	1.069 (0.950 - 1.128)	n.s.	1.107 (0.959 - 1.146)	n.s.	1.044 (0.883 - 1.149)	n.s.
SDNN (s)	0.058 (0.052 - 0.084)	0.063 (0.052 - 0.074)	n.s.	0.066 (0.051 - 0.082)	n.s.	0.060 (0.046 - 0.075)	n.s.
SDSD (s)	0.050 (0.029 - 0.096)	0.048 (0.030 - 0.081)	n.s.	0.044 (0.032 - 0.081)	n.s.	0.051 (0.032 - 0.064)	n.s.
rMSSD (s)	0.050 (0.029 - 0.096)	0.048 (0.031 - 0.081)	n.s.	0.044 (0.032 - 0.081)	n.s.	0.051 (0.032 - 0.064)	n.s.
pNN50	0.181 (0.034 - 0.274)	0.158 (0.034 - 0.247)	n.s.	0.105 (0.051 - 0.273)	n.s.	0.124 (0.065 - 0.239)	n.s.
LF (s^2)	0.001 (0.000 - 0.002)	0.001 (0.001 - 0.001)	n.s.	0.001 (0.000 - 0.001)	n.s.	0.001 (0.001 - 0.002)	n.s.
HF (s^2)	0.001 (0.001 - 0.003)	0.001 (0.000 - 0.001)	n.s.	0.001 (0.000 - 0.002)	n.s.	0.001 (0.000 - 0.001)	n.s.
LF norm	0.534 (0.301 - 0.629)	0.595 (0.467 - 0.709)	n.s.	0.543 (0.400 - 0.734)	n.s.	0.553 (0.424 - 0.667)	n.s.
HF norm	0.495 (0.381 - 0.701)	0.407 (0.310 - 0.542)	n.s.	0.468 (0.287 - 0.609)	n.s.	0.455 (0.343 - 0.584)	n.s.
LF/HF ratio	1.084 (0.431 - 1.649)	1.475 (0.862 - 2.288)	n.s.	1.175 (0.657 - 2.615)	n.s.	1.217 (0.734 - 1.953)	n.s.

comparison between results at t and baseline: n.s. not significant, * $p < 0.05$, ** $p < 0.01$

Table 4.8: Median (Q_1 - Q_3) values of HRV parameters and results of statistical tests for exposure type \mathcal{A} .

\mathcal{F}	Exposure type \mathcal{B}						
	baseline	$t = 1\text{h}$		$t = 2\text{h}$		$t = 3\text{h}$	
RR (s)	0.996 (0.915 - 1.144)	1.022 (0.932 - 1.102)	n.s.	1.004 (0.927 - 1.068)	n.s.	0.944 (0.894 - 1.042)	n.s.
SDNN (s)	0.064 (0.054 - 0.085)	0.057 (0.042 - 0.078)	n.s.	0.060 (0.051 - 0.081)	n.s.	0.065 (0.054 - 0.075)	n.s.
SDSD (s)	0.042 (0.033 - 0.073)	0.038 (0.035 - 0.066)	n.s.	0.039 (0.034 - 0.059)	n.s.	0.041 (0.029 - 0.064)	n.s.
rMSSD (s)	0.042 (0.033 - 0.073)	0.038 (0.035 - 0.066)	n.s.	0.039 (0.034 - 0.059)	n.s.	0.041 (0.029 - 0.064)	n.s.
pNN50	0.112 (0.050 - 0.205)	0.088 (0.049 - 0.197)	n.s.	0.092 (0.038 - 0.210)	n.s.	0.118 (0.040 - 0.203)	n.s.
LF (s^2)	0.001 (0.001 - 0.002)	0.001 (0.001 - 0.002)	n.s.	0.001 (0.001 - 0.002)	n.s.	0.001 (0.001 - 0.002)	n.s.
HF (s^2)	0.001 (0.000 - 0.003)	0.001 (0.001 - 0.001)	n.s.	0.001 (0.001 - 0.001)	n.s.	0.001 (0.000 - 0.002)	n.s.
LF norm	0.505 (0.438 - 0.613)	0.521 (0.446 - 0.630)	n.s.	0.618 (0.508 - 0.670)	n.s.	0.558 (0.432 - 0.665)	n.s.
HF norm	0.516 (0.397 - 0.566)	0.488 (0.385 - 0.560)	n.s.	0.397 (0.336 - 0.509)	n.s.	0.450 (0.345 - 0.575)	n.s.
LF/HF ratio	0.978 (0.773 - 1.545)	1.070 (0.796 - 1.635)	n.s.	1.568 (1.000 - 1.995)	n.s.	1.241 (0.751 - 1.957)	n.s.

comparison between results at t and baseline: n.s. not significant, * $p < 0.05$, ** $p < 0.01$

Table 4.9: Median (Q_1 - Q_3) values of HRV parameters and results of statistical tests for exposure type \mathcal{B} .

\mathcal{F}	Exposure type \mathcal{C}		
	baseline	$t = 1\text{h}$	$t = 3\text{h}$
RR (s)	1.017 (0.986 - 1.091)	1.055 (0.982 - 1.062)	0.972 (0.877 - 1.052)
SDNN (s)	0.061 (0.051 - 0.082)	0.063 (0.062 - 0.076)	0.060 (0.057 - 0.071)
SDSD (s)	0.055 (0.035 - 0.079)	0.057 (0.038 - 0.065)	0.053 (0.030 - 0.063)
rMSSD (s)	0.055 (0.036 - 0.079)	0.057 (0.038 - 0.065)	0.053 (0.030 - 0.063)
pNN50	0.188 (0.050 - 0.263)	0.137 (0.086 - 0.209)	0.154 (0.061 - 0.222)
LF (s ²)	0.001 (0.000 - 0.001)	0.001 (0.001 - 0.001)	0.001 (0.001 - 0.001)
HF (s ²)	0.001 (0.001 - 0.002)	0.001 (0.001 - 0.002)	0.001 (0.001 - 0.002)
LF norm	0.426 (0.323 - 0.566)	0.536 (0.356 - 0.585)	0.475 (0.368 - 0.634)
HF norm	0.580 (0.436 - 0.695)	0.532 (0.448 - 0.653)	0.547 (0.379 - 0.640)
LF/HF ratio	0.734 (0.466 - 1.299)	1.123 (0.545 - 1.403)	0.867 (0.576 - 1.677)

comparison between results at t and baseline: n.s. not significant, * $p < 0.05$, ** $p < 0.01$

Table 4.10: Median (Q_1 - Q_3) values of HRV parameters and results of statistical tests for exposure type \mathcal{C} .

\mathcal{F}	Exposure type \mathcal{D}		
	baseline	$t = 1\text{h}$	$t = 3\text{h}$
RR (s)	1.027 (0.926 - 1.164)	1.079 (0.950 - 1.160)	0.974 (0.892 - 1.093)
SDNN (s)	0.061 (0.049 - 0.077)	0.066 (0.051 - 0.072)	0.061 (0.051 - 0.076)
SDSD (s)	0.050 (0.036 - 0.074)	0.057 (0.029 - 0.073)	0.040 (0.027 - 0.068)
rMSSD (s)	0.050 (0.036 - 0.074)	0.057 (0.029 - 0.073)	0.040 (0.027 - 0.068)
pNN50	0.163 (0.059 - 0.236)	0.180 (0.047 - 0.248)	0.105 (0.042 - 0.227)
LF (s ²)	0.001 (0.001 - 0.002)	0.001 (0.001 - 0.002)	0.001 (0.000 - 0.001)
HF (s ²)	0.001 (0.001 - 0.002)	0.001 (0.000 - 0.001)	0.001 (0.000 - 0.001)
LF norm	0.519 (0.357 - 0.617)	0.499 (0.407 - 0.758)	0.507 (0.406 - 0.706)
HF norm	0.511 (0.407 - 0.656)	0.513 (0.244 - 0.601)	0.504 (0.301 - 0.601)
LF/HF ratio	1.017 (0.546 - 1.517)	0.964 (0.679 - 3.292)	1.006 (0.675 - 2.351)

comparison between results at t and baseline: n.s. not significant, * $p < 0.05$, ** $p < 0.01$

Table 4.11: Median (Q_1 - Q_3) values of HRV parameters and results of statistical tests for exposure type \mathcal{D} .

4.2.3 Changes in HRV parameters with exposure type

A non-parametric Friedman test, complemented by multi-comparison paired tests, was performed to assess differences in relative changes in HRV parameters with exposure types. The results show that no exposure type induces statistical changes in variations of HRV characteristics compared to \mathcal{A} or \mathcal{B} . Tables 4.12 to 4.14 illustrate the statistical significance of the multi-comparison paired tests. Median (Q_1 - Q_3) values of relative changes in HRV parameters for each exposure type and time are also summarized. Finally, functional boxplots of relative variations of all features are presented on Figure B.3 (see *Appendix B*).

\mathcal{F}	Relative changes $\Delta(\mathcal{F})^{\text{1h}}$ (%)					
	\mathcal{A}	\mathcal{B}	\mathcal{C}	\mathcal{C} vs \mathcal{A}	\mathcal{C} vs \mathcal{B}	\mathcal{D} vs \mathcal{A} \mathcal{D} vs \mathcal{B}
RR	2.3 (-3.4 - 4.8)	1.7 (-4.4 - 7.4)	2.8 (-3.9 - 7.9)	n.s.	n.s.	2.9 (-2.1 - 9.0) n.s.
SDNN	9.4 (-19.2 - 24.5)	-10.5 (-28.2 - 4.8)	2.7 (-21.7 - 24.1)	n.s.	n.s.	1.7 (-17.3 - 28.0) n.s.
SDSD	-1.3 (-21.5 - 26.4)	-3.9 (-16.2 - 28.9)	4.4 (-15.8 - 26.2)	n.s.	n.s.	-0.8 (-32.2 - 20.7) n.s.
rMSSD	-1.3 (-21.5 - 26.4)	-3.9 (-16.2 - 28.9)	4.4 (-15.8 - 26.2)	n.s.	n.s.	-0.8 (-32.3 - 20.8) n.s.
pNN50	-1.9 (-22.7 - 43.8)	0.0 (-47.6 - 91.2)	-6.5 (-27.4 - 77.3)	n.s.	n.s.	0.7 (-45.1 - 39.2) n.s.
LF	6.5 (-27.0 - 137.5)	-22.0 (-39.0 - 34.0)	-2.8 (-31.5 - 82.1)	n.s.	n.s.	-6.4 (-40.9 - 66.8) n.s.
HF	-12.7 (-35.3 - 45.5)	-2.6 (-40.9 - 31.0)	5.9 (-18.4 - 35.7)	n.s.	n.s.	-20.7 (-56.2 - 14.0) n.s.
LF norm	11.5 (-1.5 - 36.7)	2.7 (-19.6 - 9.1)	25.7 (-18.8 - 55.0)	n.s.	n.s.	8.9 (-3.9 - 39.0) n.s.
HF norm	-17.9 (-29.9 - 4.6)	-1.4 (-11.3 - 29.0)	-8.3 (-23.5 - 27.2)	n.s.	n.s.	-9.3 (-32.2 - 1.4) n.s.
LF/HF	36.0 (-8.9 - 131.3)	4.8 (-36.1 - 22.1)	52.9 (-36.2 - 67.7)	n.s.	n.s.	21.1 (-4.4 - 145.5) n.s.

n.s. not significant, * p < 0.05, ** p < 0.01.

Table 4.12: Median (Q_1 - Q_3) values of relative changes in HRV parameters after one hour and results of statistical tests.

\mathcal{F}	Relative changes $\Delta(\mathcal{F})^{\text{2h}}$ (%)					
	\mathcal{A}	\mathcal{B}	\mathcal{C}	\mathcal{C} vs \mathcal{A}	\mathcal{C} vs \mathcal{B}	\mathcal{D} vs \mathcal{A} \mathcal{D} vs \mathcal{B}
RR	3.3 (-6.1 - 7.5)	-0.5 (-5.5 - 8.4)	2.3 (0.1 - 8.9)	n.s.	n.s.	2.6 (-0.1 - 9.0) n.s.
SDNN	10.6 (-12.5 - 27.8)	-8.8 (-28.9 - 13.8)	13.7 (-18.1 - 29.7)	n.s.	n.s.	13.4 (-13.6 - 30.7) n.s.
SDSD	-1.5 (-22.8 - 21.0)	-3.5 (-34.7 - 21.6)	9.0 (-0.5 - 31.5)	n.s.	n.s.	3.1 (-6.8 - 28.8) n.s.
rMSSD	-1.5 (-22.9 - 21.0)	-3.5 (-34.7 - 21.6)	9.0 (-0.5 - 31.5)	n.s.	n.s.	3.1 (-6.9 - 28.8) n.s.
pNN50	-11.1 (-44.0 - 33.6)	-17.5 (-42.8 - 155.5)	2.2 (-7.4 - 72.7)	n.s.	n.s.	6.9 (-21.2 - 88.1) n.s.
LF	26.4 (-25.6 - 162.5)	26.4 (-36.4 - 81.2)	9.5 (-28.1 - 58.5)	n.s.	n.s.	-1.9 (-37.1 - 53.2) n.s.
HF	1.5 (-35.3 - 56.0)	-25.1 (-50.8 - 76.3)	6.3 (-18.9 - 30.4)	n.s.	n.s.	-20.9 (-44.5 - 28.8) n.s.
LF norm	15.8 (-6.5 - 39.4)	14.2 (-1.9 - 34.5)	11.9 (-8.3 - 48.3)	n.s.	n.s.	11.4 (-10.2 - 44.1) n.s.
HF norm	-13.6 (-33.9 - 9.9)	-21.4 (-29.0 - 0.1)	-12.0 (-18.8 - 15.5)	n.s.	n.s.	-10.4 (-26.3 - 18.0) n.s.
LF/HF	47.3 (-14.9 - 143.0)	44.7 (-0.6 - 100.0)	34.9 (-22.5 - 81.9)	n.s.	n.s.	26.1 (-24.7 - 90.7) n.s.

n.s. not significant, * p < 0.05, ** p < 0.01.

Table 4.13: Median (Q_1 - Q_3) values of relative changes in HRV parameters after two hours and results of statistical tests.

\mathcal{F}	Relative changes $\Delta(\mathcal{F})^{3h}$ (%)								
	\mathcal{A}	\mathcal{B}	\mathcal{B} vs \mathcal{A}	\mathcal{C}	\mathcal{C} vs \mathcal{A}	\mathcal{C} vs \mathcal{B}	\mathcal{D}	\mathcal{D} vs \mathcal{A}	\mathcal{D} vs \mathcal{B}
RR	-3.3 (-6.0 - 4.3)	-4.3 (-12.5 - 5.2)	n.s.	-4.3 (-8.1 - -1.4)	n.s.	n.s.	-5.6 (-6.9 - -2.9)	n.s.	n.s.
SDNN	-0.2 (-15.7 - 20.5)	-4.7 (-15.7 - 5.7)	n.s.	-1.5 (-21.1 - 20.6)	n.s.	n.s.	-6.1 (-18.1 - 19.3)	n.s.	n.s.
SDSD	-5.9 (-26.3 - 14.5)	-12.6 (-26.3 - 14.0)	n.s.	-3.0 (-20.3 - 19.5)	n.s.	n.s.	-19.3 (-26.7 - -6.7)	n.s.	n.s.
rMSSD	-5.9 (-26.3 - 14.5)	-12.6 (-26.3 - 14.0)	n.s.	-3.0 (-20.3 - 19.5)	n.s.	n.s.	-19.4 (-26.8 - -6.7)	n.s.	n.s.
pNN50	-16.2 (-43.6 - 30.5)	7.6 (-28.6 - 67.3)	n.s.	-10.6 (-17.6 - 9.5)	n.s.	n.s.	-35.5 (-45.0 - -2.9)	n.s.	n.s.
LF	7.8 (-19.8 - 96.8)	43.8 (-39.9 - 103.8)	n.s.	15.2 (-30.9 - 117.4)	n.s.	n.s.	-10.0 (-50.6 - 26.8)	n.s.	n.s.
HF	4.5 (-27.7 - 36.0)	-13.2 (-36.6 - 35.6)	n.s.	23.7 (-34.4 - 55.6)	n.s.	n.s.	-27.8 (-54.6 - 10.2)	n.s.	n.s.
LF norm	5.5 (-11.0 - 48.6)	0.4 (-16.6 - 26.7)	n.s.	11.3 (-5.3 - 43.8)	n.s.	n.s.	12.0 (-4.9 - 33.7)	n.s.	n.s.
HF norm	-12.2 (-27.4 - 9.1)	-4.1 (-27.9 - 16.8)	n.s.	-6.0 (-26.0 - 5.4)	n.s.	n.s.	-15.3 (-28.9 - 9.1)	n.s.	n.s.
LF/HF	24.3 (-19.7 - 105.6)	8.4 (-29.2 - 118.8)	n.s.	19.0 (-9.8 - 92.5)	n.s.	n.s.	33.6 (-12.0 - 98.9)	n.s.	n.s.

n.s. not significant, * p < 0.05, ** p < 0.01.

Table 4.14: Median (Q_1 - Q_3) values of relative changes in HRV parameters after three hours and results of statistical tests.

4.3 PTT Analysis

For this third part, the percentage of discarded PTT intervals (mean \pm std) for each stage is $4.2 \pm 9.5\%$ (\mathcal{A}), $4.8 \pm 11.9\%$ (\mathcal{B}), $3.6 \pm 9.6\%$ (\mathcal{C}) and $7.1 \pm 16.8\%$ (\mathcal{D}). These results suggest that few abnormal PTT intervals are present in ECG signal recordings in average. The results remain heterogeneous, with several recordings concerned by a percentage of discarded PTT intervals superior to 15%. For instance, two recordings of 15-minute sessions are concerned by a higher number of excluded intervals for exposure \mathcal{A} , four for \mathcal{B} , one for \mathcal{C} and four for \mathcal{D} . These recordings are however considered suitable for further analysis. Finally, the number of analyzed PTT intervals (mean \pm std) for each exposure type is 284 ± 54 (\mathcal{A}), 288 ± 55 (\mathcal{B}), 284 ± 55 (\mathcal{C}) and 273 ± 63 (\mathcal{D}). It is considered sufficient for proper computation of PTT parameters and statistical analysis of the results.

4.3.1 Changes in PTT characteristics over exposure time

Friedman tests were performed to assess the variations of PTT characteristics over exposure time. Results indicate that PTT estimates related to exposure types \mathcal{A} , \mathcal{B} and \mathcal{C} present significant variations over time. No variation of PTT parameters is observed for exposure \mathcal{D} . The non-parametric test was complemented by multi-comparison paired tests to determine which exposure duration in particular induces results statistically different from basal condition, separately for every exposure type. Tables 4.15 to 4.18 illustrate the outcomes of the multi-comparison paired tests. Median (Q_1 - Q_3) values of PTT characteristics for each exposure type and time are also summarized. The results which are statistically different from those estimated at basal condition are shown in bold. Functional boxplots of all features as functions of time are presented in Figure C.1 (*see Appendix C*).

From those tables, it can be observed that study participants exhibit a slight decrease in the mean pulse transit time estimate after one hour for exposures \mathcal{A} and \mathcal{B} , followed by a trend toward baseline values after two hours into exposure. In a second phase, the subjects present a higher decrease in PTT after three hours during sessions \mathcal{A} , \mathcal{B} and \mathcal{C} .

\mathcal{F}	Exposure type \mathcal{A}			
	baseline	$t = 1\text{h}$	$t = 2\text{h}$	$t = 3\text{h}$
PTT (s)	0.164 (0.156 - 0.175)	0.153 (0.140 - 0.163)	0.163 (0.145 - 0.167)	0.146 (0.137 - 0.159) *
SDPTT (s)	0.006 (0.005 - 0.007)	0.006 (0.004 - 0.007)	0.005 (0.004 - 0.007)	0.005 (0.004 - 0.006) n.s.
rMSSD ^{PTT} (s)	0.006 (0.005 - 0.008)	0.005 (0.004 - 0.008)	0.005 (0.004 - 0.008)	0.005 (0.004 - 0.006) n.s.
SDSD ^{PTT} (s)	0.006 (0.005 - 0.008)	0.005 (0.004 - 0.008)	0.005 (0.004 - 0.008)	0.005 (0.004 - 0.006) n.s.

comparison between results at t and baseline: n.s. not significant, * $p < 0.05$, ** $p < 0.01$

Table 4.15: Median (Q_1 - Q_3) values of PTT parameters and results of statistical tests for exposure type \mathcal{A} .

\mathcal{F}	Exposure type \mathcal{B}			
	baseline	$t = 1\text{h}$	$t = 2\text{h}$	$t = 3\text{h}$
PTT (s)	0.162 (0.157 - 0.173)	0.154 (0.145 - 0.163) *	0.158 (0.149 - 0.168)	0.149 (0.143 - 0.159) *
SDPTT (s)	0.006 (0.005 - 0.006)	0.005 (0.004 - 0.006)	0.005 (0.004 - 0.007)	0.005 (0.004 - 0.006) n.s.
rMSSD ^{PTT} (s)	0.006 (0.005 - 0.008)	0.005 0.005 (0.004 - 0.006)	0.005 (0.005 - 0.006)	0.005 (0.005 - 0.006) n.s.
SDSD ^{PTT} (s)	0.006 (0.005 - 0.008)	0.005 (0.004 - 0.006)	0.005 (0.005 - 0.006)	0.005 (0.005 - 0.006) n.s.

comparison between results at t and baseline: n.s. not significant, * $p < 0.05$, ** $p < 0.01$

Table 4.16: Median (Q_1 - Q_3) values of PTT parameters and results of statistical tests for exposure type \mathcal{B} .

\mathcal{F}	Exposure type \mathcal{C}					
	baseline	$t = 1\text{h}$	$t = 2\text{h}$	$t = 3\text{h}$		
PTT (s)	0.159 (0.144 - 0.167)	0.148 (0.141 - 0.157)	0.154 (0.148 - 0.164)	n.s.	0.143 (0.136 - 0.154)	*
SDPTT (s)	0.005 (0.004 - 0.006)	0.005 (0.004 - 0.005)	0.005 (0.005 - 0.006)	n.s.	0.005 (0.004 - 0.006)	n.s.
rMSSD ^{PTT} (s)	0.005 (0.004 - 0.007)	0.005 (0.005 - 0.006)	0.006 (0.005 - 0.007)	n.s.	0.005 (0.004 - 0.006)	n.s.
SDSD ^{PTT} (s)	0.005 (0.004 - 0.007)	0.005 (0.005 - 0.006)	0.006 (0.005 - 0.007)	n.s.	0.005 (0.004 - 0.006)	n.s.

comparison between results at t and baseline: n.s. not significant, * $p < 0.05$, ** $p < 0.01$

Table 4.17: Median (Q_1 - Q_3) values of PTT parameters and results of statistical tests for exposure type \mathcal{C} .

\mathcal{F}	Exposure type \mathcal{D}					
	baseline	$t = 1\text{h}$	$t = 2\text{h}$	$t = 3\text{h}$		
PTT (s)	0.164 (0.154 - 0.169)	0.156 (0.144 - 0.165)	0.159 (0.148 - 0.168)	n.s.	0.154 (0.141 - 0.163)	n.s.
SDPTT (s)	0.006 (0.005 - 0.007)	0.005 (0.004 - 0.006)	0.005 (0.004 - 0.006)	n.s.	0.005 (0.004 - 0.006)	n.s.
rMSSD ^{PTT} (s)	0.006 (0.005 - 0.008)	0.005 (0.004 - 0.007)	0.005 (0.005 - 0.006)	n.s.	0.005 (0.004 - 0.006)	n.s.
SDSD ^{PTT} (s)	0.006 (0.005 - 0.008)	0.005 (0.004 - 0.007)	0.005 (0.005 - 0.006)	n.s.	0.005 (0.004 - 0.006)	n.s.

comparison between results at t and baseline: n.s. not significant, * $p < 0.05$, ** $p < 0.01$

Table 4.18: Median (Q_1 - Q_3) values of PTT parameters and results of statistical tests for exposure type \mathcal{D} .

4.3.2 Variability of PTT characteristics at basal condition

No statistically significant difference is found between PTT characteristics of all exposure types at basal condition across the subjects. However, a high variability of the pre-exposure data is observed for every subject and indicator individually, as illustrated on Figure C.2 (*see Appendix C*). To assess the actual impact of each exposure type on extracted features, it is thus necessary to compute relative changes in parameters compared to baseline values.

4.3.3 Changes in PTT characteristics with exposure type

A non-parametric Friedman test, complemented by multi-comparison paired tests, was performed to assess differences in relative variations of PTT features with exposure types. The results show that no exposure type is concerned by statistically significant variations of PTT characteristics compared to results obtained during sessions \mathcal{A} or \mathcal{B} . Tables 4.19 to 4.21 illustrate the statistical significance of the multi-comparison paired tests. Median (Q_1 - Q_3) values of relative changes in PTT parameters for each exposure type and time are also summarized. Finally, functional boxplots of relative variations of all features are presented on Figure C.3 (*see Appendix C*).

\mathcal{F}	Relative changes $\Delta(\mathcal{F})^{\text{1h}}$ (%)								
	\mathcal{A}	\mathcal{B}	\mathcal{B} vs \mathcal{A}	\mathcal{C}	\mathcal{C} vs \mathcal{A}	\mathcal{C} vs \mathcal{B}	\mathcal{D}	\mathcal{D} vs \mathcal{A}	\mathcal{D} vs \mathcal{B}
P _{TT}	-6.9 (-10.4 - -4.3)	-5.1 (-11.9 - -3.2)	n.s.	-4.7 (-10.5 - 1.1)	n.s.	n.s.	-5.4 (-8.0 - 1.3)	n.s.	n.s.
SDP _{TT}	4.7 (-10.7 - 17.2)	-10.9 (-24.1 - 5.1)	n.s.	-0.5 (-17.8 - 13.1)	n.s.	n.s.	-14.5 (-27.8 - 5.6)	n.s.	n.s.
rMSSD _{P_{TT}}	-5.4 (-15.6 - 8.1)	-13.3 (-24.7 - -3.8)	n.s.	-2.5 (-17.5 - 13.4)	n.s.	n.s.	-18.6 (-26.8 - -2.4)	n.s.	n.s.
SDSD _{P_{TT}}	-5.4 (-15.7 - 8.1)	-13.3 (-24.7 - -3.8)	n.s.	-2.5 (-17.5 - 13.4)	n.s.	n.s.	-18.6 (-26.8 - -2.4)	n.s.	n.s.

n.s. not significant, * p < 0.05, ** p < 0.01.

Table 4.19: Median (Q_1 - Q_3) values of relative changes in PTT parameters after one hour and results of statistical tests.

\mathcal{F}	Relative changes $\Delta(\mathcal{F})^{\text{2h}}$ (%)								
	\mathcal{A}	\mathcal{B}	\mathcal{B} vs \mathcal{A}	\mathcal{C}	\mathcal{C} vs \mathcal{A}	\mathcal{C} vs \mathcal{B}	\mathcal{D}	\mathcal{D} vs \mathcal{A}	\mathcal{D} vs \mathcal{B}
P _{TT}	-3.7 (-7.5 - -0.9)	-5.0 (-7.4 - 0.7)	n.s.	0.9 (-5.7 - 3.7)	n.s.	n.s.	-1.2 (-4.3 - 0.9)	n.s.	n.s.
SDP _{TT}	-6.3 (-27.8 - 19.3)	-7.2 (-23.5 - 22.3)	n.s.	2.9 (-12.6 - 28.8)	n.s.	n.s.	-11.4 (-26.0 - 7.1)	n.s.	n.s.
rMSSD _{P_{TT}}	-10.8 (-27.8 - 8.2)	-12.4 (-27.7 - 10.1)	n.s.	3.9 (-14.4 - 16.9)	n.s.	n.s.	-11.7 (-25.8 - 4.6)	n.s.	n.s.
SDSD _{P_{TT}}	-10.8 (-27.8 - 8.3)	-12.4 (-27.7 - 10.2)	n.s.	3.9 (-14.4 - 16.9)	n.s.	n.s.	-11.7 (-25.8 - 4.6)	n.s.	n.s.

n.s. not significant, * p < 0.05, ** p < 0.01.

Table 4.20: Median (Q_1 - Q_3) values of relative changes in PTT parameters after two hours and results of statistical tests.

\mathcal{F}	Relative changes $\Delta(\mathcal{F})^{\text{3h}}$ (%)								
	\mathcal{A}	\mathcal{B}	\mathcal{B} vs \mathcal{A}	\mathcal{C}	\mathcal{C} vs \mathcal{A}	\mathcal{C} vs \mathcal{B}	\mathcal{D}	\mathcal{D} vs \mathcal{A}	\mathcal{D} vs \mathcal{B}
P _{TT}	-9.8 (-13.0 - -7.2)	-6.9 (-10.9 - -4.3)	n.s.	-7.4 (-14.1 - -3.1)	n.s.	n.s.	-4.7 (-9.4 - -1.8)	n.s.	n.s.
SDP _{TT}	-13.8 (-24.9 - -5.4)	0.3 (-26.0 - 23.7)	n.s.	-3.0 (-23.1 - 17.1)	n.s.	n.s.	-17.6 (-31.6 - 9.2)	n.s.	n.s.
rMSSD _{P_{TT}}	-21.6 (-34.4 - -1.6)	-15.1 (-27.2 - 8.6)	n.s.	-12.7 (-27.2 - 2.0)	n.s.	n.s.	-26.4 (-34.3 - -8.5)	n.s.	n.s.
SDSD _{P_{TT}}	-21.6 (-34.4 - -1.6)	-15.1 (-27.2 - 8.6)	n.s.	-12.7 (-27.2 - 2.0)	n.s.	n.s.	-26.4 (-34.3 - -8.5)	n.s.	n.s.

n.s. not significant, * p < 0.05, ** p < 0.01.

Table 4.21: Median (Q_1 - Q_3) values of relative changes in PTT parameters after three hours and results of statistical tests.

4.4 Correlation analysis

4.4.1 Correlation between features at basal condition

The results of the correlation analysis regarding extracted features at basal condition are presented in Table 4.22. First, this study indicates that there is a statistical positive correlation between NN and pulse transit time surrogates $T_{1j}, j \in [2, 5]$, but also a negative one with features $A_{1j}, j \in [2, 5]$. HRV statistics (SDNN, rMSSD, SDDSD and pNN50) are negatively correlated with all morphological features, except T_{14} and T_{15} . Frequency-domain measures LF and HF are then negatively correlated with pulse transit time surrogates, as well as W_1 and T_1 . HF is also negatively correlated with features A_{13}, A_{14} and A_{15} . Second, no correlation is found between PDA-derived features and PTT characteristics. However, there exist a positive correlation between the mean PTT estimate and HRV statistics, mostly NN, rMSSD and SDDSD. Finally, $rMSSD^{PTT}$ and $SDDSD^{PTT}$ are correlated with all HRV features.

4.4.2 Correlation between relative changes in features after three hours into exposure

The results of the correlation analyses regarding relative changes in features after three hours into exposure are presented in Tables 4.23 to 4.26. First, regarding PDA-derived features and HRV parameters, results indicate that there is a negative correlation between relative changes in vascular compliance related parameters $A_{i,j}, j \in [2, 5]$ and variations of HRV statistics (NN, SDNN, rMSSD, SDDSD and pNN50) after three hours for exposures \mathcal{A}, \mathcal{B} and \mathcal{C} . In the case of exposure \mathcal{D} , NN, SDNN and pNN50 correlate with these morphological features. HRV statistics are positively correlated with parameters T_{13}, T_{14} and T_{15} for \mathcal{A} and \mathcal{D} only, and negatively with T_1 and W_1 for \mathcal{B} and \mathcal{D} . Parameters $A_{1j}, j \in [2, 5]$ correlate negatively with HF and positively with LF/HF ratio. Secondly, results related to PDA-derived features and PTT characteristics indicate that no persistent correlation exists between relative changes in those features. For exposure \mathcal{C} only, a statistically significant positive correlation is found between PTT estimate and parameters $T_1, T_{1j}, j \in [2, 5]$ and W_1 . Thirdly, results related to HRV features and PTT characteristics are similar. The variations of parameter NN correlate positively with those of the mean PTT estimate for all exposure type. A positive correlation is found between HRV and PTT statistical measures for exposure \mathcal{A} and \mathcal{B} only. No such correlation exists for \mathcal{C} and \mathcal{D} . Lastly, for exposure \mathcal{A} , there is a statically significant negative correlation between LF, as well as LF/HF, and PTT statistics. Parameter HF norm is also positively correlated with all PTT indicators.

	NN	SDNN	rMSSD	SDSD	pNN50	LF	HF	LF norm	HF norm	LF/HF
T ₁	0.059	-0.289**	-0.269**	-0.269**	-0.294**	-0.260**	-0.27**	0.116	-0.109	-0.008
T ₁₂	0.138	-0.297**	-0.278**	-0.278**	-0.277**	-0.392**	-0.351**	0.071	-0.068	-0.044
T ₁₃	0.313**	-0.217**	-0.204**	-0.204**	-0.203**	-0.368**	-0.319**	0.049	-0.049	-0.075
T ₁₄	0.438**	-0.121	-0.117	-0.116	-0.124	-0.312**	-0.257**	0.033	-0.033	-0.084
T ₁₅	0.599**	-0.020	-0.002	-0.002	-0.013	-0.338**	-0.209**	-0.029	0.027	-0.118
W ₁	0.041	-0.302**	-0.284**	-0.284**	-0.308**	-0.262**	-0.281**	0.142	-0.134	0.012
A ₁₂	-0.440**	-0.231**	-0.252**	-0.253**	-0.180*	0.252**	-0.021	0.078	-0.076	-0.018
A ₁₃	-0.446**	-0.462**	-0.433**	-0.433**	-0.424**	-0.055	-0.227**	0.113	-0.106	-0.068
A ₁₄	-0.522**	-0.464**	-0.484**	-0.484**	-0.452**	-0.001	-0.238**	0.134	-0.128	-0.024
A ₁₅	-0.582**	-0.517**	-0.550**	-0.550**	-0.520**	0.005	-0.263**	0.192**	-0.187**	0.039

	NN	SDNN	rMSSD	SDSD	pNN50	LF	HF	LF norm	HF norm	LF/HF
PTT	0.205**	0.130	0.214**	0.214**	0.126	0.135	0.237**	-0.132	0.142	-0.089
SDPTT	-0.151*	0.097	0.123	0.123	0.041	0.259**	0.206**	-0.075	0.090	-0.121
rMSSD ^{PTT}	-0.102	0.224**	0.300**	0.300**	0.223**	0.209**	0.363**	-0.333**	0.348**	-0.282**
SDSD ^{PTT}	-0.102	0.224**	0.299**	0.299**	0.223**	0.209**	0.363**	-0.334**	0.348**	-0.281**

	T ₁	T ₁₂	T ₁₃	T ₁₄	T ₁₅	W ₁	A ₁₂	A ₁₃	A ₁₄	A ₁₅
PTT	0.007	0.748	0.364	0.014	0.001	0.057	0.023	0.456	0.715	0.760
SDPTT	0.275	0.031	0.001	0.000	0.000	0.215	0.596	0.551	0.291	0.264
rMSSD ^{PTT}	0.121	0.026	0.004	0.001	0.004	0.033	0.771	0.644	0.307	0.277
SDSD ^{PTT}	0.122	0.026	0.004	0.002	0.004	0.034	0.771	0.646	0.308	0.278

* p < 0.01, ** p < 0.001

Table 4.22: Correlation coefficients between PDA, HRV and PTT features at baseline condition.

	Exposure type \mathcal{A}									
	$\Delta(\text{NN})$	$\Delta(\text{SDNN})$	$\Delta(\text{rMSSD})$	$\Delta(\text{SDSD})$	$\Delta(\text{pNN50})$	$\Delta(\text{LF})$	$\Delta(\text{HF})$	$\Delta(\text{LF norm})$	$\Delta(\text{HF norm})$	$\Delta(\text{LF/HF})$
$\Delta(\text{T}_1)$	-0.120	-0.099	-0.090	-0.090	-0.078	-0.058	-0.197	0.123	0.119	0.220
$\Delta(\text{T}_{12})$	0.045	-0.108	0.032	0.032	0.131	-0.108	-0.172	0.171	0.144	0.180
$\Delta(\text{T}_{13})$	0.341*	0.119	0.240	0.240	0.352*	-0.192	-0.086	-0.006	0.222	-0.044
$\Delta(\text{T}_{14})$	0.545**	0.315*	0.403**	0.403**	0.411**	-0.216	-0.007	-0.124	0.309*	-0.190
$\Delta(\text{T}_{15})$	0.726**	0.498**	0.560**	0.560**	0.466**	-0.229	0.077	-0.194	0.440**	-0.308*
$\Delta(\text{W}_1)$	-0.188	-0.182	-0.140	-0.140	-0.105	-0.001	-0.212	0.183	0.004	0.302*
$\Delta(\text{A}_{12})$	-0.581**	-0.481**	-0.480**	-0.480**	-0.346*	0.027	-0.273	0.282	-0.256	0.423**
$\Delta(\text{A}_{13})$	-0.603**	-0.510**	-0.504**	-0.504**	-0.349*	0.077	-0.317*	0.268	-0.384**	0.477**
$\Delta(\text{A}_{14})$	-0.647**	-0.546**	-0.562**	-0.562**	-0.450	0.078	-0.340*	0.311*	-0.333*	0.494**
$\Delta(\text{A}_{15})$	-0.651**	-0.558**	-0.590**	-0.590**	-0.448	0.023	-0.377**	0.306*	-0.296*	0.476**

	$\Delta(\text{NN})$	$\Delta(\text{SDNN})$	$\Delta(\text{rMSSD})$	$\Delta(\text{SDSD})$	$\Delta(\text{pNN50})$	$\Delta(\text{LF})$	$\Delta(\text{HF})$	$\Delta(\text{LF norm})$	$\Delta(\text{HF norm})$	$\Delta(\text{LF/HF})$
$\Delta(\text{PTT})$	0.496**	0.379**	0.286	0.286	-0.029	-0.504**	-0.228	-0.229	0.558**	-0.239
$\Delta(\text{SDPTT})$	0.486**	0.378**	0.362**	0.362**	-0.004	-0.369**	-0.057	-0.343*	0.538**	-0.321*
$\Delta(\text{rMSSD}^{\text{PTT}})$	0.626**	0.583**	0.486**	0.486**	0.144	-0.320*	0.040	-0.450**	0.550**	-0.419**
$\Delta(\text{SDSD}^{\text{PTT}})$	0.627**	0.583**	0.487**	0.487**	0.145	-0.320*	0.040	-0.450**	0.550**	-0.419**

	$\Delta(\text{T}_1)$	$\Delta(\text{T}_{12})$	$\Delta(\text{T}_{13})$	$\Delta(\text{T}_{14})$	$\Delta(\text{T}_{15})$	$\Delta(\text{W}_1)$	$\Delta(\text{A}_{12})$	$\Delta(\text{A}_{13})$	$\Delta(\text{A}_{14})$	$\Delta(\text{A}_{15})$
$\Delta(\text{PTT})$	0.268	0.175	0.127	0.227	0.335*	0.209	-0.012	-0.083	-0.088	-0.120
$\Delta(\text{SDPTT})$	0.26	0.148	0.108	0.229	0.312*	0.196	-0.037	-0.036	-0.072	-0.120
$\Delta(\text{rMSSD}^{\text{PTT}})$	-0.018	-0.055	0.087	0.245	0.371**	-0.095	-0.182	-0.214	-0.270	-0.300*
$\Delta(\text{SDSD}^{\text{PTT}})$	-0.018	-0.055	0.087	0.245	0.371**	-0.095	-0.182	-0.214	-0.270	-0.300*

* p < 0.01, ** p < 0.001

Table 4.23: Correlation coefficients between relative changes in PDA, HRV and PTT features for exposure \mathcal{A} after three hours.

		Exposure type \mathcal{B}									
	$\Delta(\text{NN})$	$\Delta(\text{SDNN})$	$\Delta(\text{rMSSD})$	$\Delta(\text{SDSD})$	$\Delta(\text{pNN50})$	$\Delta(\text{LF})$	$\Delta(\text{HF})$	$\Delta(\text{LF norm})$	$\Delta(\text{HF norm})$	$\Delta(\text{LF/HF})$	
$\Delta(\text{T}_1)$	-0.244	-0.344*	-0.432**	-0.432**	-0.412**	-0.213	-0.080	-0.128	-0.029	-0.087	
$\Delta(\text{T}_{12})$	-0.145	-0.381**	-0.279	-0.280	-0.358*	-0.174	0.027	-0.138	0.002	-0.162	
$\Delta(\text{T}_{13})$	0.016	-0.274	-0.095	-0.095	-0.259	-0.078	-0.038	-0.033	-0.070	-0.059	
$\Delta(\text{T}_{14})$	0.111	-0.234	-0.033	-0.033	-0.221	-0.074	-0.098	-0.004	-0.104	-0.025	
$\Delta(\text{T}_{15})$	0.332*	-0.216	0.115	0.115	-0.154	-0.176	-0.150	-0.089	-0.031	-0.130	
$\Delta(\text{W}_1)$	-0.210	-0.325*	-0.405**	-0.405**	-0.413**	-0.167	-0.083	-0.069	-0.079	-0.042	
$\Delta(\text{A}_{12})$	-0.497**	-0.214	-0.348*	-0.348*	-0.179	0.095	0.270	-0.008	0.178	0.020	
$\Delta(\text{A}_{13})$	-0.670**	-0.204	-0.508**	-0.508**	-0.264	0.336*	0.244	0.296*	-0.121	0.295*	
$\Delta(\text{A}_{14})$	-0.739**	-0.267	-0.594**	-0.594**	-0.334*	0.294*	0.117	0.258	-0.085	0.276	
$\Delta(\text{A}_{15})$	-0.800**	-0.330*	-0.641**	-0.641**	-0.384**	0.350*	0.114	0.335*	-0.095	0.325*	

	$\Delta(\text{NN})$	$\Delta(\text{SDNN})$	$\Delta(\text{rMSSD})$	$\Delta(\text{SDSD})$	$\Delta(\text{pNN50})$	$\Delta(\text{LF})$	$\Delta(\text{HF})$	$\Delta(\text{LF norm})$	$\Delta(\text{HF norm})$	$\Delta(\text{LF/HF})$
$\Delta(\text{PTT})$	0.314*	-0.016	-0.033	-0.033	-0.016	-0.092	-0.383**	0.026	-0.236	0.111
$\Delta(\text{SDPTT})$	0.166	0.441**	0.251	0.251	0.432**	0.269	-0.075	0.265	-0.495**	0.328*
$\Delta(\text{rMSSD}^{\text{PTT}})$	0.194	0.325*	0.366**	0.366**	0.444**	0.235	0.152	0.128	-0.284	0.151
$\Delta(\text{SDSD}^{\text{PTT}})$	0.194	0.325*	0.365**	0.365**	0.445**	0.235	0.152	0.127	-0.284	0.151

	$\Delta(\text{T}_1)$	$\Delta(\text{T}_{12})$	$\Delta(\text{T}_{13})$	$\Delta(\text{T}_{14})$	$\Delta(\text{T}_{15})$	$\Delta(\text{W}_1)$	$\Delta(\text{A}_{12})$	$\Delta(\text{A}_{13})$	$\Delta(\text{A}_{14})$	$\Delta(\text{A}_{15})$
$\Delta(\text{PTT})$	0.234	-0.108	-0.169	-0.032	0.093	0.249	-0.105	-0.135	-0.097	-0.124
$\Delta(\text{SDPTT})$	-0.213	-0.182	-0.115	-0.058	-0.003	-0.165	-0.443**	-0.264	-0.262	-0.277
$\Delta(\text{rMSSD}^{\text{PTT}})$	-0.317*	-0.158	0.007	0.035	0.079	-0.290*	-0.374**	-0.290*	-0.215	-0.243
$\Delta(\text{SDSD}^{\text{PTT}})$	-0.317*	-0.159	0.005	0.034	0.078	-0.300*	-0.374**	-0.290*	-0.215	-0.243

* p < 0.01, ** p < 0.001

Table 4.24: Correlation coefficients between relative changes in PDA, HRV and PTT features for exposure \mathcal{B} after three hours.

		Exposure type \mathcal{C}									
$\Delta(\text{NN})$	$\Delta(\text{SDNN})$	$\Delta(\text{rMSSD})$	$\Delta(\text{SDSD})$	$\Delta(\text{pNN50})$	$\Delta(\text{LF})$	$\Delta(\text{HF})$	$\Delta(\text{LF norm})$	$\Delta(\text{HF norm})$	$\Delta(\text{LF/HF})$		
$\Delta(\text{T}_1)$	-0.180	-0.0580	-0.218	-0.219	-0.304*	-0.308*	-0.297*	0.035	0.056	-0.012	
$\Delta(\text{T}_2)$	-0.204	-0.347*	-0.453**	-0.454**	-0.376**	-0.411**	-0.541**	0.128	-0.036	0.146	
$\Delta(\text{T}_3)$	0.148	-0.300*	-0.200	-0.200	-0.253	-0.550**	-0.547**	-0.118	0.163	-0.113	
$\Delta(\text{T}_4)$	0.434**	-0.112	0.118	0.118	-0.114	-0.559**	-0.414**	-0.304*	0.276	-0.319*	
$\Delta(\text{T}_5)$	0.612**	0.005	0.310*	0.310*	-0.043	-0.535**	-0.306*	-0.414**	0.348*	-0.438**	
$\Delta(\text{W}_1)$	-0.174	-0.024	-0.201	-0.202	-0.269	-0.301*	-0.276	0.012	0.054	-0.029	
$\Delta(\text{A}_2)$	-0.529**	-0.477**	-0.567**	-0.568**	-0.304*	-0.072	-0.309*	0.470**	-0.157	0.462**	
$\Delta(\text{A}_3)$	-0.545**	-0.448**	-0.587**	-0.588**	-0.304*	-0.238	-0.355*	0.260	-0.048	0.278	
$\Delta(\text{A}_4)$	-0.569**	-0.420**	-0.609**	-0.610**	-0.325*	-0.185	-0.367**	0.352*	-0.122	0.356*	
$\Delta(\text{A}_5)$	-0.580**	-0.403**	-0.592**	-0.592**	-0.317*	-0.153	-0.324*	0.334*	-0.089	0.313*	

		$\Delta(\text{NN})$	$\Delta(\text{SDNN})$	$\Delta(\text{rMSSD})$	$\Delta(\text{SDSD})$	$\Delta(\text{pNN50})$	$\Delta(\text{LF})$	$\Delta(\text{HF})$	$\Delta(\text{LF norm})$	$\Delta(\text{HF norm})$	$\Delta(\text{LF/HF})$
$\Delta(\text{PTT})$		0.323*	-0.117	0.206	0.205	-0.393**	-0.194	-0.291*	0.284	-0.047	0.235
$\Delta(\text{SDPTT})$		-0.338*	0.283	0.058	0.062	-0.097	0.649**	0.522**	0.081	-0.117	0.096
$\Delta(\text{rMSSD}^{\text{PTT}})$		-0.328*	0.155	-0.009	-0.006	-0.153	0.630**	0.482**	0.114	-0.078	0.120
$\Delta(\text{SDSD}^{\text{PTT}})$		-0.329*	0.155	-0.010	-0.007	-0.153	0.630**	0.482**	0.114	-0.078	0.121

		$\Delta(\text{T}_1)$	$\Delta(\text{T}_2)$	$\Delta(\text{T}_3)$	$\Delta(\text{T}_4)$	$\Delta(\text{T}_5)$	$\Delta(\text{W}_1)$	$\Delta(\text{A}_2)$	$\Delta(\text{A}_3)$	$\Delta(\text{A}_4)$	$\Delta(\text{A}_5)$
$\Delta(\text{PTT})$		0.421**	0.393**	0.411**	0.446**	0.419**	0.398**	0.000	-0.092	0.095	0.083
$\Delta(\text{SDPTT})$		-0.186	-0.119	-0.161	-0.190,	-0.184	-0.172	-0.175	-0.274	-0.204	-0.208
$\Delta(\text{rMSSD}^{\text{PTT}})$		-0.238	-0.118	-0.129	-0.168	-0.156	-0.233	-0.153	-0.270	-0.208	-0.203
$\Delta(\text{SDSD}^{\text{PTT}})$		-0.238	-0.118	-0.129	-0.168	-0.157	-0.233	-0.153	-0.270	-0.207	-0.202

* p < 0.01, ** p < 0.001

Table 4.25: Correlation coefficients between relative changes in PDA, HRV and PTT features for exposure \mathcal{C} after three hours.

		Exposure type \mathcal{D}									
	$\Delta(\text{NN})$	$\Delta(\text{SDNN})$	$\Delta(\text{rMSSD})$	$\Delta(\text{SDSD})$	$\Delta(\text{pNN50})$	$\Delta(\text{LF})$	$\Delta(\text{HF})$	$\Delta(\text{LF norm})$	$\Delta(\text{HF norm})$	$\Delta(\text{LF/HF})$	
$\Delta(\text{T}_1)$	-0.286	-0.351*	-0.202	-0.202	-0.295*	0.054	-0.062	0.171	-0.021	0.139	
$\Delta(\text{T}_{12})$	-0.048	0.003	-0.027	-0.027	-0.130	-0.036	-0.111	0.303*	-0.049	0.276	
$\Delta(\text{T}_{13})$	0.122	0.279	0.382**	0.382**	0.184	0.049	0.155	0.043	0.098	-0.012	
$\Delta(\text{T}_{14})$	0.236	0.333*	0.522**	0.522**	0.299*	0.016	0.209	-0.107	0.162	-0.165	
$\Delta(\text{T}_{15})$	0.463**	0.436**	0.645**	0.645**	0.439**	-0.106	0.146	-0.202	0.185	-0.267	
$\Delta(\text{W}_1)$	-0.237	-0.360*	-0.224	-0.224	-0.310*	0.032	-0.124	0.208	-0.030	0.160	
$\Delta(\text{A}_{12})$	-0.597**	-0.232	-0.231	-0.231	-0.324*	0.218	0.283	-0.035	0.017	0.071	
$\Delta(\text{A}_{13})$	-0.472**	-0.339*	-0.140	-0.140	-0.288*	0.272	0.295*	-0.045	-0.017	0.135	
$\Delta(\text{A}_{14})$	-0.669**	-0.267	-0.194	-0.194	-0.341*	0.412**	0.445**	-0.041	0.050	0.031	
$\Delta(\text{A}_{15})$	-0.701**	-0.308*	-0.210	-0.210	-0.390**	0.350*	0.435**	-0.068	0.117	-0.016	

	$\Delta(\text{NN})$	$\Delta(\text{SDNN})$	$\Delta(\text{rMSSD})$	$\Delta(\text{SDSD})$	$\Delta(\text{pNN50})$	$\Delta(\text{LF})$	$\Delta(\text{HF})$	$\Delta(\text{LF norm})$	$\Delta(\text{HF norm})$	$\Delta(\text{LF/HF})$
$\Delta(\text{PTT})$	0.422**	0.079	0.087	0.087	0.118	-0.309*	-0.256	0.015	-0.037	0.086
$\Delta(\text{SDPTT})$	0.151	0.159	0.094	0.095	0.323*	0.082	-0.008	0.024	-0.158	0.048
$\Delta(\text{rMSSD}^{\text{PTT}})$	0.154	0.014	0.213	0.213	0.422**	0.009	0.032	-0.072	-0.032	-0.034
$\Delta(\text{SDSD}^{\text{PTT}})$	0.151	0.013	0.209	0.209	0.419**	0.010	0.031	-0.071	-0.033	-0.032

	$\Delta(\text{T}_1)$	$\Delta(\text{T}_{12})$	$\Delta(\text{T}_{13})$	$\Delta(\text{T}_{14})$	$\Delta(\text{T}_{15})$	$\Delta(\text{W}_1)$	$\Delta(\text{A}_{12})$	$\Delta(\text{A}_{13})$	$\Delta(\text{A}_{14})$	$\Delta(\text{A}_{15})$
$\Delta(\text{PTT})$	-0.165	-0.046	-0.248	-0.213	-0.097	-0.155	-0.205	-0.037	-0.386**	-0.422**
$\Delta(\text{SDPTT})$	-0.315*	-0.193	-0.264	-0.272	-0.225	-0.335*	-0.091	-0.190	-0.280	-0.378**
$\Delta(\text{rMSSD}^{\text{PTT}})$	-0.255	-0.206	-0.185	-0.163	-0.121	-0.293*	-0.066	-0.110	-0.229	-0.299*
$\Delta(\text{SDSD}^{\text{PTT}})$	-0.255	-0.205	-0.185	-0.165	-0.124	-0.294*	-0.064	-0.111	-0.228	-0.298*

* p < 0.01, ** p < 0.001

Table 4.26: Correlation coefficients between relative changes in PDA, HRV and PTT features for exposure \mathcal{D} after three hours.

Chapter 5

Discussion

The present work investigates the influence of exposure to biodiesel exhaust gases on cardiovascular function in human. Measurements of changes in PPG pulse waveform, by implementing a pulse decomposition analysis (PDA), and study of pulse transit time over exposure time are performed for assessment of vascular compliance properties. In addition, HRV analysis is used for the purpose of evaluation of ANS functioning. A discussion interpreting the results is presented in this part of the report. Ethical considerations, limitations of this work, as well as opportunities for further development are also addressed.

5.1 Critical review of the results

Minor changes in PDA-derived features with exposure types are highlighted during this study. Indeed, an increase in amplitude loss between main wave and reflected ones is observed after three hours into exposure to biodiesel exhaust. This mainly concerns morphological features A_{13} (during session \mathcal{D}) and A_{14} (during session \mathcal{C}), but also A_{15} (for \mathcal{B} and \mathcal{C}). Previously described changes in vascular compliance related features A_{13} and A_{14} are observed in, respectively, 13 out of 18 and 12 out of 17 study participants, allowing to conclude that they are reasonably consistent among test persons. However, they are not found to be statistically significant compared to results obtained during exposure to air enriched with NaCl salt particles (\mathcal{B}). Still, they could be construed as first signs of an increase in arterial stiffness during exposure to biodiesel exhaust. In fact, the reduced distensibility of arteries implies an earlier return of reflected waves, which arrive during systole rather than diastole [9]. Thus, an increment in parameters A_{13} , A_{14} and A_{15} relates to a larger rise in systolic pressure and a larger decline in diastolic blood pressure [17]. No change in any other PDA-derived features is observed with exposure types. In addition, PTT

parameters remain nearly unchanged across all stages of the experimental protocol, providing no further information about the relationship between exposure to biodiesel exhaust and vascular compliance properties. HRV analysis does not highlight any statistical variation with exposure types. Exposure to biodiesel exhaust is therefore not proven to imply any significant change in ANS functioning. However, a negative correlation was found between vascular compliance related parameters A_{13} , A_{14} and A_{15} and time-domain HRV statistics. A decreased HRV is usually associated with cardiac failure or myocardial infarction. It would be in line with a shift in the autonomic balance, inducing a stress response of the cardiovascular system during exposure to biodiesel exhaust. Finally, the Pearson analyses also indicate that there exists a statistical positive correlation between mean NN interval and mean PTT estimate, for all exposure types. Further investigations are required regarding the relationships between those variables, to determine its potential usefulness for future applications.

This work is one of the first studies to assess the effects of biodiesel exhaust on cardiovascular function, making the comparison to current literature further complicated. On a first side, heart rate variability analysis is a major method used in research related to air pollution, mainly applied to explore mechanisms by which it may induce an increased respiratory and cardiovascular mortality. However, the assessed effects of air pollutants on HRV are not entirely consistent across studies. Some of them reported a decrease in heart rate variability statistics in elderly subjects [6], while others determined that there was no consistent effect of exposure to diesel exhaust on HRV parameters [25]. Potential factors that may explain these divergences are, for instance, age, gender and health status of test persons, composition of gases, or even the use of different methods for HRV analysis. On the other side, the relationship between exposure to diesel exhaust and arterial stiffness was previously observed. Diesel exhaust inhalation was proven to induce a decrease in vascular compliance of elastic arteries immediately after exposure [7]. Very few studies were available to assess the impact of biodiesel exhaust gases on cardiovascular function in human. No change in HRV indexes or in arterial stiffness was reported in any of them. However, one study demonstrated that exhaust from biodiesel induced acute adverse cardiovascular effects of increased thrombus formation and impaired vasomotor function in man [26].

5.2 Limits of the study

A limitation in this study is the high dependency on recording quality regarding both pulse decomposition and heart rate variability analyses. In fact, poor quality may directly impact the PPG pulse waveform, not en-

abling proper computation of inner waves and extraction of morphological features. Moreover, poor quality affects the accuracy in detecting the fiducial points in PPG signals, and thus necessarily the computation of PTT series. In any case, these issues highly depend on the sampling frequency and the morphology of the pulse waveform. If the pulse shape stays consistent over time, the analysis of PTT series remains reliable. Otherwise, another method less sensitive to those variations should be used for accurate PPG pulse detection and definition. For example, wave definition by least-square optimization would likely be a more robust alternative to define accurate parameters in this case [27]. It can be noted that this also applies to detection of heart beats in ECG recordings, even though R waves reach larger amplitudes and therefore remain far easier to detect. In this study, several recordings were of poor quality, not enabling further analysis of the signals. Since the number of study participants was already low, the reduced quality of some recordings constitutes a significant limit of this work.

Another limitation of this study is the high variability of individual responses during the experimental protocol. In our case, 19 study participants completed the whole experimental protocol. Pre-exposure, no statistical difference was found between results of study participants. However, the significant range of PDA, HRV and PTT responses forced us to compute relative changes in all parameters to compare the actual effects of every exposure type. As an example, results obtained during exposure to filtered air (\mathcal{A}) or air enriched in NaCl salt particles (\mathcal{B}) were quite dissimilar, sometimes following opposite trends, and thus making the comparison with exposure to biodiesel exhaust even more complicated. Therefore it is likely that the large range of responses during exposure to various gases may have overwhelmed the small adverse effects of exposure to biodiesel exhaust on ANS and regarding vascular compliance properties. To increase the number of study participants could contribute to reduce the intra- and inter-subjects variability of the responses and obtain statistically relevant results regarding vascular compliance properties or HRV statistics. Also, this would allow for sub-group analysis, which was not possible in this study with only 19 participants. For example, the relationship between arterial stiffening and air pollution is assumed to be age-dependent. It was not possible to study it accurately in the context of this thesis.

5.3 Ethical considerations

In this study, all participants were volunteers and gave their informed consent before the whole experiment was carried out. The study was conducted in accordance with the Declaration of Helsinki, and approved by the local research ethics committee. Study participants who completed the experi-

mental protocol were exposed to various gases, like biodiesel exhaust, in a controlled and ethically-approved manner. This makes the ethical aspects considered.

5.4 Future work

Next steps in possible future work would be to pursue studies related to adverse effects of exposure to greenhouse gases in human. By now, many researches focused on studying the relationship between air pollution and human health effects, but the exact connection between both variables remains poorly understood. Moreover, this thesis is one of the first studies to assess the effects of exposure to biofuel exhaust on cardiovascular function in human. Very little information exists in the current literature, making the comparison with our results complex. Thus, it is of substantial interest to pursue studies related to exposure to air pollution, but more precisely to biofuel exhaust inhalation.

Given the large range of responses obtained by PDA, HRV or PTT analysis in this thesis, further studies should be based on larger groups of subjects. This is primordial, to ensure that results are statistically relevant, but also to be able to detect minor changes due to exposure to toxicant particles among variations related to natural intra- and inter-subject variability. Larger groups of study participants would also enable subgroup analyses, for instance based on age, sex or even health status of persons.

Finally, during this work, but also in previous studies [17], pulse decomposition analysis was only performed with on fingertip PPG signals. PPG segments recorded at other locations of the body may have a different morphology from that studied in this thesis. The current PDA method can not be generalized to all types of PPG signals in an automatic way and should be adapted. Therefore, further studies, based on PPG signals acquired from various sites of the body, should be conducted for assessing the impact of the recording location on the PDA results.

Chapter 6

Conclusion

In conclusion, the aim of this thesis was to investigate the effects of exposure to biodiesel exhaust gases on cardiovascular function in human. It was fulfilled by analyzing both ECG and PPG signals from study participants. Measures of changes in PPG waveforms, complemented by computation of pulse transit time (PTT) were performed for assessment of vascular compliance properties. In addition, calculation of heart rate variability (HRV) statistics was used for evaluation of the autonomic nervous system (ANS). PDA-derived results may be related to an increase in arterial stiffness after three hours into exposure to biodiesel exhaust. No statistical change in PTT parameters was estimated, which does not confirm the previous observation. There was also no effect of exposure to biodiesel exhaust on HRV indicators. The large range of responses obtained for PDA, HRV and PTT series during exposure to various gases constitutes the major limitation to this work. Further studies are necessary to determine the exact connection between exposure to biofuel exhaust and cardiovascular effects in human. Those researches should definitely be based on larger groups of study participants to compensate for the high intra- and inter-subject variability of responses.

Bibliography

- [1] A.C. Pinto, L.L.N. Guarieiro, M.J.C. Rezende, N.M. Ribeiro, E.A. Torres, W.A. Lopes, P.A.P. Pereira, and J.B. de Andrade. Biodiesel: An overview. *J Braz Chem Soc*, 16(6B):1313–1330, 2005.
- [2] S. Steiner, C. Bisig, A. Petri-Fink, and B. Rothen-Rutishauser. Diesel exhaust: current knowledge of adverse effects and underlying cellular mechanisms. *Arch Toxicol*, 90:1541–1553, 2016.
- [3] A. Lankoff, K. Brzoska, J. Czarnocka, M. Kowalska, H. Lisowska, R. Mruk, J. Øvrevik, A. Wegierek-Ciuk, M. Zuberek, and M. Kruszewski. A comparative analysis of in vitro toxicity of diesel exhaust particles from combustion of 1st- and 2nd-generation biodiesel fuels in relation to their physicochemical properties — the fuelhealth project. *Environ Sci Pollut Res*, 24:19357–19374, 2017.
- [4] D.W. Dockery, C.A. Pope, X. Xu, J.D. Spengler, J.H. Ware, M.E. Fay, B.G. Ferris, and F.E. Speizer. An association between air pollution and mortality in six u.s. cities. *N Engl J Med*, 329(24):1753–1759, 1993.
- [5] D.H. Rivero, S.R. Soares, G. Lorenzi-Filho, M. Saiki, J.J. Godleski, L. Antonangelo, M. Dolhnikoff, and P.H. Saldiva. Acute cardiopulmonary alterations induced by fine particulate matter of são paulo, brazil. *Toxicological Sciences*, 85:898–905, 2005.
- [6] C.A. 3rd Pope, M.L. Hansen, R.W. Long, K.R. Nielsen, N.L. Eatough, W.E. Wilson, and D.J. Eatough. Ambient particulate air pollution, heart rate variability, and blood markers of inflammation in a panel of elderly subjects. *Environ. Health Perspect*, 112:339–345, 2004.
- [7] M. Lundbäck, N.L. Mills, A. Lucking, S. Barath, K. Donaldson, D.E. Newby, T. Sandström, and A. Blomberg. Experimental exposure to diesel exhaust increases arterial stiffness in man. *Particle and Fibre Toxicology*, 6(7), 2009.
- [8] J.M. Brito, L. Belotti, A.C. Toledo, L. Antonangelo, F.S. Silva, D.S. Alvim, P.A. Andre, P.H.N. Saldiva, and D.H.R.F. Rivero. Acute car-

- diovascular and inflammatory toxicity induced by inhalation of diesel and biodiesel exhaust particles. *Toxicological Sciences*, 116:67–68, 2010.
- [9] M. Elgendi. On the analysis of fingertip photoplethysmogram signals. *Current Cardiology Reviews*, 8:14–25, 2012.
- [10] E. Gil, M. Orini, E. Bailòn, J.M. Vergara, L. Mainardi, and P. Laguna. Photoplethysmography pulse rate variability as a surrogate measurement of heart rate variability during non-stationary conditions. *Physiol. Meas.*, 31:1271–1290, 2010.
- [11] T. Tamura, Y. Maeda, M. Sekine, and M. Yoshida. Wearable photoplethysmographic sensors - past and present. *Electronics*, 3:282–302, 2014.
- [12] L. Sörnmo and P. Laguna. *Bioelectrical signal processing in cardiac and neurological applications*. Elsevier, 2005.
- [13] U. Rubins. Finger and ear photoplethysmogram waveform analysis by fitting with gaussians. *Med Biol Eng Comput*, 46:1271–1276, 2008.
- [14] Q. Yousef, M.B.I. Reaz, and M.A.M. Ali. The analysis of ppg morphology: Investigating the effects of aging on arterial compliance. *Measurement Science Review*, 12, 2012.
- [15] K. Pilt, R. Ferenets, K. Meigas, L.G. Lindberg, K. Temitski, and M. Viigimaa. New photoplethysmographic signal analysis algorithm for arterial stiffness estimation. *The Scientific World Journal*, 2013.
- [16] C. Liu, D. Zheng, A. Murray, and C. Liu. Modeling carotid and radial artery pulse pressure waveforms by curve fitting with gaussian functions. *Biomedical Signal Processing and Control*, 8:449–454, 2013.
- [17] S. Kontaxis, E. Gil, V. Marozas, J. Lazaro, E. Garcia, M. Posadas-de Miguel, S. Siddi, M.L. Bernal, J. Aguilo, J.M. Haro, C. De La Camara, P. Laguna, and R. Bailon. Photoplethysmographic waveform analysis for autonomic reactivity assessment in depression. *IEEE Trans Biomed Eng*, 2020.
- [18] A. Wang, L. Yang, W. Wen, S. Zhang, G. Gu, and D. Zheng. Gaussian modelling characteristics changes derived from finger photoplethysmographic pulses during exercise and recovery. *Microvascular Research*, 116:20–25, 2018.
- [19] R. Sassi, S. Cerutti, F. Lombardi, M. Malik, H.V. Huikuri, C.K. Peng, G. Schmidt, and Y. Yamamoto. Advances in heart rate variability signal analysis: joint position statement by the e-cardiology esc working

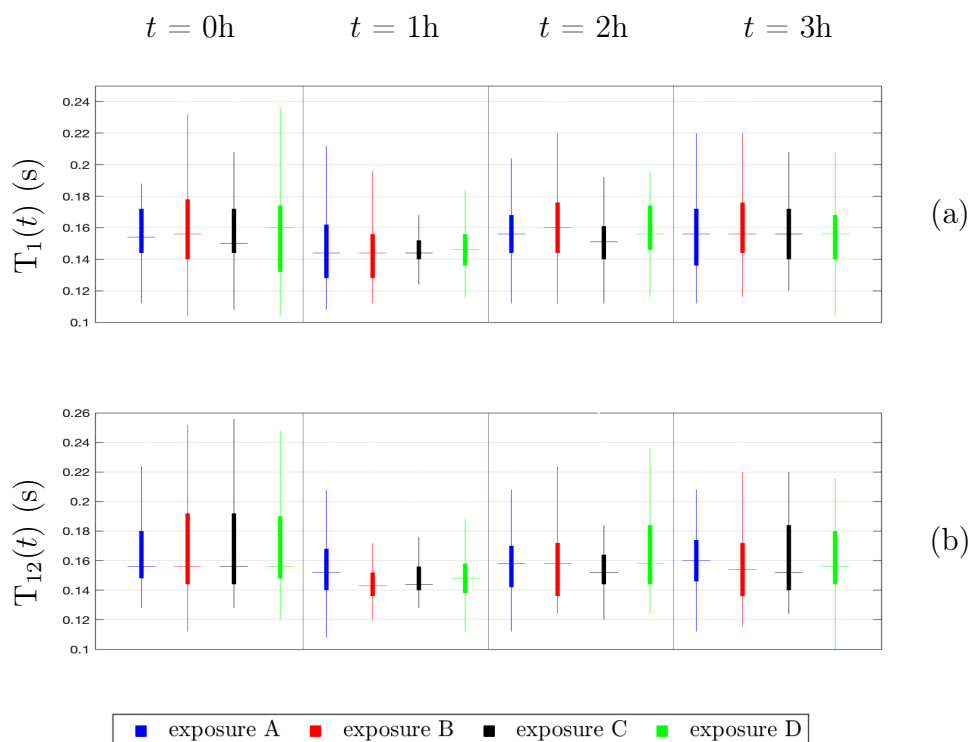
- group and the european heart rhythm association co-endorsed by the asia pacific heart rhythm society. *Europace*, 17:1341–1353, 2015.
- [20] R. Mukkamala, J.O. Hahn, O.T. Inan, L.K. Mestha, C.S. Kim, H. Töreyn, and S. Kyal. Toward ubiquitous blood pressure monitoring via pulse transit time: Theory and practice. *IEEE Transactions on Biomedical Engineering*, 62(8), 2015.
- [21] B. Olde and M. Holmer. Functional description of cardio logger. 2014.
- [22] P. Armañac, P. Kontaxis, J. Lázaro, P. Laguna, R. Bailón, and E. Gil. Cardiovascular changes induced by acute emotional stress estimated from the pulse transit time difference. *Computing in Cardiology*, 46:1–4, 2019.
- [23] E.J. Argüello-Prada. The mountaineer’s method for peak detection in photoplethysmographic signals. *Revista Facultad de Ingeniería, Universidad de Antioquia*, 90:42–50, 2019.
- [24] M. Lagerholm, C. Peterson, G. Braccini, L. Edenbrandt, and L. Sörnmo. Clustering ecg complexes using hermite functions and self-organizing maps. *IEEE Transactions on Biomedical Engineering*, 47(7):838–848, 2000.
- [25] A. Peretz, J.D. Kaufman, C.A. Trenga, J. Allen, C. Carlsten, M.R. Aulet, S.D. Adar, and J.H. Sullivan. Effects of diesel exhaust inhalation on heart rate variability in human volunteers. *Environmental Research*, 107:178–184, 2008.
- [26] J. Unosson. Acute cardiovascular effects of biofuel exhaust exposure. *Phd Dissertation, Umeå Universitet*, 2014.
- [27] A. Sološenkoa, A. Petrénsa, V. Marozasa, and L. Sörnmo. Modeling of the photoplethysmogram during atrial fibrillation. *Computers in Biology and Medicine*, 81:130–138, 2017.

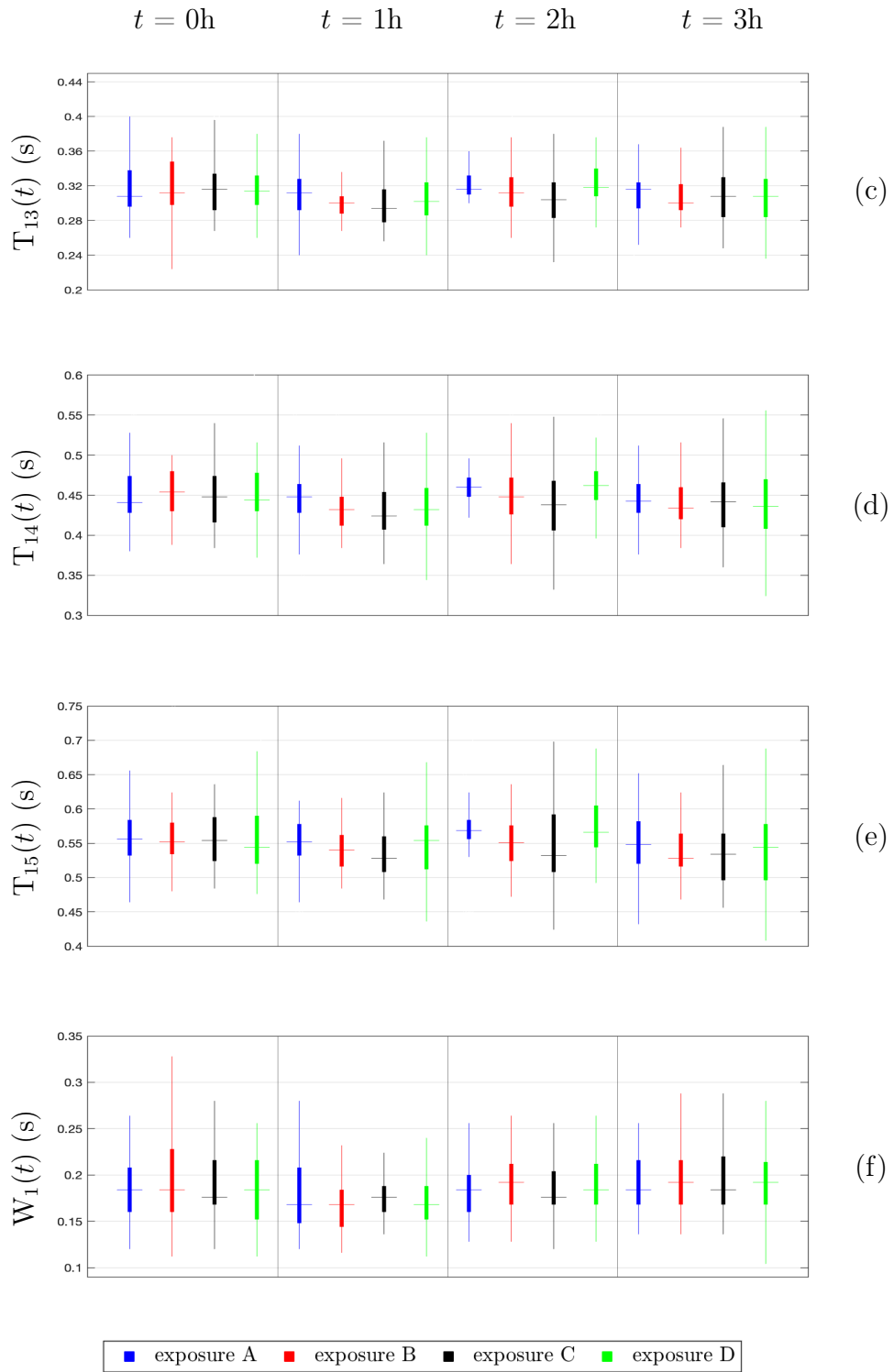
Appendix A

Pulse waveform analysis

Preliminary comment: In the following appendices, functional boxplots are presented. For each boxplot, the mid-line corresponds to the median value. The broadest part is limited by the quantiles 25 and 75. The wide line begins at the non-outlier minimum and ends at the non-outlier maximum.

A.1 Changes in PDA-derived features over time





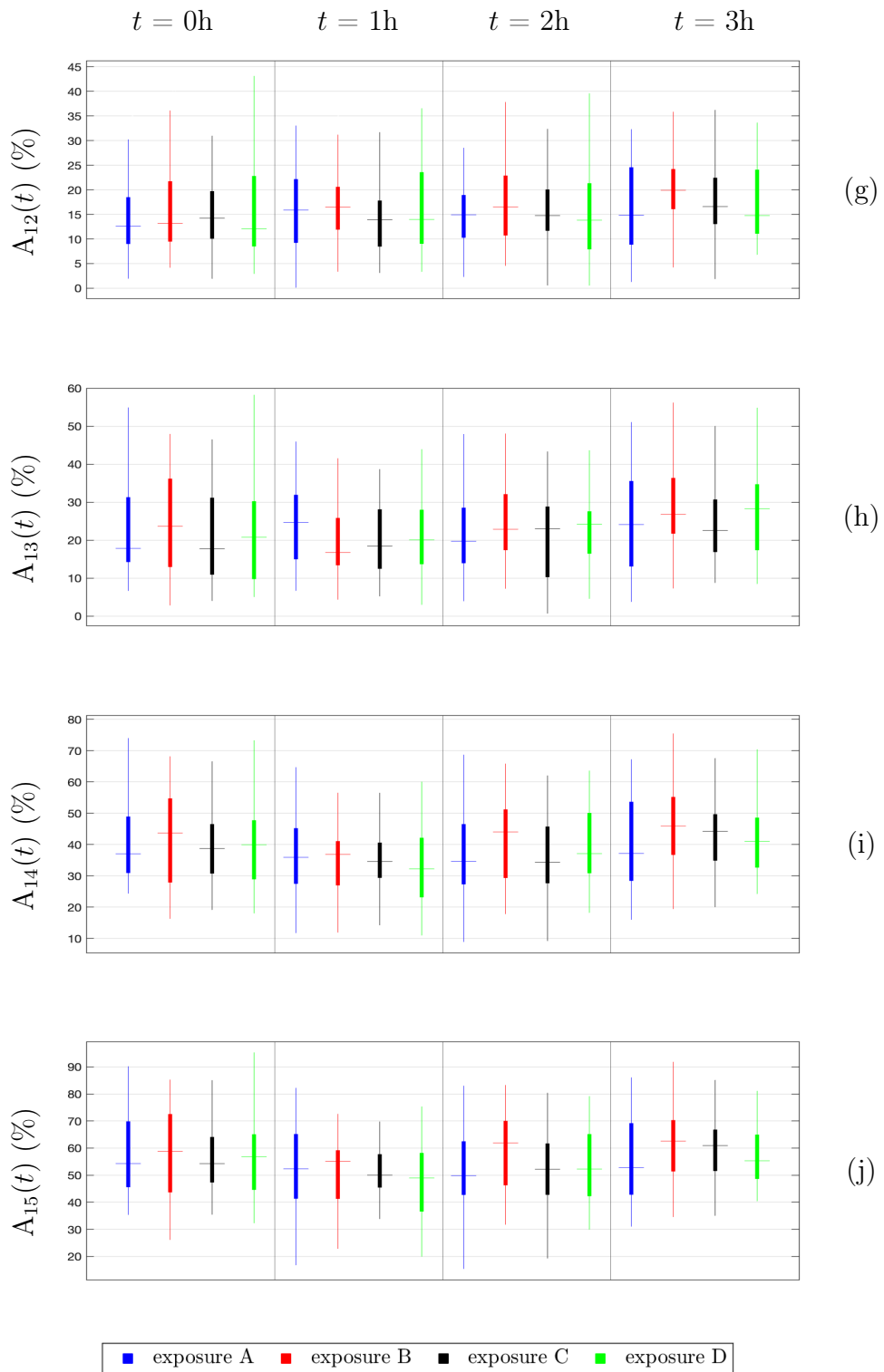
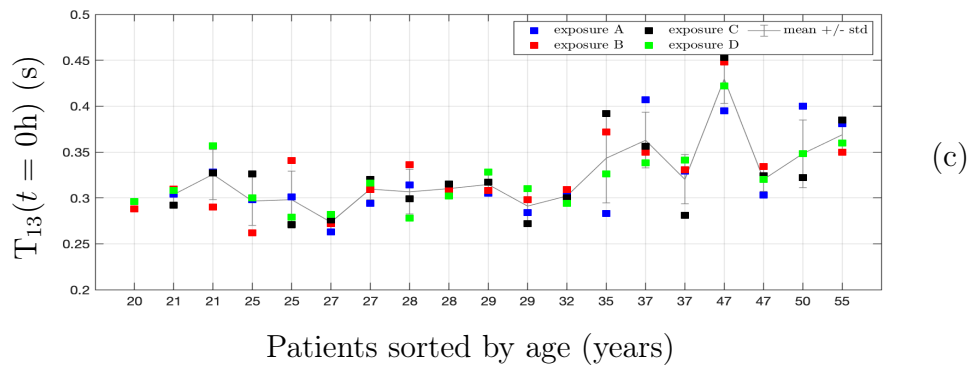
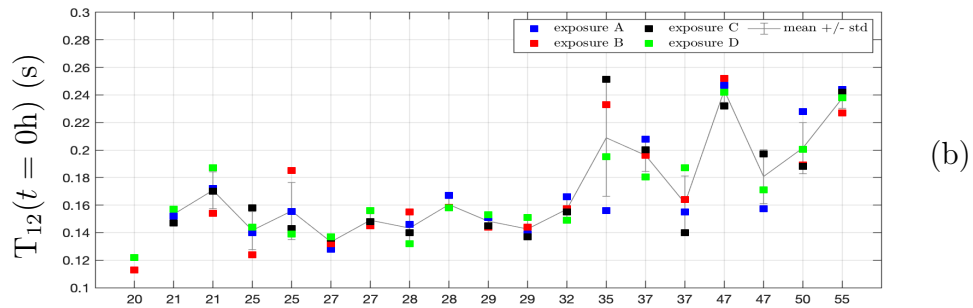
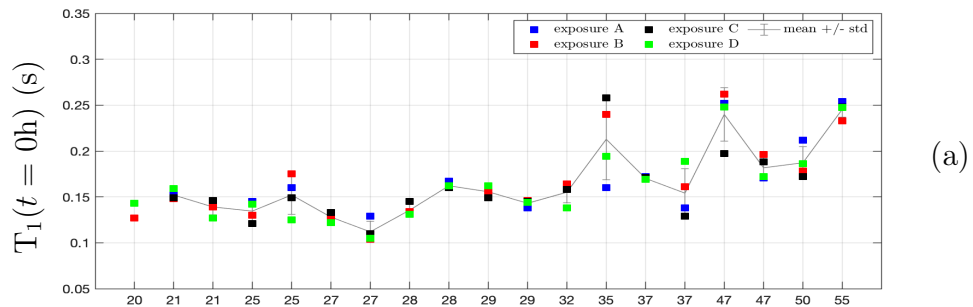
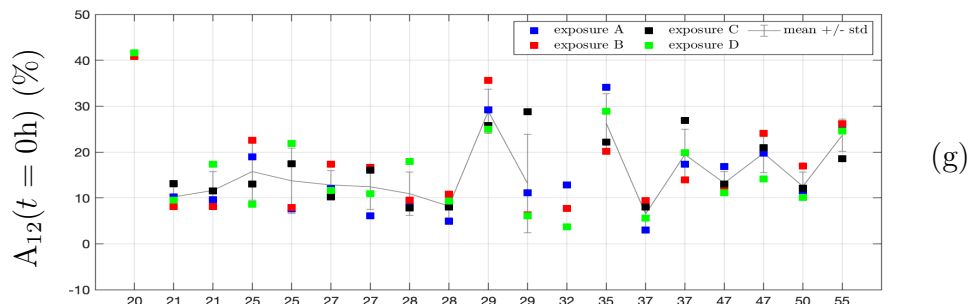
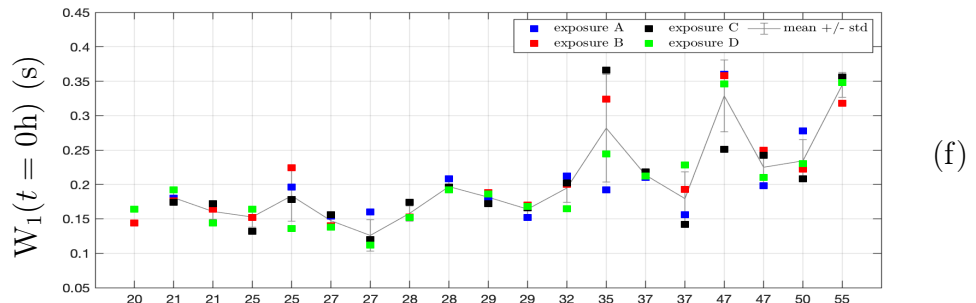
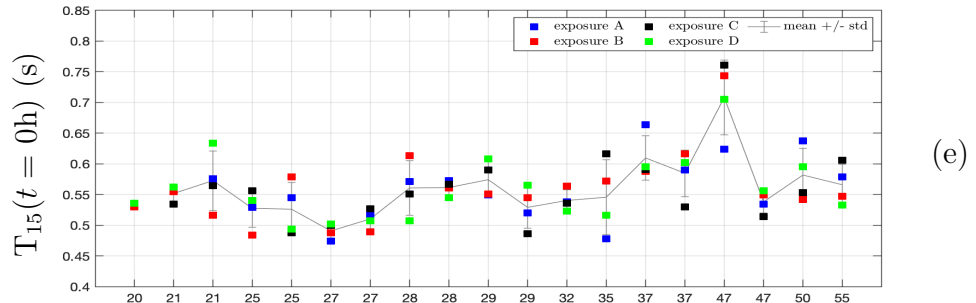
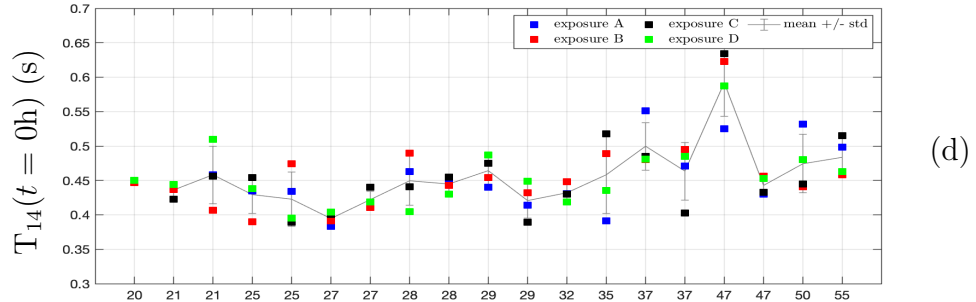


Figure A.1: Functional boxplots of PDA-derived characteristics.

A.2 Variability of PDA-derived features at basal condition



Patients sorted by age (years)



Patients sorted by age (years)

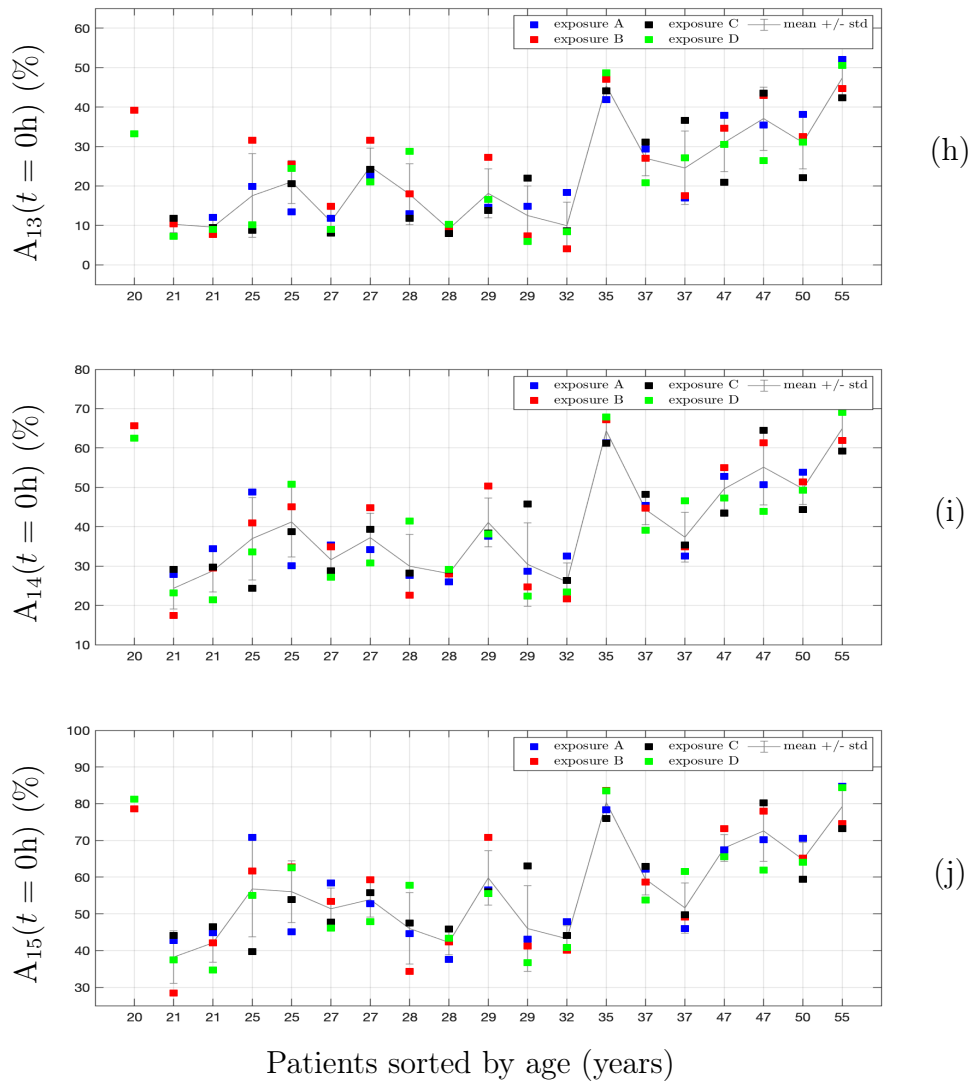
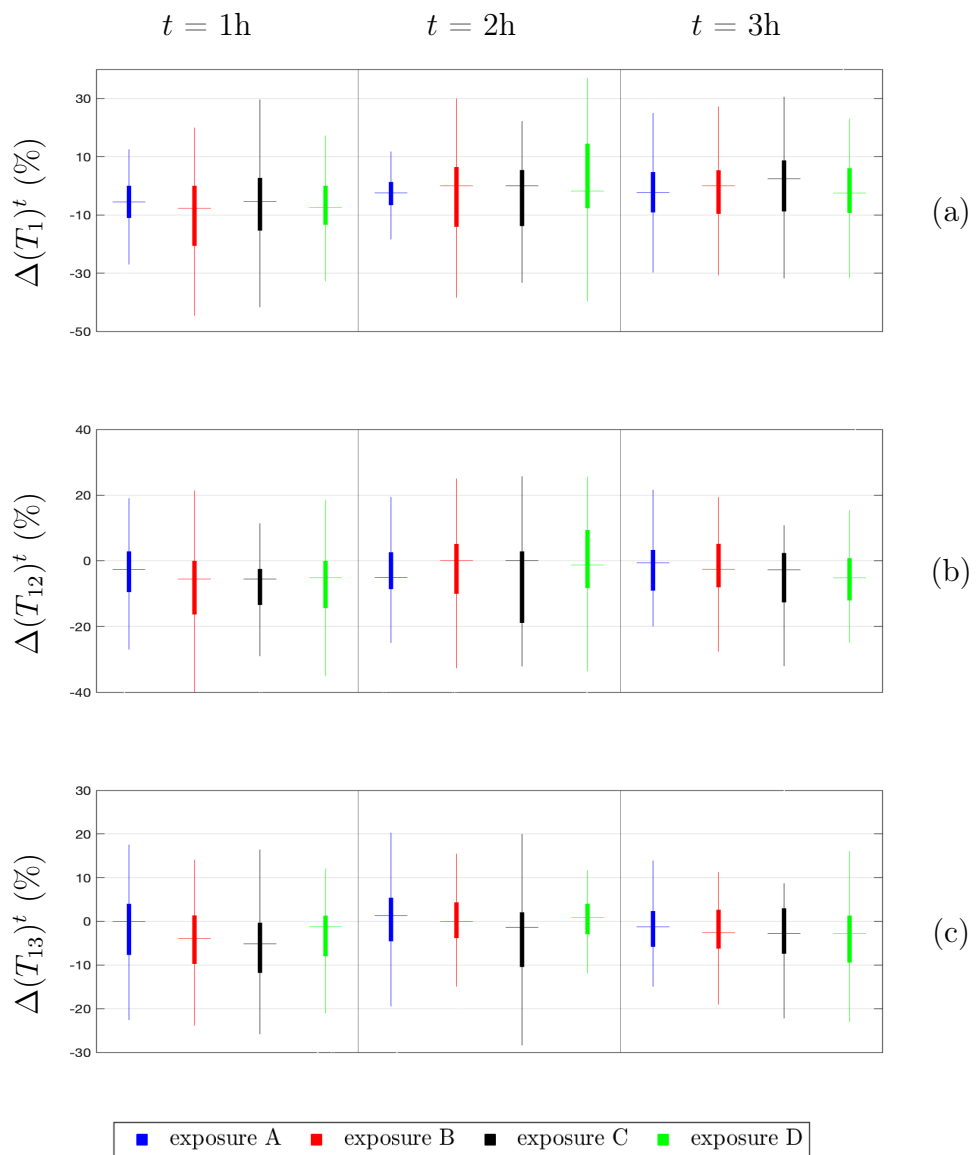
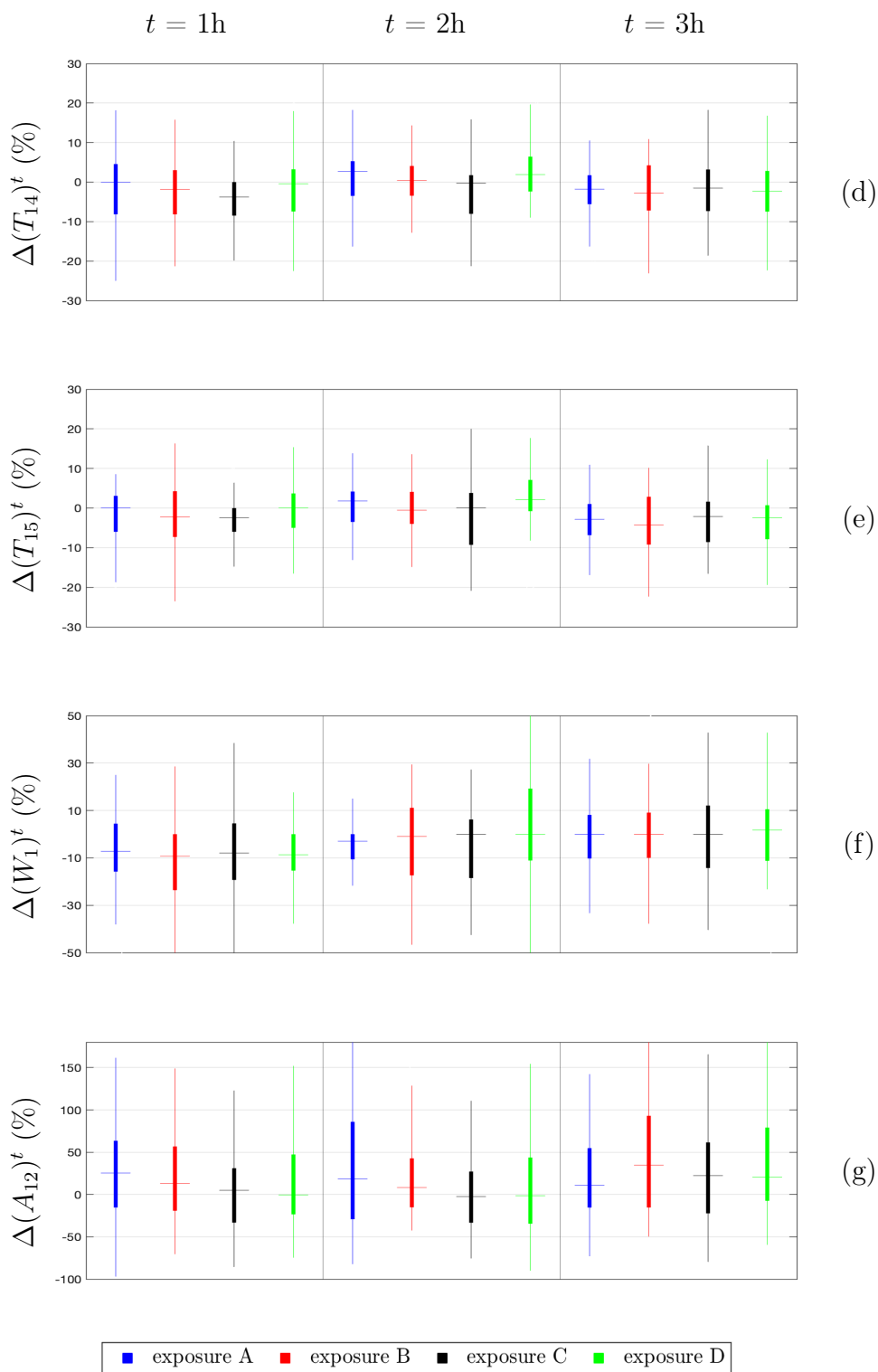


Figure A.2: Median values of PDA-derived features at basal condition for every patient and exposure type.

A.3 Changes in PDA-derived features with exposure type





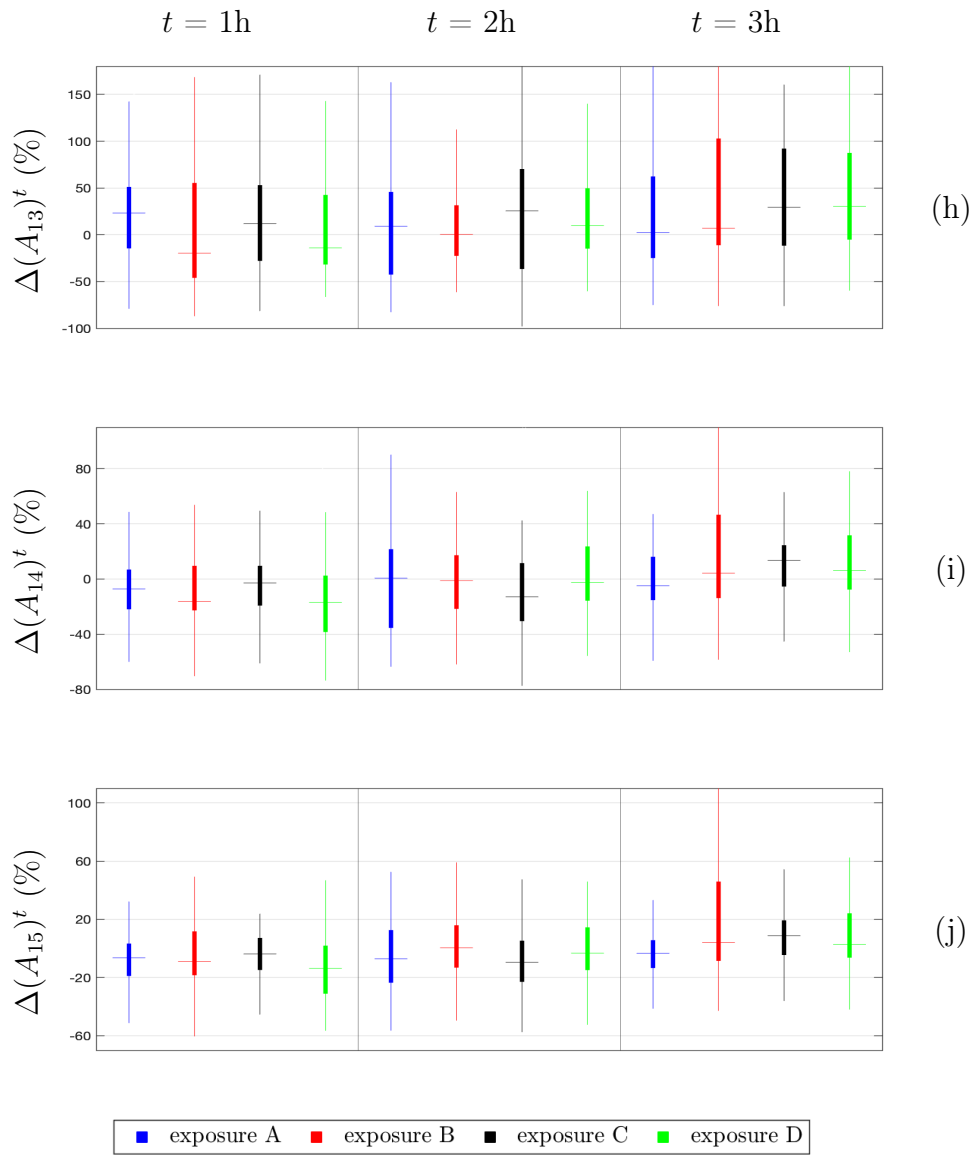
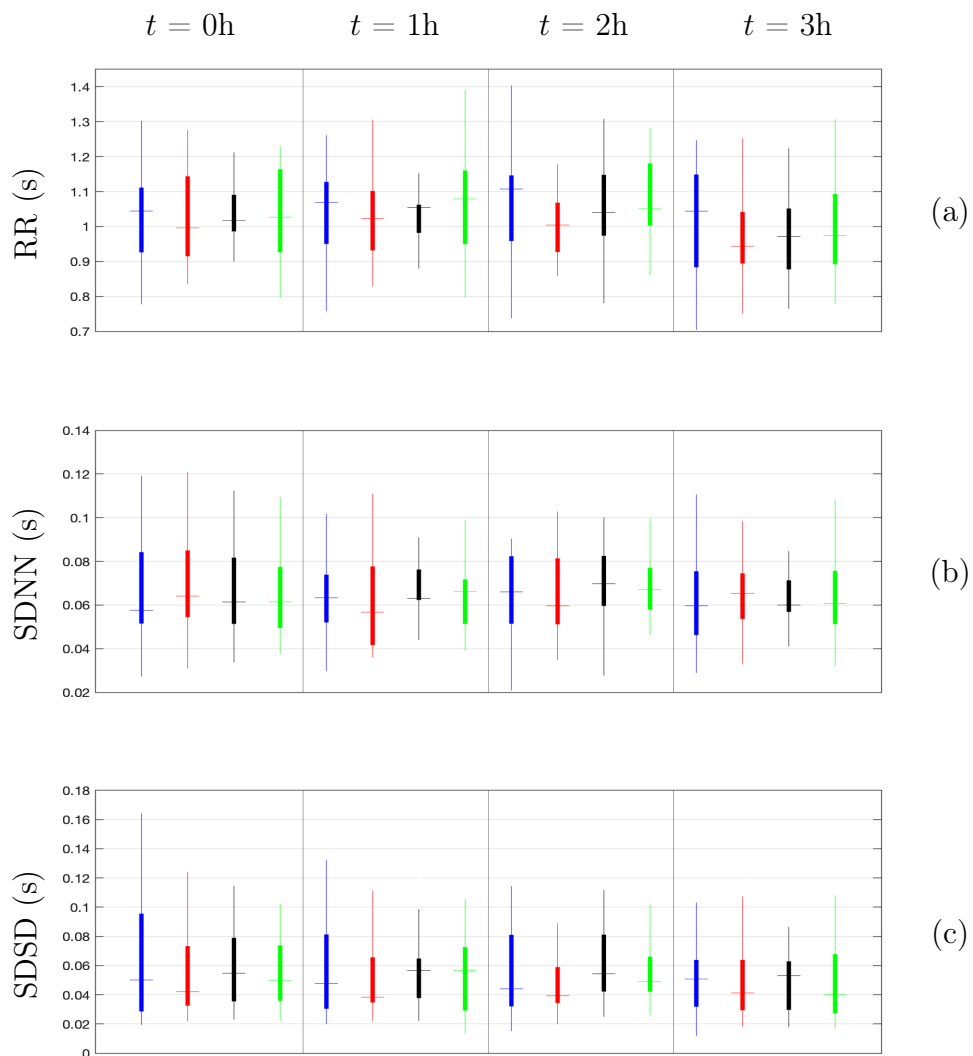


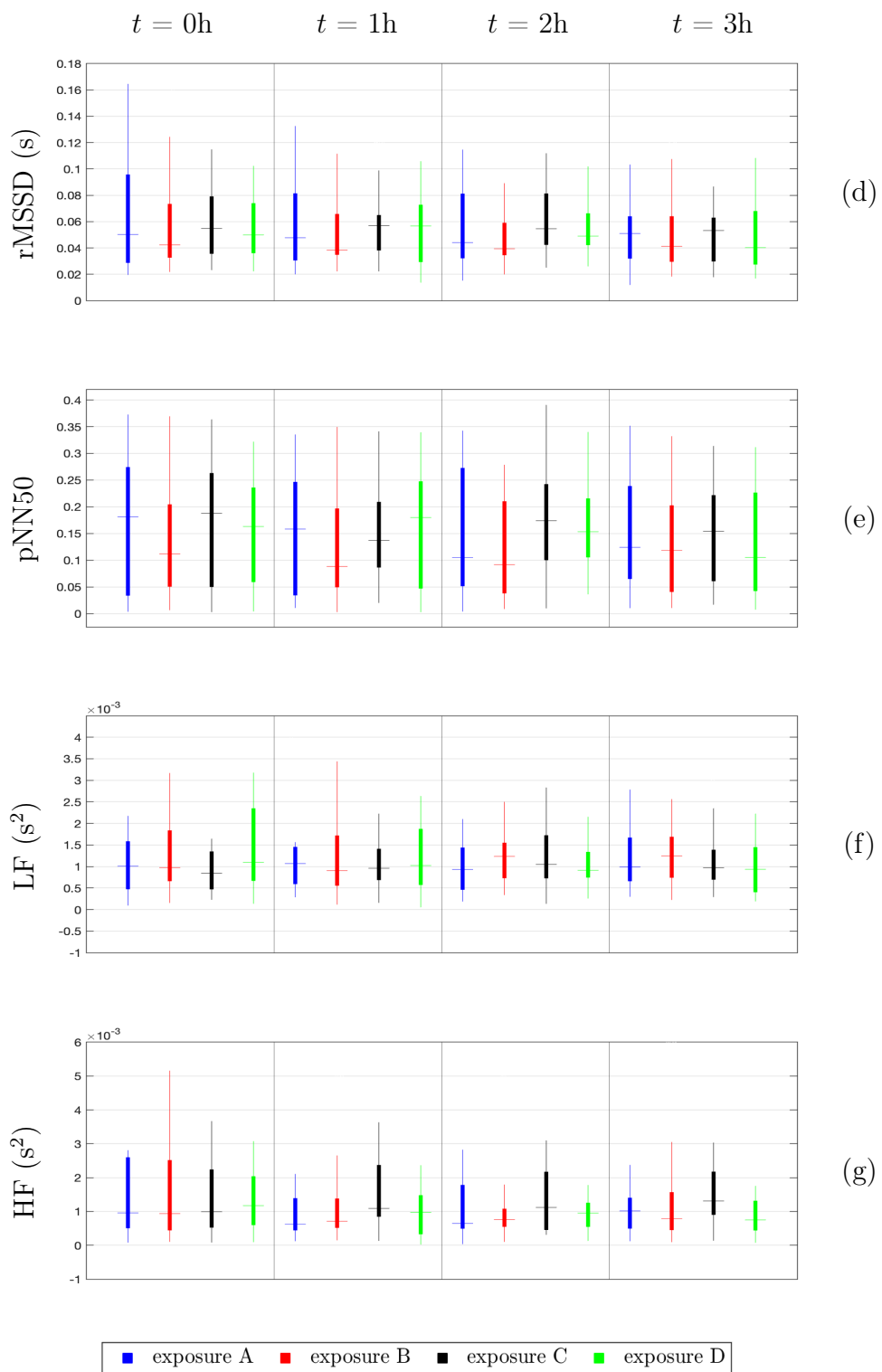
Figure A.3: Functional boxplots of relative changes in PDA-derived features.

Appendix B

Heart rate variability analysis

B.1 Changes in HRV parameters over time





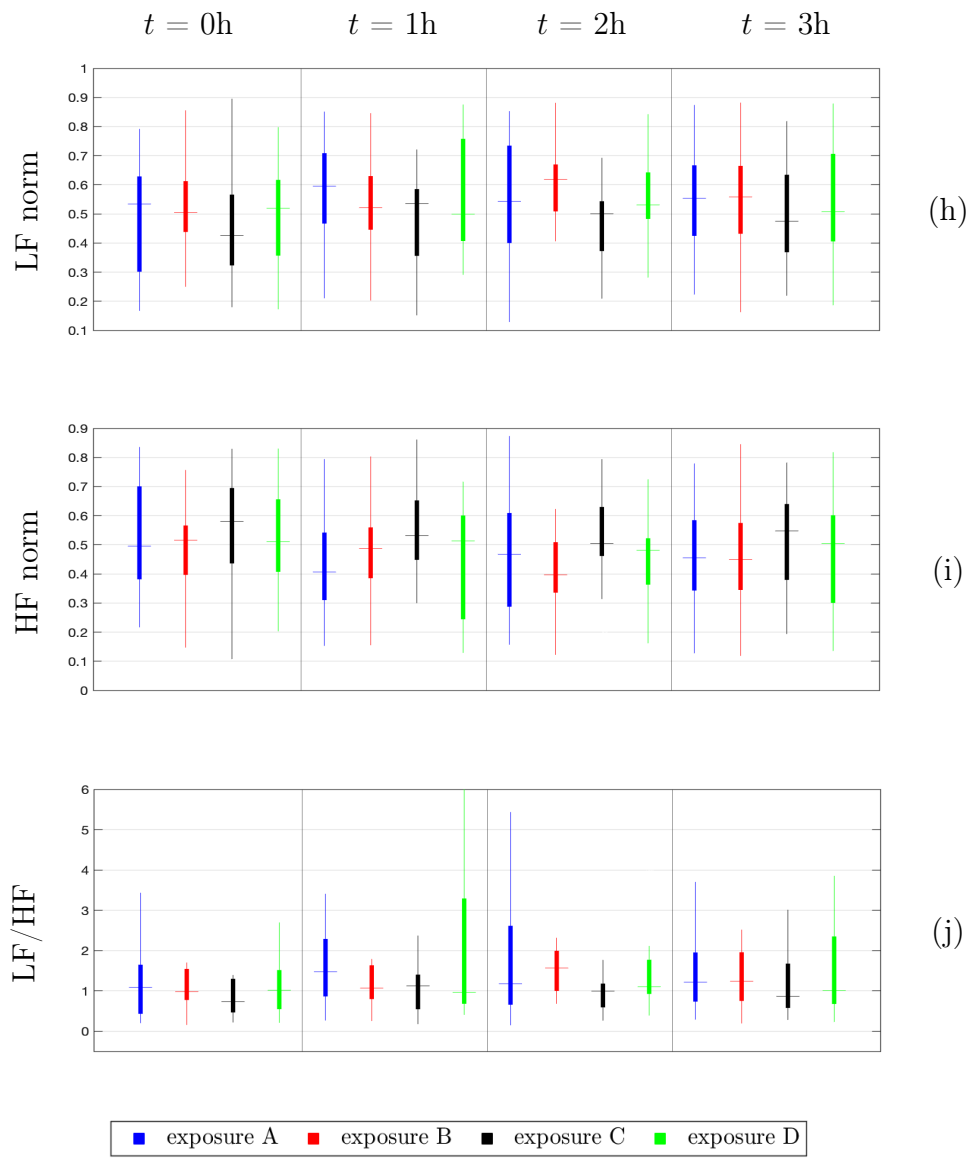
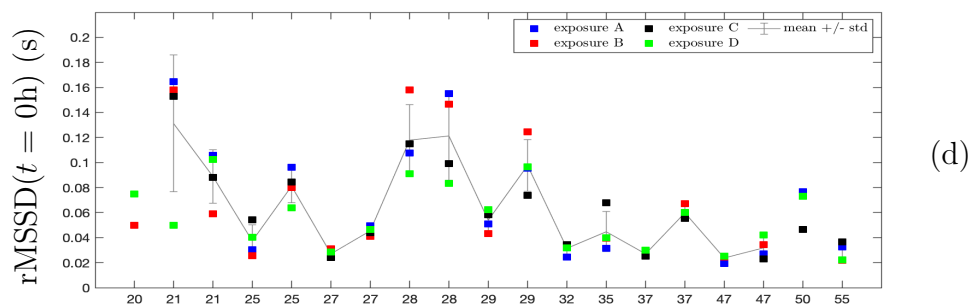
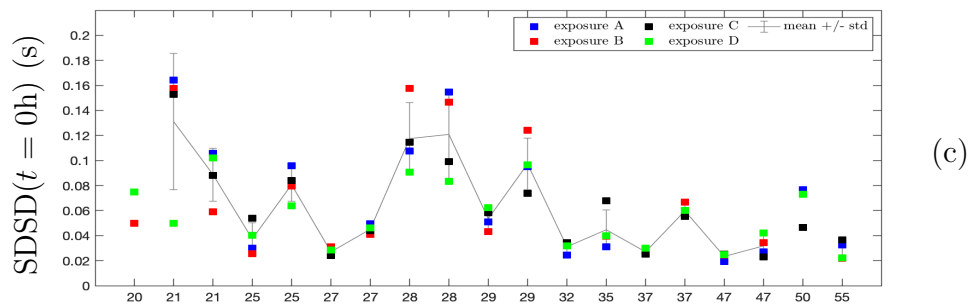
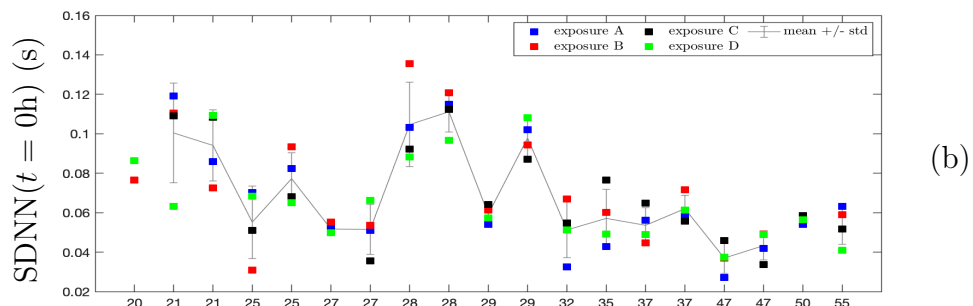
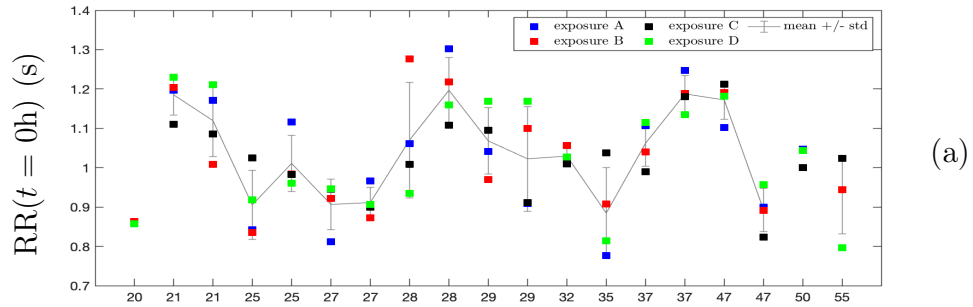
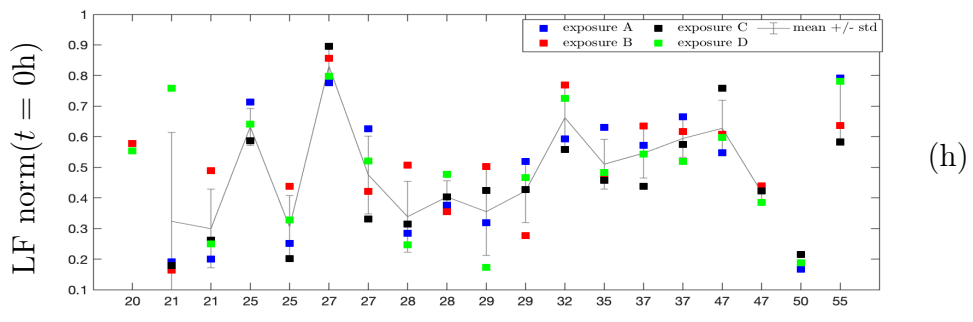
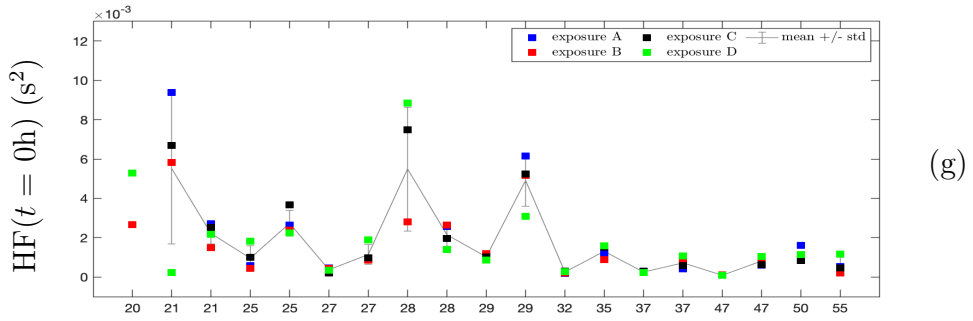
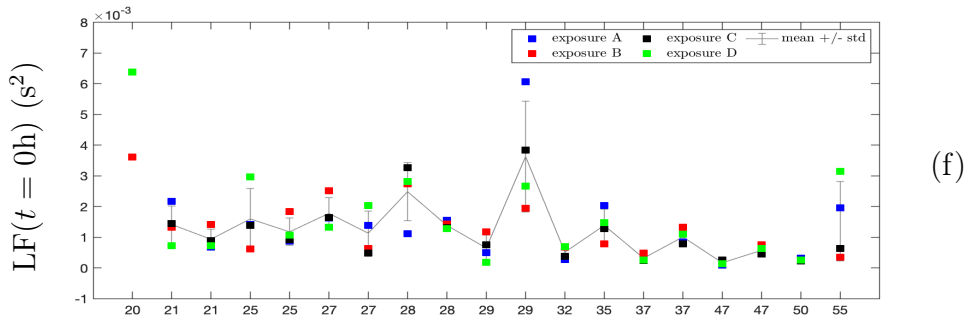
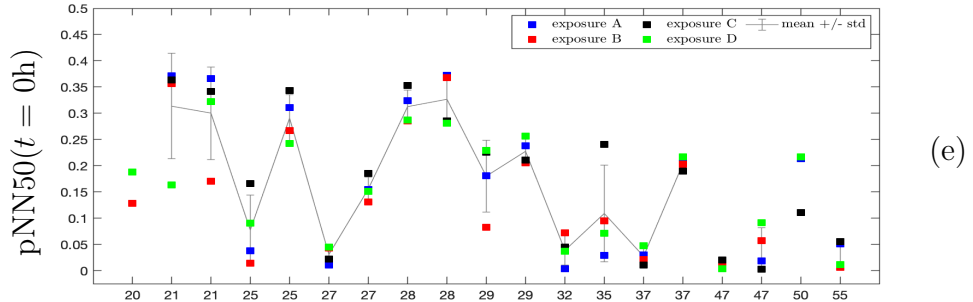


Figure B.1: Functional boxplots of HRV parameters.

B.2 Variability of HRV parameters at basal condition



Patients sorted by age (years)



Patients sorted by age (years)

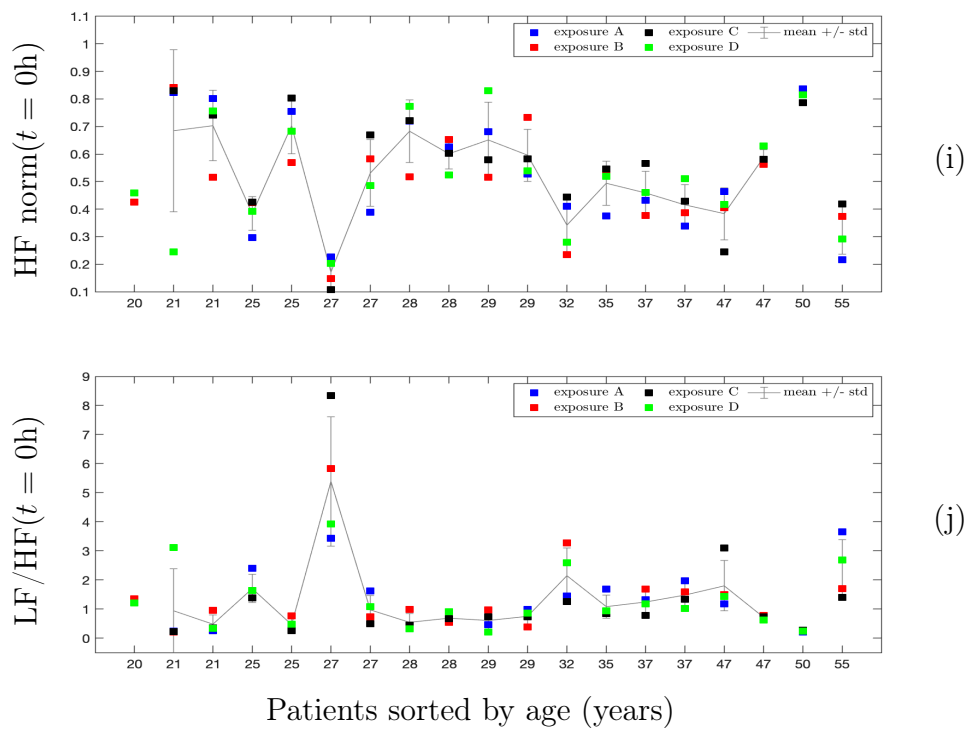
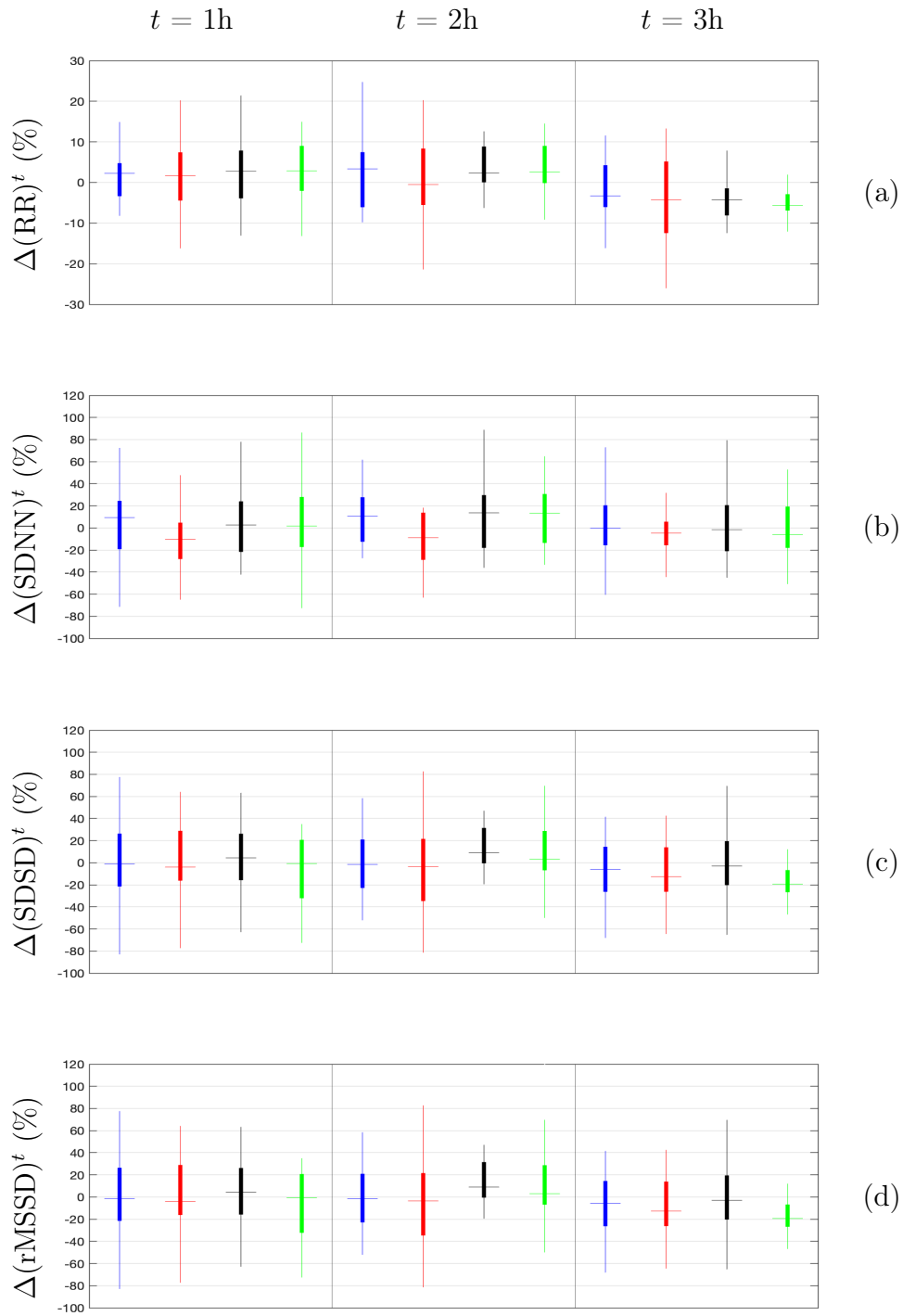
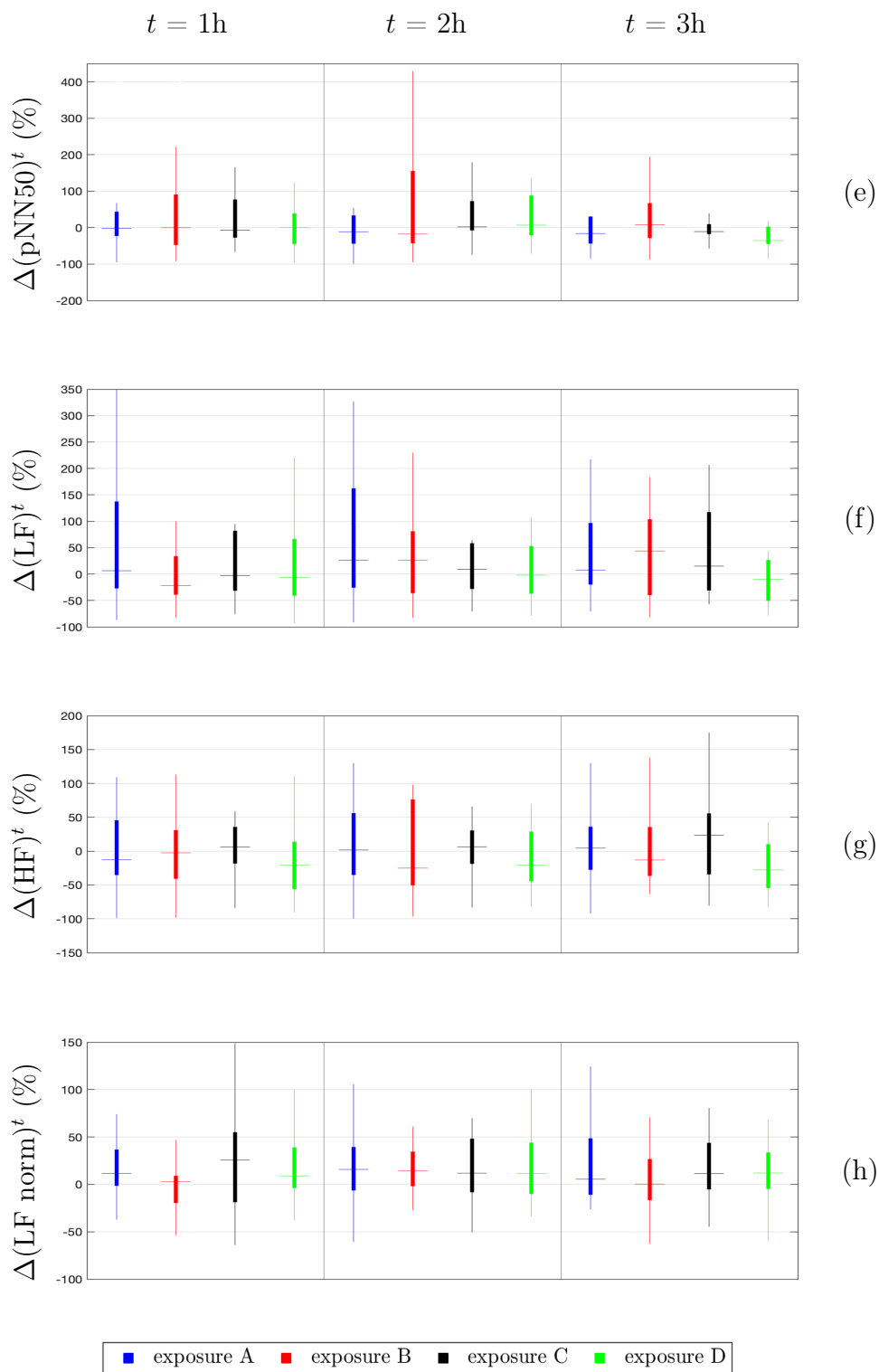


Figure B.2: Median values of HRV parameters at basal condition for every patient and exposure type.

B.3 Changes in HRV parameters with exposure type





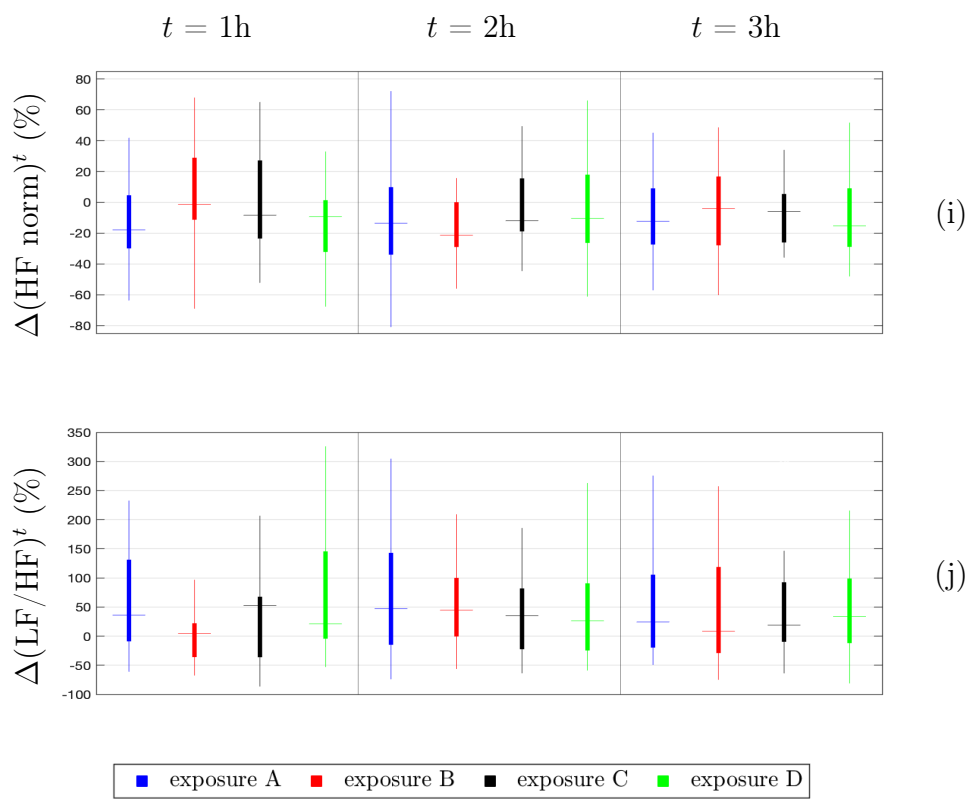
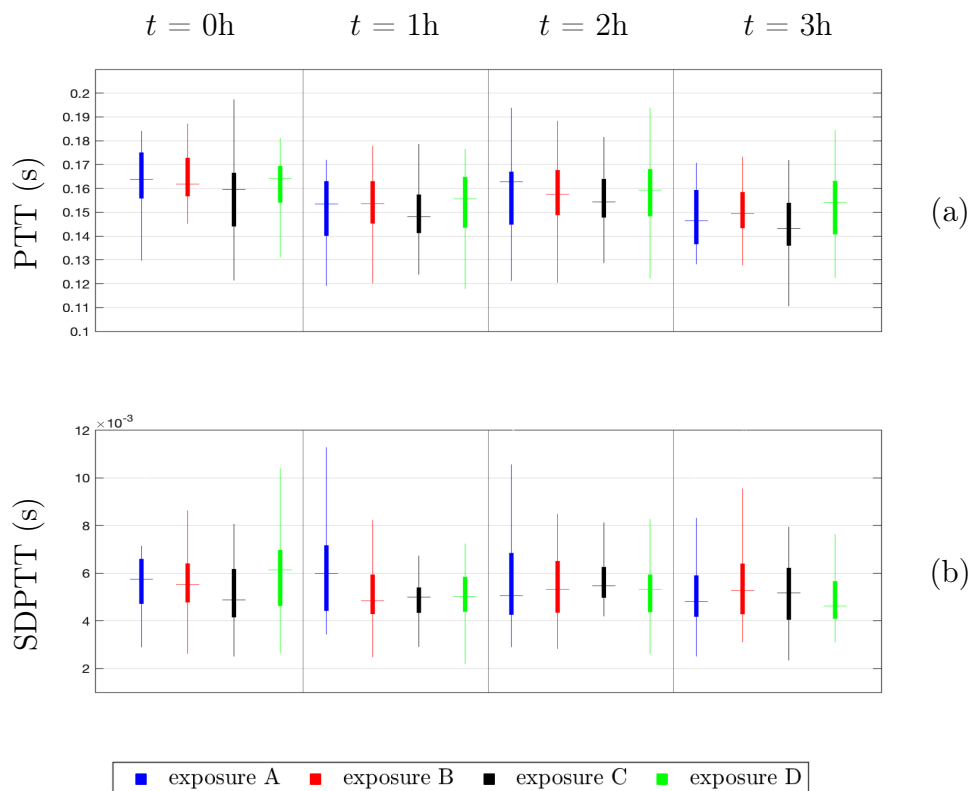


Figure B.3: Functional boxplots of relative changes in HRV parameters.

Appendix C

Pulse transit time analysis

C.1 Changes in PTT characteristics over time



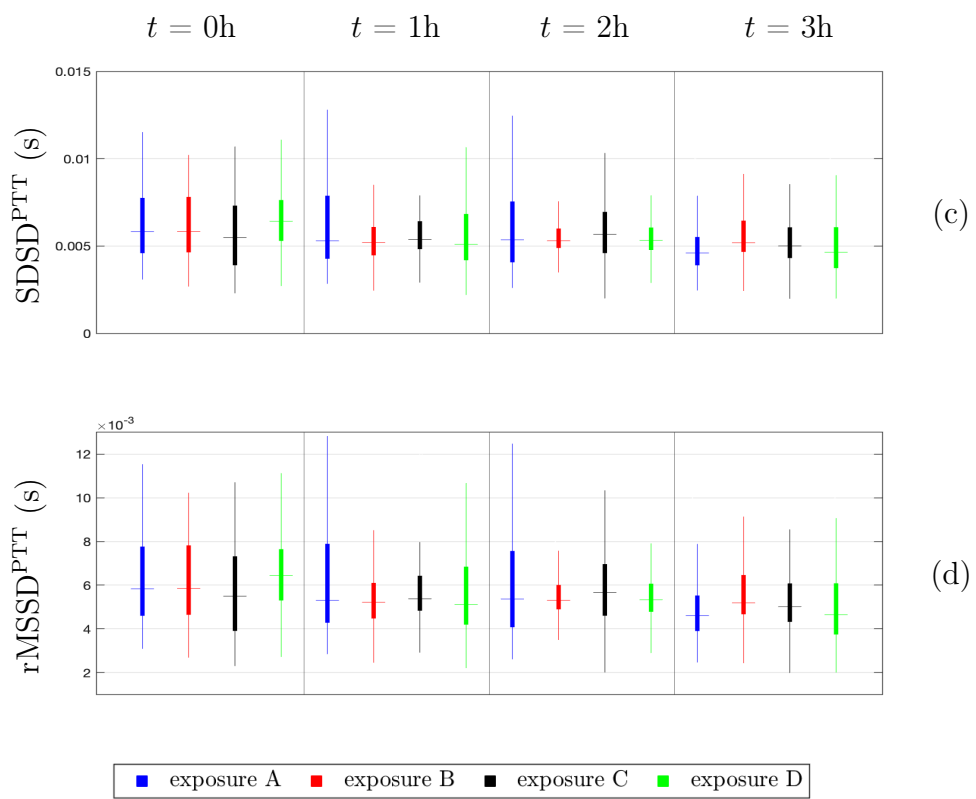


Figure C.1: Functional boxplots of PTT characteristics.

C.2 Variability of PTT characteristics at basal condition

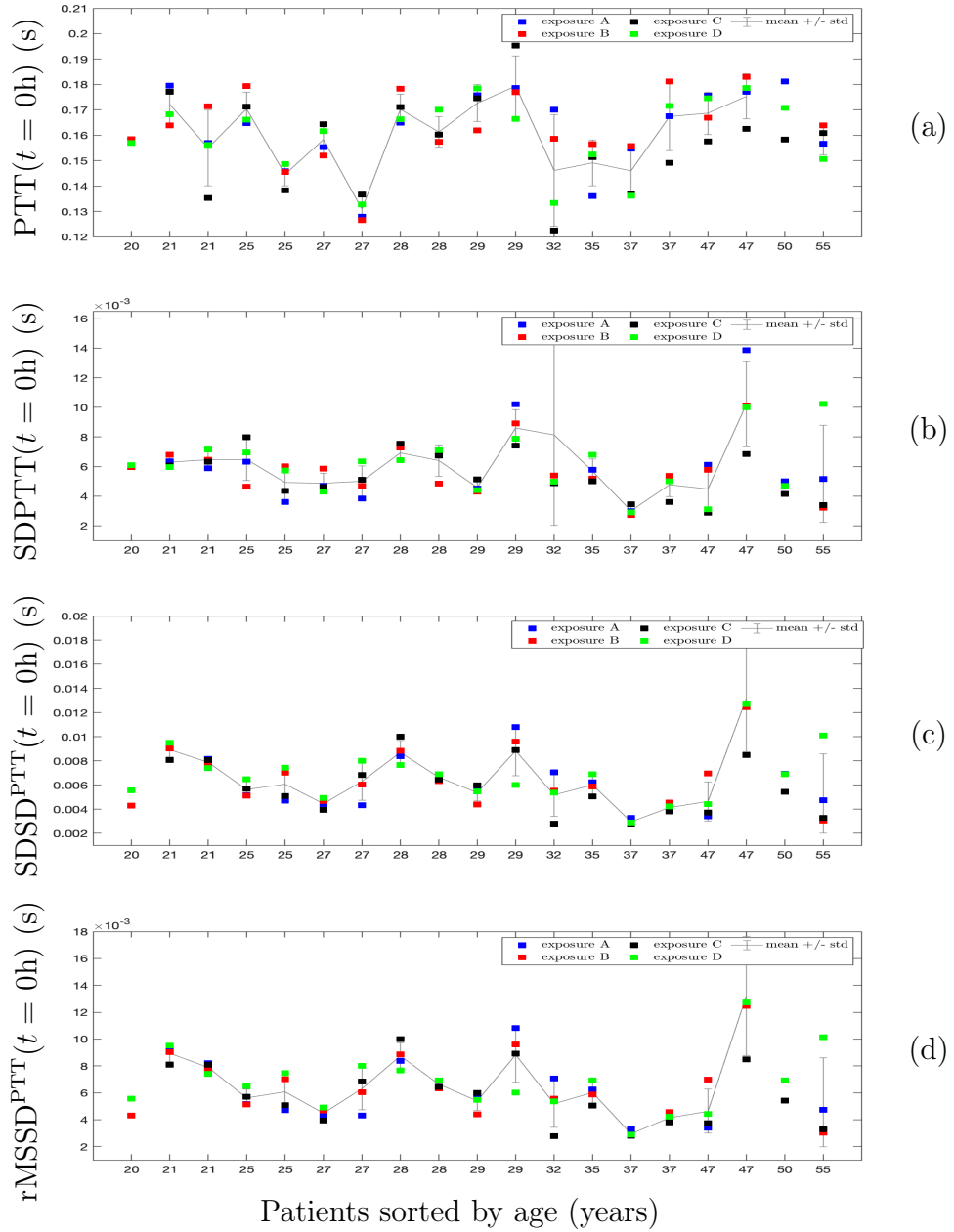


Figure C.2: Median values of PTT characteristics at basal condition for every patient and exposure type.

C.3 Changes in PTT characteristics with exposure type

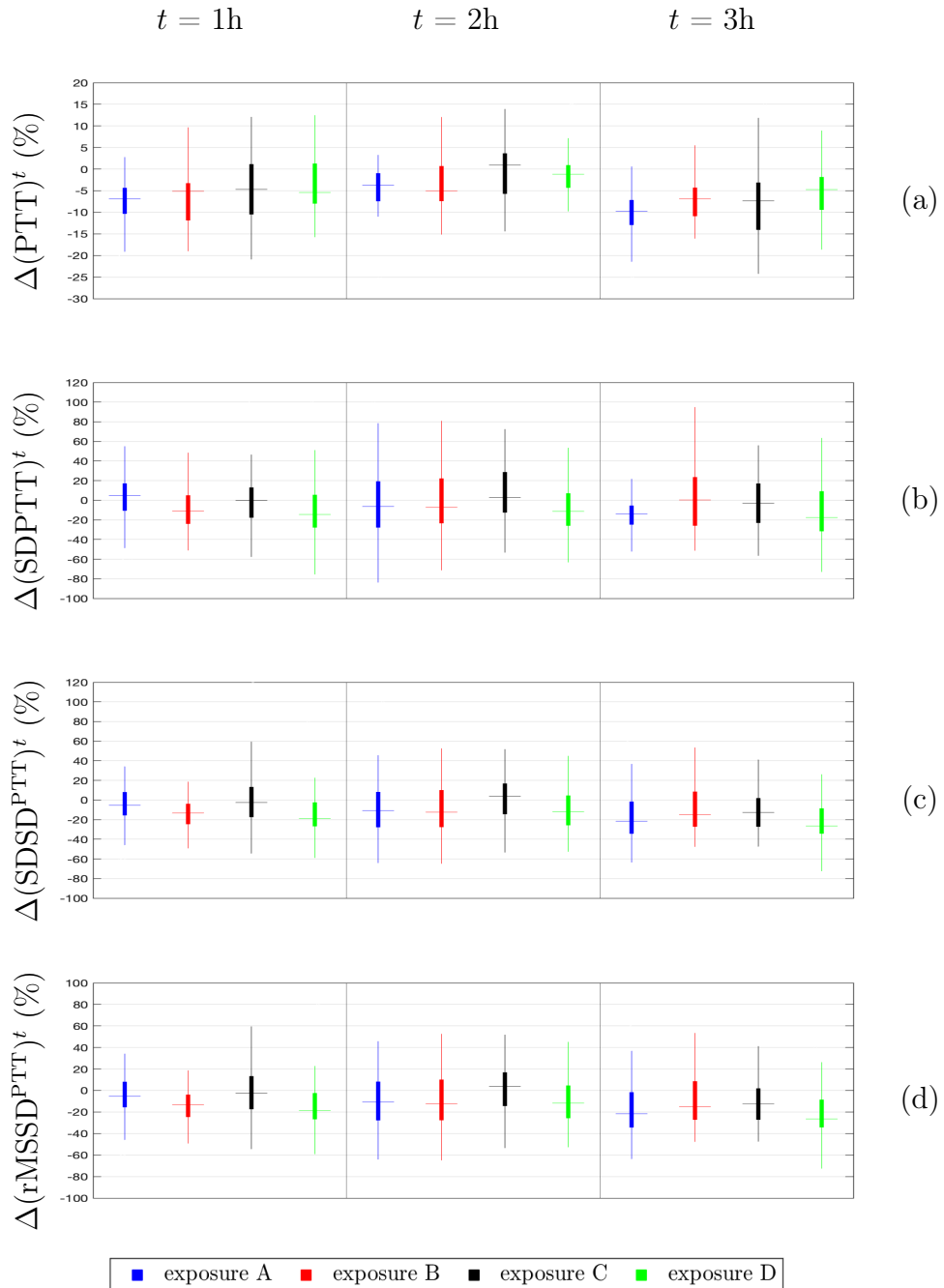


Figure C.3: Functional boxplots of relative changes in PTT characteristics.

